

Retrieval of total and tropospheric ozone from observations by the Global Ozone Monitoring Experiment

Citation for published version (APA):

Valks, P. J. M. (2003). *Retrieval of total and tropospheric ozone from observations by the Global Ozone Monitoring Experiment*. [Phd Thesis 2 (Research NOT TU/e / Graduation TU/e), Applied Physics and Science Education]. Technische Universiteit Eindhoven. <https://doi.org/10.6100/IR571922>

DOI:

[10.6100/IR571922](https://doi.org/10.6100/IR571922)

Document status and date:

Published: 01/01/2003

Document Version:

Publisher's PDF, also known as Version of Record (includes final page, issue and volume numbers)

Please check the document version of this publication:

- A submitted manuscript is the version of the article upon submission and before peer-review. There can be important differences between the submitted version and the official published version of record. People interested in the research are advised to contact the author for the final version of the publication, or visit the DOI to the publisher's website.
- The final author version and the galley proof are versions of the publication after peer review.
- The final published version features the final layout of the paper including the volume, issue and page numbers.

[Link to publication](#)

General rights

Copyright and moral rights for the publications made accessible in the public portal are retained by the authors and/or other copyright owners and it is a condition of accessing publications that users recognise and abide by the legal requirements associated with these rights.

- Users may download and print one copy of any publication from the public portal for the purpose of private study or research.
- You may not further distribute the material or use it for any profit-making activity or commercial gain
- You may freely distribute the URL identifying the publication in the public portal.

If the publication is distributed under the terms of Article 25fa of the Dutch Copyright Act, indicated by the "Taverne" license above, please follow below link for the End User Agreement:

www.tue.nl/taverne

Take down policy

If you believe that this document breaches copyright please contact us at:

openaccess@tue.nl

providing details and we will investigate your claim.

Retrieval of total and tropospheric ozone from observations by the Global Ozone Monitoring Experiment

PROEFSCHRIFT

ter verkrijging van de graad van doctor aan de
Technische Universiteit Eindhoven, op gezag van de
Rector Magnificus, prof.dr. R.A. van Santen, voor een
commissie aangewezen door het College voor
Promoties in het openbaar te verdedigen
op donderdag 18 december 2003 om 16.00 uur

door

Pieter Valks

geboren te Velsen

Dit proefschrift is goedgekeurd door de promotoren:

prof.dr. H. Kelder

en

prof.dr. U. Platt

Copromotor:

dr. R.F. van Oss

The work described in this thesis was performed at the Royal Netherlands Meteorological Institute (KNMI). The research was supported by the European Space Agency (ESA) and the European Organisation for the Exploitation of Meteorological Satellites (EUMETSAT).

Druk: Universiteitsdrukkerij Technische Universiteit Eindhoven

CIP-DATA LIBRARY TECHNISCHE UNIVERSITEIT EINDHOVEN

Valks, Pieter

Retrieval of total and tropospheric ozone from observations by the Global Ozone Monitoring Experiment / by Pieter Valks. - Koninklijk Nederlands Meteorologisch Instituut (KNMI). - Eindhoven : Technische Universiteit Eindhoven, 2003. - Proefschrift. ISBN 90-386-1825-5

NUR 932

Trefw.: atmosferisch ozon / aardobservatiesatellieten / stratosfeer / troposfeer / luchtverontreiniging

Subject headings: ozone / GOME / remote sensing / atmospheric-composition / retrieval

Contents

| | |
|---|------------|
| Samenvatting | vii |
| 1 Introduction | 1 |
| 1.1 The importance of ozone | 1 |
| 1.2 Ozone in the stratosphere | 2 |
| 1.3 Observations of ozone from the ground | 4 |
| 1.4 Satellite observations of ozone..... | 6 |
| 1.5 The DOAS retrieval method | 8 |
| 1.6 Ozone in the tropical troposphere | 11 |
| 1.7 Global chemistry transport models | 14 |
| 1.8 Thesis outline | 15 |
| 2 A Fast Delivery System for the retrieval of near-real time ozone columns from GOME data | 17 |
| 2.1 Introduction | 18 |
| 2.2 The Fast Delivery system..... | 19 |
| 2.2.1 GOME instrument | 19 |
| 2.2.2 Data transport | 19 |
| 2.2.3 Operational Environment | 20 |
| 2.2.4 Time delays | 21 |
| 2.3 Total ozone retrieval algorithm | 22 |
| 2.3.1 Level 0-1 processor | 22 |
| 2.3.2 Level 1-2 processor | 23 |
| 2.3.3 FD versus off-line GDP ozone columns | 25 |
| 2.4 Ground-based validation | 26 |
| 2.5 Concluding remarks | 29 |
| 3 Ozone mini-hole observed over Europe, influence of low stratospheric temperature on observations | 31 |
| 3.1 Introduction | 32 |
| 3.2 Ground-based observations | 32 |
| 3.3 Satellite observations..... | 35 |
| 3.4 Conclusions | 38 |

| | | |
|----------|---|-----------|
| 4 | Variability in tropical tropospheric ozone: analysis with GOME observations and a global model | 39 |
| 4.1 | Introduction | 40 |
| 4.2 | GOME measurements | 41 |
| 4.2.1 | FRESCO cloud algorithm | 42 |
| 4.2.2 | GOME total ozone | 44 |
| 4.3 | Tropical tropospheric ozone from GOME | 46 |
| 4.3.1 | GOME-CCD method..... | 46 |
| 4.3.2 | Zonal variations in the ozone column above 200 hPa..... | 47 |
| 4.3.3 | The tropical tropospheric ozone column below 200 hPa | 48 |
| 4.4 | TTOC variability examined with the GOME-CCD method and the TM3 model ... | 52 |
| 4.4.1 | The TM3 chemistry-transport model | 52 |
| 4.4.2 | Southern Tropics | 53 |
| 4.4.3 | Northern Tropics | 58 |
| 4.5 | Conclusions and future outlook..... | 60 |
| 4.6 | Appendix: GOME retrieval efficiency | 61 |
| 5 | Improved GOME total ozone columns: an empirical DOAS method that accounts for Raman scattering | 65 |
| 5.1 | Introduction | 66 |
| 5.2 | Improvement of the GOME (ir)radiance spectra | 67 |
| 5.2.1 | The GomeCal package | 67 |
| 5.2.2 | Reduced effective spectral resolution | 68 |
| 5.3 | DOAS slant column fit..... | 68 |
| 5.3.1 | Common DOAS fit-equation | 68 |
| 5.3.2 | Accounting for Raman scattering..... | 69 |
| 5.3.3 | Instrumental slit function | 72 |
| 5.3.4 | GOME fit results | 74 |
| 5.4 | DOAS fit-window and temperature dependence | 77 |
| 5.4.1 | Ozone cross-section data sets..... | 77 |
| 5.4.2 | The 325-335 nm GOME fit-window..... | 78 |
| 5.4.3 | The 331.6-336.6 nm OMI fit-window..... | 81 |
| 5.5 | Air Mass Factor calculations..... | 82 |
| 5.5.1 | Empirical Air Mass Factor | 82 |
| 5.5.2 | Slant column dependent Air Mass Factor | 83 |
| 5.6 | Cloud correction and vertical ozone column..... | 84 |
| 5.6.1 | Cloud correction | 84 |
| 5.6.2 | Vertical ozone column | 87 |
| 5.6.3 | Error analysis..... | 87 |
| 5.7 | Ozone column comparisons | 89 |
| 5.7.1 | Fit window comparison..... | 89 |
| 5.7.2 | Comparisons with FD ozone columns | 89 |
| 5.7.3 | Comparisons with GDP ozone columns..... | 92 |
| 5.7.4 | Validation with ground-based measurements | 94 |
| 5.8 | Concluding Remarks | 95 |

| | | |
|----------|---|------------|
| 6 | Summary and Outlook | 99 |
| 6.1 | Overview | 99 |
| 6.2 | Summary and Conclusions | 99 |
| 6.2.1 | Scientific questions | 99 |
| 6.2.2 | Answers to the scientific questions | 100 |
| 6.3 | Outlook and future work | 104 |
| 6.3.1 | Total ozone columns | 104 |
| 6.3.2 | Tropical tropospheric ozone..... | 105 |
| | Bibliography | 107 |
| | Abbreviations and Acronyms | 119 |
| | Nawoord | 121 |
| | Curriculum Vitae | 123 |

Samenvatting

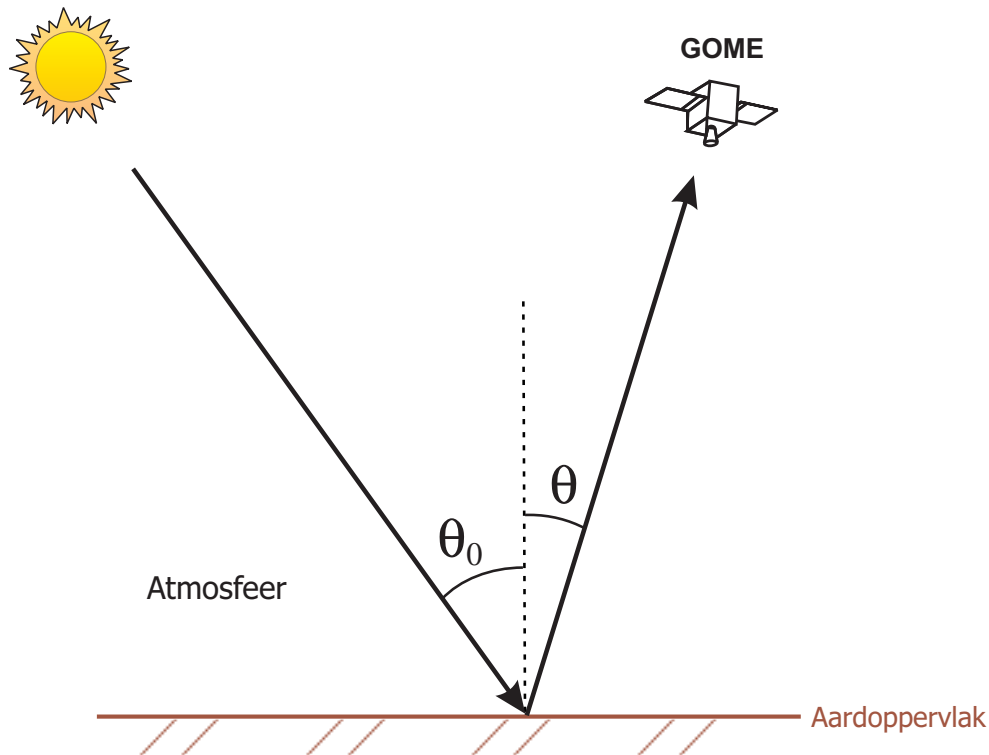
Het onderzoek in dit proefschrift richt zich op de bepaling van atmosferische ozonhoeveelheden uit metingen van het satellietinstrument GOME (*Global Ozone Monitoring Experiment*). In dit hoofdstuk wordt daarom eerst het belang van ozon in de atmosfeer toegelicht en het meetprincipe van het GOME instrument uitgelegd. Daarna wordt een korte samenvatting van de inhoud van dit proefschrift gegeven en worden de belangrijkste onderzoeksresultaten beschreven.

Ozon in de atmosfeer

Ozon (O_3), een verbinding van zuurstof, is een van de belangrijkste sporegassen in de aardatmosfeer. Ongeveer 90% van de ozon bevindt zich in de stratosfeer, tussen 12 en 50 km hoogte. De ozonlaag in de stratosfeer absorbeert schadelijk ultraviolet zonlicht en beschermt zo onze biosfeer. Hoge ozonconcentraties op leefniveau, ook wel zomersmog genoemd, zijn echter schadelijk voor de gezondheid van mensen, dieren en gewassen. Aan de grond en in de rest van de troposfeer, die zich uitstrekt tot een hoogte van ongeveer 12 km, wordt ozon gevormd door chemische omzettingen van o.a. stikstofoxiden en koolwaterstoffen, onder invloed van zonlicht. Verder is ozon ook van belang voor mogelijke klimaatveranderingen. Het is namelijk een sterk broeikasgas, vooral hoog in de troposfeer in de (sub)tropen.

De grootschalige afname van de ozonconcentraties in de stratosfeer boven de Zuidpool tussen augustus en november is een bekend fenomeen. Het ozongat boven de Zuidpool wordt veroorzaakt door chemische afbraak van ozon, voornamelijk als gevolg van chloorfluorkoolwaterstoffen (CFK's) die door de mens in de atmosfeer zijn gebracht. Door de lage temperaturen tijdens de poolwinter op het zuidelijk halfrond ontstaan hoge parelmoerwolken. Aan het oppervlak van deze wolken worden chloor-reservoirstoffen door chemische (heterogene) reacties omgezet in actief chloor. Als in de lente de zon terugkeert boven de Zuidpool, wordt ozon door de actieve chloorradicalen katalytisch afgebroken. In het ozongat is de totale ozonhoeveelheid daardoor nog maar een derde van de normale hoeveelheid.

Metingen van ozon en andere belangrijke atmosferische sporegassen vormen de basis van onze kennis over de atmosfeer. De totale ozonhoeveelheid in de atmosfeer (de ozonkolomdichtheid) boven een bepaalde locatie kan vanaf de grond worden bepaald met Dobson en Brewer spectrometers, genoemd naar de personen die deze instrumenten hebben ontwikkeld. Informatie over de verticale verdeling van ozon (het ozonprofiel) kan worden verkregen door



Satellietmeting met het GOME instrument. De pijlen geven het pad aan dat het licht door de atmosfeer aflegt. De stand van de zon is hier aangeduid met θ_0 . Het zonlicht wordt gereflecteerd door het aardoppervlak of verstrooid door lucht moleculen. GOME kijkt onder een hoek van 0 tot 30° naar het aardoppervlak en meet zo het gereflecteerde zonlicht.

een meetinstrument, een ozonsonde, aan een ballon op te laten. Ozonmetingen vanaf de grond geven nauwkeurige informatie over de ozonkolomdichtheid of het ozonprofiel op een bepaalde plaats. Om de ozonhoeveelheden op een globale schaal te bepalen zijn echter metingen met satellietinstrumenten noodzakelijk.

Satellietmetingen van ozon

Voor het onderzoek in dit proefschrift is gebruik gemaakt van metingen door het GOME instrument, gelanceerd op de ERS-2 satelliet in April 1995. GOME meet het zonlicht dat gereflecteerd is door het aardoppervlak en de atmosfeer. Hiertoe kijkt GOME naar beneden de atmosfeer in (*nadir*), onder een hoek van maximaal 30° (zie figuur). De sterkte van het gereflecteerde zonlicht hangt af van de golflengte ervan. GOME meet deze stralingssterkte bij duizenden golflengtes tegelijkertijd in het ultraviolette, zichtbare en nabij-infrarode golflengtegebied (een spectrum). Omdat ozon in de atmosfeer het ultraviolette zonlicht (gedeeltelijk) absorbeert en de mate van absorptie afhangt van de golflengte, kan uit het door GOME gemeten aardspectrum de ozonkolomdichtheid in de atmosfeer worden berekend. De bepaling van de ozonkolomdichtheid uit het gemeten aardspectrum wordt *retrieval* (terugvinden) genoemd. De retrieval-techniek die in dit proefschrift wordt gebruikt om de ozonkolomdichtheid te bepalen heet Differentiële Optische Absorptie Spectroscopie (DOAS). Deze methode maakt

optimaal gebruik van de mogelijkheden van het GOME instrument om de fijne absorptiestructuren in het gereflecteerde aardspectrum te meten.

De DOAS methode bestaat uit twee stappen: eerst wordt uit een gedeelte van het gemeten aardspectrum de totale ozonhoeveelheid langs het lichtpad door de atmosfeer bepaald: dit wordt de schuine ozonkolomdichtheid genoemd. Het golflengtegebied van het aardspectrum dat wordt gebruikt in de DOAS retrieval wordt *fit-window* genoemd. Voor de bepaling van de schuine ozonkolomdichtheid wordt vaak een fit-window tussen 325 en 335 nm genomen. Daarna wordt uit de schuine ozonkolom de verticale ozonkolomdichtheid bepaald met behulp van de zogenaamde luchtmassafactor, die een maat is voor de afgelegde weg van het licht door de atmosfeer. De luchtmassafactor wordt berekend met behulp van een computermodel (stralingstransportmodel). De computerberekeningen zijn complex, omdat de luchtmassafactor afhangt van de verticale verdeling van ozon, van de aanwezigheid van andere gassen, wolken en aërosolen, en van de reflectie-eigenschappen van het aardoppervlak. Retrieval-technieken, zoals de DOAS methode, zijn daarom nog in ontwikkeling.

Overzicht van dit proefschrift

Zoals gezegd handelt dit proefschrift over metingen van ozon met het GOME satellietinstrument. In **hoofdstuk 2** wordt een snel retrieval systeem beschreven dat binnen drie uur na een GOME meting de ozonkolomdichtheid bepaalt uit het gemeten aardspectrum, en beschikbaar stelt via het Internet. Dit retrieval systeem wordt het *Fast-Delivery* (FD) systeem genoemd. De FD-ozonkolommen zijn van belang voor verschillende toepassingen: ze worden bijvoorbeeld gebruikt in weermodellen om de weersverwachting op middellange termijn te verbeteren, om de dikte van de ozonlaag te monitoren, en om de zonkrachtverwachting in de lente en zomer te verbeteren. Het snelle retrieval systeem maakt gebruik van een klein gedeelte van de ruwe GOME gegevens die al binnen een paar uur na de satellietmeting beschikbaar zijn. Het algoritme dat wordt gebruikt om de ozonkolomdichtheid te bepalen maakt gebruik van de DOAS-techniek en is gebaseerd op het operationele algoritme van de GOME Data Processor (GDP), dat is ontwikkeld door het Duitse centrum voor Lucht- en Ruimtevaart (DLR), in opdracht van de Europese ruimtevaartorganisatie ESA.

Er is echter een aantal veranderingen in het FD-algoritme aangebracht om de ozonkolomdichtheid nauwkeuriger te kunnen bepalen. Zo wordt in het algoritme rekening gehouden met de actuele temperatuur van de atmosfeer. Dit is van belang omdat de hoeveelheid absorptie van het zonlicht door ozon afhangt van de temperatuur van de atmosfeer. Verder worden voor de bepaling van de luchtmassafactor met het stralingstransportmodel betere aannames gemaakt over de verticale verdeling van ozon (door gebruik te maken van de Fortuin en Kelder ozonklimatologie). Tenslotte wordt beter rekening gehouden met de aanwezigheid van wolken in de atmosfeer. Wolken hebben namelijk een versturende invloed op de retrieval van de ozonkolomdichtheid uit GOME metingen, met name omdat GOME niet door de wolken heen kan 'kijken'. Om hiervoor zo goed mogelijk te kunnen corrigeren worden uit het door GOME gemeten aardspectrum belangrijke bewolkingseigenschappen (de bedekkingsgraad en wolken-tophoogte) afgeleid. Daartoe wordt gebruik gemaakt van het zogenaamde FRESCO (Fast Retrieval Scheme for Cloud Observables) wolkenalgoritme.

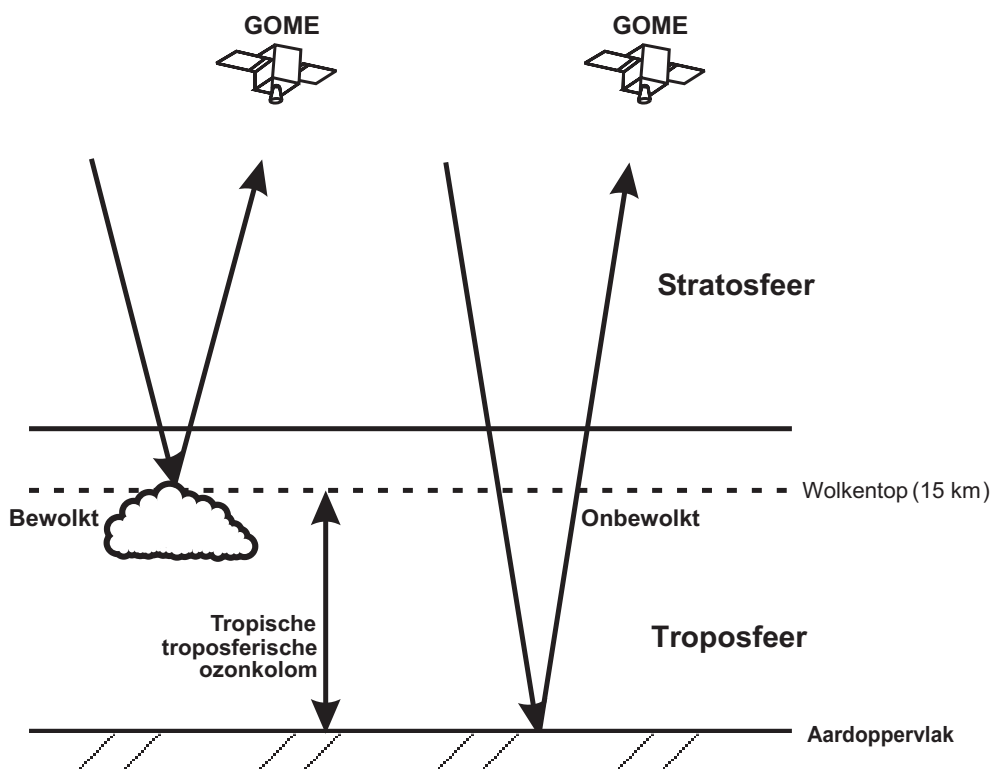
Om de nauwkeurigheid van de snelle GOME ozonkolommen te bepalen zijn ze vergeleken met grondwaarnemingen van de ozonkolomdichtheid op ongeveer 20 plaatsen, verspreid over de hele aarde. Deze wereldwijde *validatie* laat een redelijk goede overeenstemming zien tussen de GOME ozonkolommen en de grondwaarnemingen (over het algemeen zijn de verschillen kleiner dan 5%).

In **hoofdstuk 3** worden grond- en satellietmetingen beschreven van een mini-ozongat, dat op 30 November en 1 December 1999 over noord-west Europa trok. Mini-ozongaten komen regelmatig voor op de gematigde breedten van beide halfronden. In tegenstelling tot het grote ozongat boven de Zuidpool zijn het relatief kort durende gebeurtenissen en speelt chemische afbraak van ozon geen grote rol. Het mini-ozongat boven Europa werd voornamelijk veroorzaakt door transport van ozon-arme lucht uit de subtropen naar het mini-gat gebied. In het mini-ozongat was de totale ozonhoeveelheid met meer dan 30% afgenomen en werden ozonkolomdichtheden onder de 200 Dobson Units gemeten*. De metingen werden uitgevoerd vanaf de grond met een Brewer spectrometer en met een ozonsonde in De Bilt, en vanuit de ruimte met het GOME instrument. De metingen laten zien dat de grootste afname in de ozonhoeveelheden optrad tussen 10 tot 20 km hoogte.

Tijdens het mini-ozongat verschijnsel was de temperatuur in de stratosfeer erg laag. In deze studie is daarom ook gekeken naar de invloed van de lage temperatuur op de nauwkeurigheid van de ozonmetingen. Zoals gezegd is het belangrijk om rekening te houden met de actuele temperatuur van de atmosfeer en wordt dit ook gedaan in het FD-algoritme. Meestal wordt echter een klimatologische (gemiddelde) temperatuur gebruikt in ozon retrieval algoritmen. Uit deze studie blijkt dat door het gebruik van een klimatologische temperatuur in het retrieval algoritme voor GOME, in plaats van de actuele temperatuur, een fout wordt gemaakt van 4% in de bepaling van de ozonkolomdichtheid in het mini-ozongat. Voor de Brewer spectrometer is deze fout 2%.

Hoofdstuk 4 gaat over de variaties in de ozonhoeveelheid in de troposfeer, in de tropen. In de tropen worden grote hoeveelheden vervuilende stoffen, zoals stikstofdioxide, koolmonoxide en koolwaterstoffen geëmitteerd door zowel menselijke als natuurlijke bronnen. De belangrijkste natuurlijke emissiebron van stikstofdioxide in de tropen is bliksem. Bij een bliksemontlading wordt de lucht sterk verhit en worden stikstofdioxide gevormd. De belangrijkste menselijke bron van vervuilende gasen in de tropen zijn biomassa-verbrandingen. Tijdens de droge seizoenen worden in Afrika en Zuid-Amerika op grote schaal bossen, struikgewas en agrarisch afval verbrand, waardoor enorme hoeveelheden stikstofdioxide, koolmonoxide en koolwaterstoffen vrijkomen. In deze vervuilde gebieden worden daardoor in de troposfeer, via chemische reacties aangedreven door het sterke tropische zonlicht, grote hoeveelheden ozon geproduceerd. In de tropen kan de gevormde ozon over grote afstanden worden getransporteerd door de wind en zo ook gebieden ver weg van de emissiebronnen vervuilen.

* De hoeveelheid ozon in de atmosfeer wordt vaak uitgedrukt in Dobson Units (DU). Een Dobson Unit is gelijk aan de hoogte van de ozonkolom (in honderdste millimeters) als alle ozonmoleculen naar de grond zouden worden gebracht. Gemiddeld is de ozonkolom ongeveer 300 DU, wat overeen komt met een kolom van 3 mm hoog!



Principe van de CCD (Convective-Cloud-Differential) methode om de troposferische ozonkolom in de tropen te bepalen. Hierbij wordt gebruik gemaakt van GOME ozonkolom-metingen boven hoge convectieve wolken in de tropen en metingen in onbewolkte situaties. Uit het verschil tussen deze twee type metingen wordt de troposferische ozonkolom bepaald.

De troposferische ozonhoeveelheid in deze vervuilde tropische gebieden kan met de zogenaamde *Convective-Cloud-Differential* (CCD) methode worden bepaald uit satellietmetingen van het GOME instrument. Deze methode maakt gebruik van GOME ozonmetingen boven dikke convectieve wolken, die in de tropen tot grote hoogten reiken (12 tot 16 km). Zoals gezegd kan GOME niet door de wolken heen 'kijken' en het instrument meet dus eigenlijk alleen de ozonhoeveelheid boven de wolken. In het geval van een wolkenvrije hemel kan GOME echter wel de ozonhoeveelheid tot aan de grond meten. In de CCD methode wordt van deze twee type metingen gebruik gemaakt, door het verschil te berekenen tussen de totale (wolkenvrije) GOME ozonkolomdichtheid en de GOME ozonkolomdichtheid boven hoge tropische wolken, met als resultaat de ozonkolomdichtheid *onder* de wolk (zie figuur). Uit deze resultaten kunnen kaarten van de maandgemiddelde ozonkolomdichtheid in de troposfeer (tot een hoogte van ongeveer 15 km) worden samengesteld voor de tropen (tussen 20°NB en 20°ZB). Voor de CCD-methode is een nauwkeurige bepaling van de bedekkingsgraad en wolkentophoogte van groot belang. Deze wolkeneigenschappen worden afgeleid uit de GOME metingen met behulp van het FRESCO algoritme (hierboven beschreven). Om de nauwkeurigheid van de GOME troposferische ozonkolommen te bepalen zijn ze vergeleken met ozonsonde metingen uitgevoerd vanaf zeven tropische plaatsen, waaronder Paramaribo. Deze vergelijkingen laten een goede overeenkomst zien tussen de satelliet- en grondmetingen van de troposferische ozonkolom.

De GOME-CCD methode is gebruikt om de grote variabiliteit in troposferisch ozon in de tropen te onderzoeken. Zo worden boven de zuidelijke tropische Atlantische Oceaan vaak hoge troposferische ozonhoeveelheden gemeten, terwijl boven de Stille Oceaan de ozonwaarden juist heel laag zijn. De grootte en de precieze locatie van dit troposferisch ozonmaximum boven de Atlantische Oceaan variëren echter van jaar tot jaar. Bij het onderzoek naar de ozonvariabiliteit is ook gebruik gemaakt van een chemie-transportmodel, genaamd TM3. Dit is een computermodel dat de atmosfeer opdeelt in een rooster en berekeningen maakt van de emissies van gassen, de chemische omzetting in de atmosfeer en het transport van deze stoffen door de wind en door turbulentie. Met een chemie-transportmodel is het mogelijk om de afzonderlijke effecten van bliksem en biomassa verbrandingen op de ozonhoeveelheden in de troposfeer te berekenen. Analyses van de GOME troposferische ozonkolommen met behulp van het TM3 model, laten zien dat de variabiliteit in troposferisch ozon in de tropen het gevolg is van een complexe interactie tussen verschillende processen, zoals de emissies door biomassa verbrandingen en bliksem, maar ook het transport van ozon over grote afstanden door de wind.

In **Hoofdstuk 5** van dit proefschrift wordt een nieuw en verbeterd retrieval algoritme voor de bepaling van de ozonkolomdichtheid uit GOME metingen beschreven. Uit de validatie van de Fast-Delivery ozonkolommen met grondwaarnemingen, beschreven in hoofdstuk 2, kwam namelijk een aantal punten naar voren voor verdere verbetering van het retrieval algoritme. Het belangrijkste punt is dat de nauwkeurigheid van de FD-ozonkolommen afhangt van de zonnestand en het seizoen. Het nieuwe algoritme, *TOGOMI* genaamd, maakt ook gebruik van de DOAS methode en is gebaseerd op het ozon retrieval algoritme, ontwikkeld voor het OMI (Ozon Monitoring Instrument) instrument dat in 2004 zal worden gelanceerd op de EOS-Aura satelliet.

Een van de belangrijkste verbeteringen van het nieuwe TOGOMI algoritme is dat rekening wordt gehouden met inelastische verstrooiing door luchtmoleculen. Een groot gedeelte van het door GOME gemeten zonlicht is verstrooid door luchtmoleculen, met name in de troposfeer. Bij verstrooiing door een luchtmolecuul heeft het verstrooide licht normaal gesproken dezelfde golflengte als het inkomende licht. In ongeveer 4 procent van de gevallen treedt echter een verschuiving op in de golflengte van het verstrooide licht t.o.v. de golflengte van het inkomende licht. Deze inelastische verstrooiing heeft een versturende invloed op de DOAS methode, waarmee in het nieuwe TOGOMI algoritme nu rekening wordt gehouden. Een andere verbetering van het TOGOMI algoritme is dat gebruik wordt gemaakt van de zogenaamde *empirische* DOAS methode, waardoor de luchtmassafactor nauwkeuriger kan worden berekend. Verder biedt het TOGOMI algoritme de mogelijkheid gebruik te maken van een speciaal golflengtegebied (fit-window) rond 334,1 nm, waardoor de bepaling van de ozonkolomdichtheid minder gevoelig wordt voor de natuurlijke variaties in de temperatuur en de verticale verdeling van ozon.

Met het verbeterde TOGOMI algoritme worden schuine ozonkolomdichtheden gevonden die 3 tot 10% groter zijn dan de waarden die met de gebruikelijke GOME-DOAS algoritmes worden gevonden. Dit komt voornamelijk doordat nu op een juiste manier rekening wordt gehouden met inelastische verstrooiing. De nieuwe GOME ozonkolommen zijn ook vergeleken met metingen vanaf de grond, uitgevoerd met Brewer en Dobson spectrometers. Deze voorlopige validatie laat een zeer goede overeenkomst zien tussen de satelliet- en grondme-

tingen. De verschillen tussen de GOME ozonkolomdichtheid en de grondwaarnemingen zijn meestal kleiner dan 2%. Verder is de nauwkeurigheid van de GOME ozonkolomdichtheid nu veel minder afhankelijk van de zonnestand en het seizoen.

Chapter 1

Introduction

This chapter provides a general overview of ozone in the troposphere and the stratosphere, and introduces the main topics of this thesis: the retrieval of ozone columns from satellite observations of the Global Ozone Monitoring Experiment (GOME), and the variability in tropical tropospheric ozone. First, a short overview of the important role of ozone in the atmosphere is given. Then, the introduction focuses on ozone in the stratosphere and on low-ozone phenomena, such as the Antarctic ozone hole and ozone mini-holes. This is followed by an overview of various ozone observation techniques, both from the ground and from space. A short description of the GOME satellite instrument is given and the Differential Optical Absorption Spectroscopy (DOAS) retrieval method is described. Then, the importance of ozone in the tropical troposphere is explained, and some methods to derive a tropical tropospheric ozone column from satellite observations are discussed. Finally, the motivation and scientific aims and results of this research are summarized.

1.1 The importance of ozone

The composition of the atmosphere has undergone dramatic changes in the last decades due to human activities [e.g. *IPCC*, 2001; *WMO*, 2003]. The quasi-exponential growth in the world population and the industrialization have led to a strong growth in fossil fuel and biomass burning emissions of trace gases such as carbon dioxide (CO_2), carbon monoxide (CO), nitrogen oxides (NO_x), methane (CH_4), and other hydrocarbons [*Van Aardenne et al.*, 2001]. The emissions of nitrogen oxides and hydrocarbons have resulted in an increase of ozone (O_3) near the surface and a degradation of air quality on a global scale, while the increases of CO_2 , CH_4 and other greenhouse gases have caused a rise in global mean temperature (global warming) [*IPCC*, 2001]. Furthermore, the release in the atmosphere of manmade chlorofluorocarbons has resulted in depletion in stratospheric ozone and the formation of an ozone hole over Antarctica in austral spring [*Crutzen*, 1970; *Molina and Rowland*, 1974; *Farman et al.*, 1985].

Although ozone is a trace gas and constitutes less than 0.001% of the air by volume, it is one of the most important constituents of the atmosphere. The ozone layer in the stratosphere protects the biosphere by absorbing harmful solar ultraviolet (UV) radiation. Downward transport of ozone from the stratosphere contributes to the ozone abundance in the troposphere, but ozone is also produced in the troposphere by sunlight driven chemical reaction cycles, involving NO_x , CO, CH_4 and other hydrocarbons. This can lead to excessive amounts of ozone near the surface ('summer smog'), which are toxic to ecosystem, animals and men. Ozone also acts as a greenhouse gas, with highest efficiency in the upper troposphere and lowermost stratosphere [Lacis *et al.*, 1990]. In this region, the emissions by subsonic aviation are an important source of nitrogen oxides, and locally enhance the photochemical production of ozone [e.g. IPCC, 1999; Valks *et al.*, 1999]. This aircraft induced ozone increase in the upper troposphere and lower stratosphere has a significant climate effect, with a positive radiative forcing of 0.02-0.05 W/m^2 [Brasseur *et al.*, 1998; IPCC, 1999]. The total increase of tropospheric ozone since pre-industrial times has led to a globally averaged positive radiative forcing of about 0.35 W/m^2 [IPCC, 2001; Hansen *et al.*, 1997].

1.2 Ozone in the stratosphere

About 90% of the atmospheric ozone is located in the stratosphere. This atmospheric region extends from the tropopause, at an altitude of ~12 km, up to the stratopause at 50 km. The formation of ozone in the stratosphere is initiated by the photolysis of molecular oxygen (O_2) (at wavelengths shorter than 242 nm) [Chapman, 1930]:



Ozone in the stratosphere absorbs solar UV radiation, which heats the stratosphere, resulting in an increase in temperature with increasing altitude and a strong stability. Most ozone is produced in the tropics, where the solar irradiance is highest. However, the highest ozone abundances are found at mid and high-latitudes (Figure 1.1), as a result of the poleward transport of ozone-rich air in the stratosphere by the Brewer-Dobson circulation [Brewer, 1949; Dobson, 1956].

The dramatic depletion of stratospheric ozone over Antarctica between August and November is caused by chemical destruction [Molina and Rowland, 1974; Farman *et al.*, 1985]. The anthropogenic emissions of chlorofluorocarbons over the past 40 years have resulted in a build-up of chlorine and bromine in the stratosphere. In the polar vortex during the Southern Hemisphere winter, the low temperatures lead to the formation of Polar Stratospheric Clouds (PSCs). The heterogeneous reactions on the surfaces of PSCs convert chlorine reservoir species (mainly ClONO_2 and HCl) into active chlorine. When the sun returns over Antarctica in the austral spring, the activated chlorine (Cl) catalytically destroys ozone:

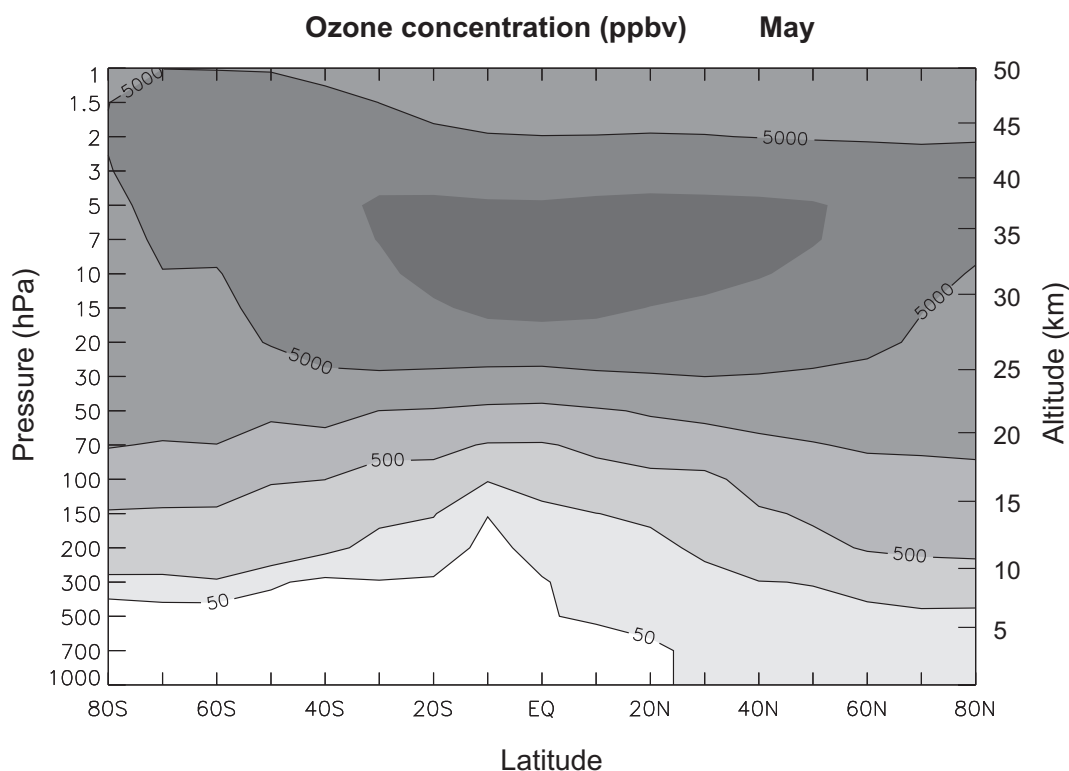


Figure 1.1 Zonal distribution of ozone for the month May (average over the years 1980-1991). The ozone concentration is given in parts per billion (ppb). Clearly visible is the ozone maximum in the stratosphere at ~ 10 hPa (30 km), with ozone concentrations > 8000 ppb. The highest ozone concentrations below 50 hPa (20 km) are found at mid- and high latitudes, as a result of the Brewer-Dobson circulation. The data are from the Fortuin and Kelder [1998] ozone climatology, which is based on ozonesonde and satellite measurements.



The ozone destruction becomes apparent by calculating the net result of reactions (1.3) – (1.5):



The largest ozone losses occur in the lower stratosphere, at altitudes between 10 and 20 km. The springtime ozone column over Antarctica decreased from about 320 Dobson Units (DU) before 1980 to less than 150 DU at present [Uchino *et al.*, 1999; WMO, 2003]*. Nowadays, the abundance of stratospheric chlorine is at its peak and is expected to decrease since the

* The column abundance of ozone is usually expressed in Dobson Units (DU). One DU corresponds to the height (in 10^{-3} cm) the column ozone would have if all the gas were at standard pressure and temperature. One DU is equivalent to a column of 2.687×10^{16} molecules cm^{-2} .

production of chlorofluorocarbons was drastically reduced and regulated by the Montreal Protocol (1987), and the subsequent amendments [WMO, 2003].

Because the Arctic does not get as cold as the Antarctic and the Arctic vortex is not as persistent, the ozone destruction in the Arctic has not been as large as in Antarctica. However, in cold Arctic winters losses up to 35% have been measured, as a result of the same mechanisms [Müller *et al.*, 1997; Rex *et al.*, 1997]. Ozone observations show a negative trend in the Arctic ozone abundance in spring since the late 1980s [Newman *et al.*, 1997; WMO, 2003].

A different low-ozone phenomenon is the ozone mini-holes that occur regularly throughout the mid-latitudes of both hemispheres [James, 1998; Newman *et al.*, 1988]. In contrast to the Antarctic ozone-hole, mini-holes are relatively short-lived events, mainly caused by dynamics in the upper troposphere and lower stratosphere. The most important mechanisms are the uplifting of the tropopause in tropospheric anti-cyclones, and the advection of ozone-poor air into the mini-hole region [McKenna *et al.*, 1989; Vaughan and Timmis, 1998; Teitelbaum *et al.*, 2001]. On average, the ozone abundance is reduced by about 10% in mini-holes. However, on some occasions the ozone amount above the Northern Hemisphere has been reduced by more than 30%, and the ozone value drops below 200 DU [Weber *et al.*, 2002]. Ozone mini-holes occur most frequent in the Northern Hemisphere at the end of the Atlantic and Pacific storm tracks, during the winter months December-March. The number of mini-hole events has increased since the begin of the 1980s and may account for up to a third of observed ozone trend in the mid-latitude winter and spring [Reid *et al.*, 2000].

Ozone depletion in the stratosphere results in enhanced levels of solar UV radiation at the Earth's surface. UV radiation has the potential to damage DNA in living cells, damages animal and human skin, increases the likelihood of especially skin cancer, damages eye cornea, effects the immune system and reduces plant growth. Most relevant to living organisms is the radiation in the UV-B (280-315 nm) and UV-A (315-400 nm) ranges. The biological effect of the solar radiation is generally expressed in terms of the UV-dose, taking into account the wavelength dependence of the sensitivity of a particular biological system to UV radiation, e.g. erythema induction (sunburn) [McKinlay and Diffey, 1987]. The Antarctic ozone hole resulted in strong increases in the UV-dose in the polar region of the Southern Hemisphere in October and November. A positive trend in the UV-dose is also found at the Northern mid-latitudes in winter and spring [WMO, 2003].

1.3 Observations of ozone from the ground

Measurements of the atmospheric gases form the basis of our knowledge of the atmosphere. The first regular measurements of surface ozone were already performed in the 19th century in Vienna, using potassium iodide papers (Schönbein method, see Lauscher [1984]), and in Montsouris, near Paris, by chemical analysis of collected air (method of Houzeau and Levy). Soon after the optical properties of ozone were discovered at the end of the 19th century, UV measurements were used to determine the total ozone column above the ground. This indirect spectroscopic method uses the fact that ozone absorbs solar radiation differently at specific

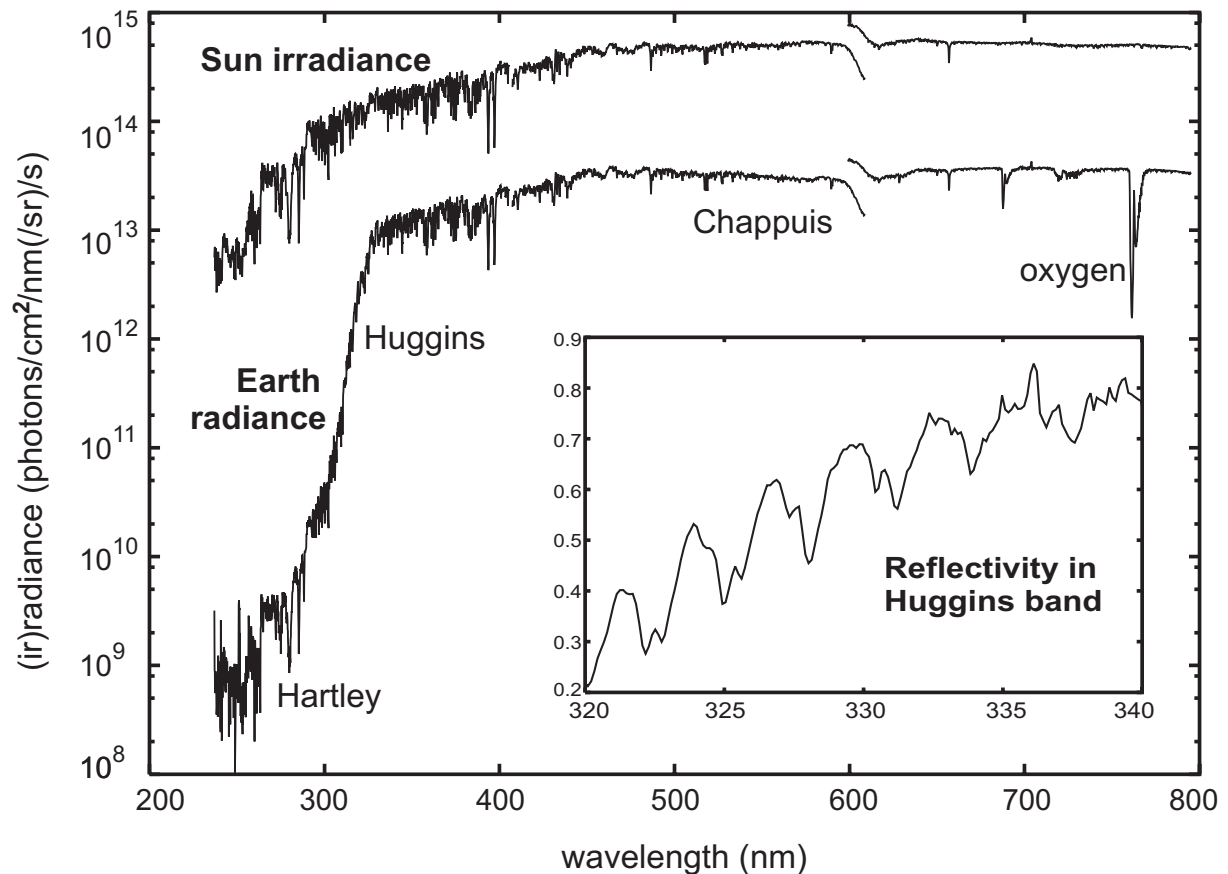


Figure 1.2 Extraterrestrial solar irradiance spectrum and Earthshine radiance spectrum for ultraviolet (UV), visible (VIS) and near-infrared (NIR) wavelengths. These spectra were measured by the Global Ozone Monitoring Experiment (GOME) on 1 May 1998. The UV ozone absorption is very strong in the Hartley band (<310 nm) and decreases at higher wavelengths in the Huggins band (310-350 nm). The visible Chappuis band shows weak ozone absorption features. The inset shows the reflectivity $R(\lambda)$ for the 320-340 nm region in the Huggins band, used for the DOAS ozone column retrieval.

wavelengths: the ozone absorption is very strong below 310 nm (Hartley band) and rapidly decreases at higher wavelengths in the Huggins band (310-350 nm), with little ozone absorption at 350 nm (Figure 1.2). By measuring the UV radiation at different wavelengths on the ground, information about the ozone abundance between the surface and the top of the atmosphere can be deduced.

Dobson [1930, 1968] developed a UV-spectrophotometer to measure ozone by its absorption features. The Dobson spectrometer measures direct or scattered sunlight at several wavelength pairs in the Huggins band, about 20 nm apart, at which the ozone absorption differs markedly. By using more than one pair of wavelengths, the ozone absorption can be separated from other effects, such as scattering by air molecules and aerosols, and the total ozone column above the instrument can be determined. The Dobson instrument forms the basis for the current global network of ground based measurement stations and has been in use since the 1930s. The Brewer spectrophotometer is based on the same principle as the Dobson instrument, and has been in use for 25 years. It also uses differential absorption in the

UV, and measures five narrow wavelength bands between 306 and 320 nm [Brewer, 1973]. The sensitivity of the Brewer instrument is better, which means that measurements can be made with lower sun. There are now more than 200 Brewer and Dobson instruments installed at different locations all over the world.

The most common method to measure the vertical distribution of ozone in the atmosphere (the ozone profile) is with a lightweight ozone measuring instrument carried aloft a small balloon. This ozonesonde is an electrochemical device that contains electrodes in a Potassium Iodine (KI) solution [Komhyr, 1967]. When ambient air is pumped through the cell, the ozone reacts with the KI solution and causes an electric current in the cell and provides a measure of the ozone concentration. Since the 1960s, two types of ozonesondes, the Brewer-Mast sonde and the electrochemical concentration cell (ECC), are used to measure the ozone profile in the atmosphere at over 100 stations in the world, usually one's a week. The Brewer-Mast and ECC sondes measure the ozone profile with a vertical resolution of 50-100 m, and usually reach altitudes of ~30 km. Measurements of the ozone profile can also be made from the ground by means of a differential absorption lidar using laser light, or by a microwave spectrometer. Lidar measurements have a vertical resolution of 1-2 km, and can reach altitudes around 50 km [e.g. McDermid *et al.*, 1990], while microwave measurements go to altitudes of ~80 km, with a resolution of 5-10 km [e.g. Parrish *et al.*, 1992].

Ground-based instruments provide accurate information about the ozone column or profile at a particular place. Although the number of measurements stations is quite large, the spatial coverage is still limited, especially in the developing countries in the (sub)tropics and the Southern Hemisphere, and over the oceans.

1.4 Satellite observations of ozone

Ozone measurements from satellites are essential to obtain a global coverage. Satellite instruments use a passive spectroscopic method to detect ozone. They measure the solar radiation scattered by the atmosphere and the Earth's surface, or the thermal infrared (IR) radiation emitted by the Earth's atmosphere in a nadir-viewing mode. Other satellite instruments measure the radiation from the Sun or a star that has travelled through the atmosphere in a limb-viewing mode. Regular global satellite measurements started at the end of the 1970s with the launch of the NIMBUS-7 satellite, carrying the Solar Backscatter Ultra-Violet (SBUV), Total Ozone Mapping Spectrometer (TOMS), Tiros Operational Vertical Sounder (TOVS), and Stratospheric Aerosol and Gas Experiment (SAGE) [Krueger *et al.*, 1980; Miller, 1989]. The TOMS instrument determines the ozone column by comparing the radiation scattered back from the atmosphere with the incident solar radiation at six wavelengths between 309 and 380 nm, at which the ozone absorption differs [Klenk *et al.*, 1982; McPeters *et al.*, 1998]. TOMS provides a global picture of the ozone distribution in one day and subsequent versions on different satellites are maintaining a (nearly) continuous dataset of ozone columns from 1978 until today. TOMS was the first instrument that provided a picture of the huge geographical extent of the Antarctic ozone hole [Farman *et al.*, 1985], and is invaluable for the determination of long-term trends in ozone [e.g. Stolarski *et al.*, 1991].

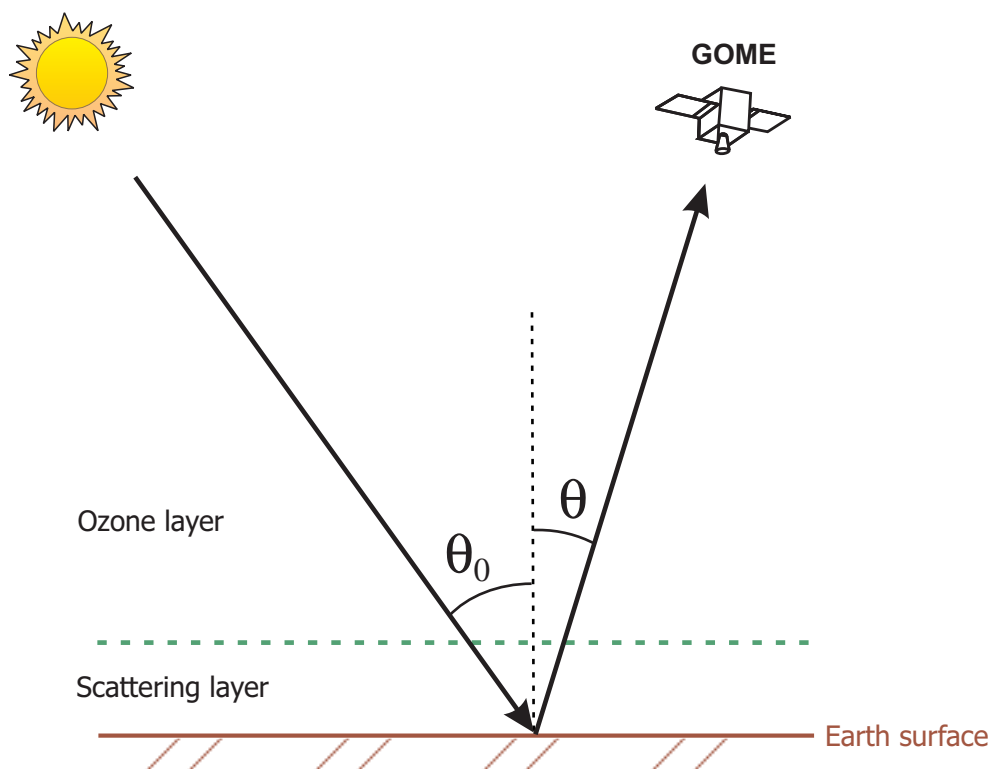


Figure 1.3 Schematic illustration of a light path through the atmosphere. The light travels through the ozone absorption layer and is scattered back to GOME by air molecules, aerosols or the surface. The solar zenith angle is θ_0 and the GOME viewing zenith angle is θ .

The Global Ozone Monitoring Experiment (GOME), launched on the ERS-2 satellite in April 1995, measures the Earth's radiance spectrum contiguously as a function of wavelength. GOME is a nadir-viewing spectrometer and measures the radiance from 240 to 790 nm, i.e. from the Hartley-UV band to near infrared wavelengths, with a spectral resolution of 0.2 to 0.4 nm [Burrows *et al.*, 1999a] (Figure 1.2). Although the emphasis of GOME is on ozone, the contiguous spectral measurements provide the possibility to derive abundances of other important trace gases, such as nitrogen dioxide (NO_2), formaldehyde (HCHO), sulphur dioxide (SO_2), bromine oxide (BrO), and the chlorine specie OCIO [e.g. Richter and Burrows, 2002; Wagner and Platt, 1998; Eisinger and Burrows, 1998]. Like ozone, these gases have specific absorption features in the UV. However, the concentrations of these trace gases in the atmosphere are much smaller than that of ozone, and measurements at many wavelengths are needed to detect their spectral signatures.

A retrieval process to determine the abundance of ozone (and other trace gases) that makes use of the contiguous spectral measurements of GOME is the Differential Optical Absorption Spectroscopy (DOAS) method [Platt, 1994]. This method has been in use for more than 25 years to measure abundances of ozone, NO_2 , formaldehyde and other trace gases from the ground [e.g. Noxon, 1975; Platt *et al.*, 1979], but the launch of GOME made it possible to use the DOAS method from space. The DOAS retrieval technique for GOME is described in the next section.

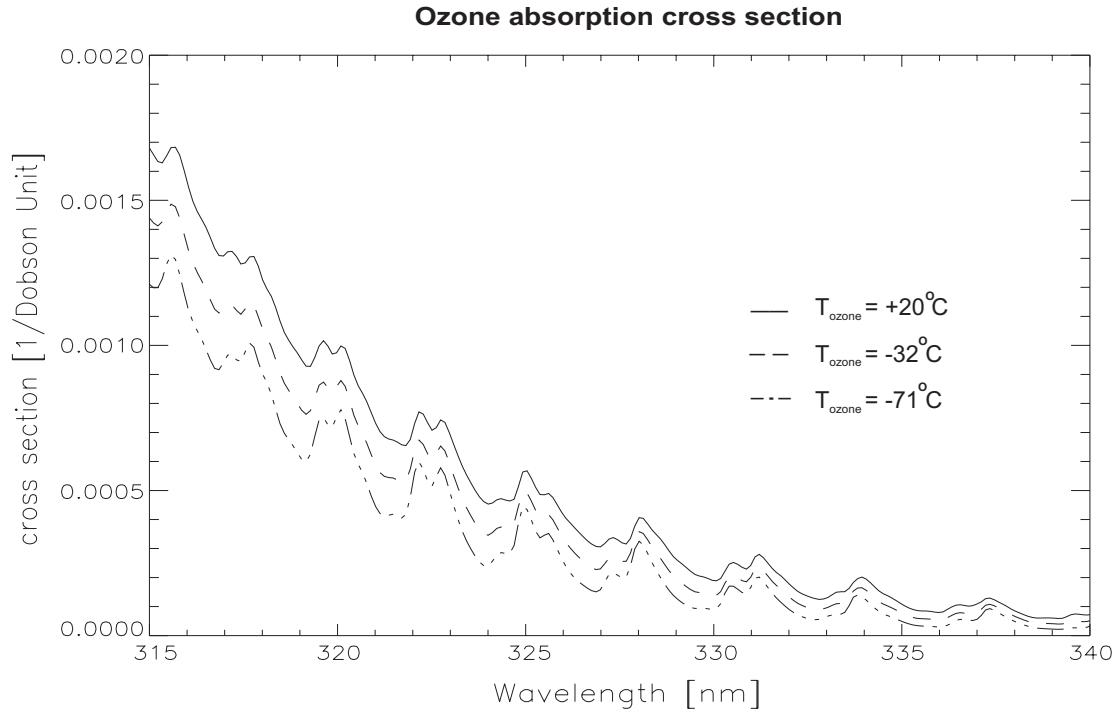


Figure 1.4 Ozone absorption cross-sections in the Huggins band for three atmospheric temperatures. The data are from Burrows et al. [1999b].

1.5 The DOAS retrieval method

The GOME instrument measures the radiance backscattered from the atmosphere and reflected by the Earth's surface in the nadir direction, with a maximum viewing angle of 32° w.r.t. nadir (Figure 1.3). To a first approximation, the scattering and ozone absorption processes are separated for this solar and viewing geometry. Most of scattering occurs in the lower part of the atmosphere (0-7 km), because this layer contains about 80% of the air molecules of the atmosphere. Since about 90% of the ozone is located in the stratosphere, most ozone absorption takes place above this scattering layer.

The Earthshine radiance $I(\lambda)$ measured by GOME contains spectral features of the absorption by ozone (and other trace gases). The relative depth of these absorption bands is related to the abundance of ozone in the atmosphere. To isolate the atmospheric signal, the reflectivity $R(\lambda)$ is calculated by dividing the measured Earthshine radiance by the extraterrestrial solar spectrum (which is regularly measured by GOME):

$$R(\lambda) = \frac{I(\lambda)}{\mu_0 F_0(\lambda)} \quad (1.7)$$

where μ_0 is the cosine of the solar zenith angle, and $\pi F_0(\lambda)$ is the solar irradiance perpendicular to the solar beam (Figure 1.2). The variation of the absorption by ozone with wavelength is given by the absorption cross-section $\sigma(\lambda)$, which is a molecular property of ozone (Figure 1.4). The spectral features of the ozone cross-sections in the wavelength region

325-337 nm are most useful for DOAS retrieval of ozone [Diebel *et al.*, 1995]. In the simple case of Figure 1.3, with the absorption layer on top of the scattering layer, the reflectivity can be expressed in terms of the Lambert-Beer law:

$$R(\lambda) = R_0(\lambda)e^{-\sigma(\lambda) \cdot N_s} \quad (1.8)$$

where $R_0(\lambda)$ is the reflectivity of the atmosphere in the absence of ozone. $R_0(\lambda)$ varies smoothly as a function of wavelength, due to scattering by air molecules, reflectance by the surface and aerosol scattering and absorption. N_s is referred to as the ozone slant column density, which is the number of ozone molecules along the light path through the atmosphere (per unit area). In the basic DOAS method, the ozone slant column is determined by fitting the logarithm of the GOME reflectivity spectrum to the ozone absorption cross sections, using linear regression. The smoothly varying $R_0(\lambda)$ is filtered out with a low-order polynomial in wavelength.

Figure 1.5 shows an example of a DOAS fit in the wavelength region 325-337 nm. The difference between the measured and fitted spectra in Figure 1.5 is mainly due to the effect of inelastic Raman scattering, which is called Ring effect [Grainger and Ring, 1962]. Inelastic Raman scattering causes a filling-in of solar Fraunhofer lines in the Earthshine spectrum and a filling-in of ozone absorption features. For an accurate retrieval of the ozone slant column, inelastic Raman scattering needs to be accounted for in the DOAS fit. Another complication in the DOAS fit is the dependence of the ozone cross-section on the atmospheric temperature (see Figure 1.4). One way to deal with this is to determine an effective (representative) temperature for the ozone cross-section, using temperature data from Numerical Weather Prediction (NWP) models.

A main advantage of DOAS fitting is that knowledge about the surface reflection, aerosol and cloud properties is not required. Another advantage of the DOAS method is that it is insensitive to (non-additive) radiometric calibration errors of the measured GOME spectra, as long as they vary only slowly over the fitting window.

To determine the vertical ozone column N_v , the ozone slant column is dividing by the so-called air mass factor M :

$$N_v = \frac{N_s}{M} \quad (1.9)$$

In the simply case of Figure 1.3, the air mass factor is given by the ratio of the light path length through the absorbing layer, L , and the thickness of the absorbing layer, H , and is called the geometrical air mass factor:

$$M_{geo} = \frac{L}{H} = \frac{1}{\mu_0} + \frac{1}{\mu} \quad (1.10)$$

where μ is the cosine of the GOME viewing zenith angle.

The assumption of a separated absorption and scattering layer (Figure 1.3), and the use of a geometrical air mass factor, result in reasonably accurate ozone columns for small solar- and

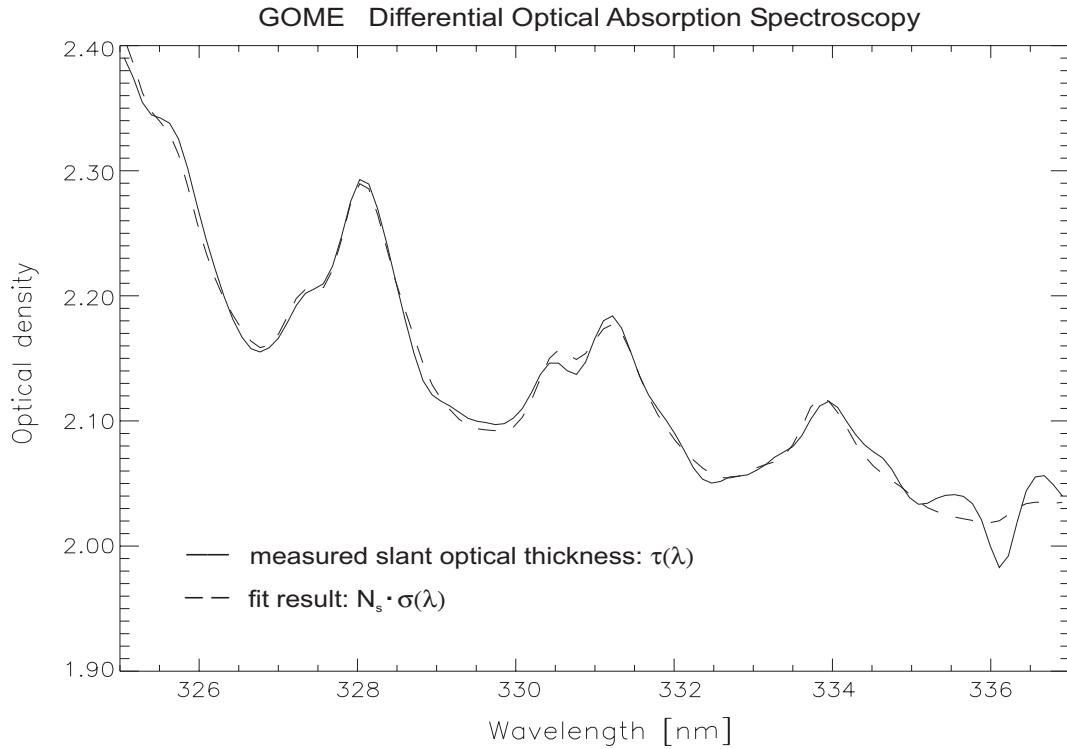


Figure 1.5 DOAS method applied to a GOME reflectivity measurement of 16 June 1996, for the wavelength region 325–337 nm. The measured slant optical thickness $\tau(\lambda) = -\ln\{R(\lambda)\}$ is plotted, together with the fitted slant column N_s ($=891$ DU), multiplied by the ozone absorption cross-section $\sigma(\lambda)$. In this DOAS fit example, no correction was made for inelastic Raman scattering, resulting in differences between the measured and fitted spectra, especially around 336 nm.

viewing zenith angles. However, in the real atmosphere, the ozone molecules and the scattering particles are mixed, and the real air mass factor differs from the geometrical air mass factor, especially for larger solar zenith angles. Therefore, radiative transfer theory is used to calculate the air mass factor for different model atmospheres. A common method is to calculate the ratio R/R_0 with a radiative transfer model, for a wavelength that is representative for the DOAS fitting window [Burrows *et al.*, 1999a]. The air mass factor can then be derived using Eq. (1.8):

$$M = \frac{-\ln(R/R_0)}{\sigma \cdot N_v} \quad (1.11)$$

where the vertical ozone column N_v is now known from the model atmosphere, and it is assumed that the air mass factor does not depend on the wavelength and the ozone column. Usually the air mass factors are not computed on-line for each measured GOME spectrum, but a look-up table approach is used. The air mass factors are pre-calculated with a radiative transfer model for various model atmospheres, surface albedos and different solar and

viewing geometries, and are stored in a look-up table. In this thesis, the Doubling-Adding-KNMI (DAK) radiative transfer model [De Haan *et al.*, 1987] has been used to calculate the air mass factor look-up table.

The DOAS retrieval is more complicated in the presence of clouds, since GOME can only detect ozone above the clouds. The amount of ozone below the cloud is called the ghost vertical column, and is derived from an ozone profile climatology. Clouds are treated as elevated bright reflecting surfaces, and the cloud-fraction and cloud-top pressure are needed to determine the ghost vertical column and the air mass factor. The cloud-fraction and cloud-top pressure are retrieved with the Fast Retrieval Scheme for Cloud Observables (FRESCO) algorithm, using the GOME reflectivities at a few wavelengths in the oxygen absorption A-band (758-766 nm) [Koelemeijer *et al.*, 2001, 2002].

Since on-line radiative transfer calculations are not needed, the DOAS fitting is a very fast retrieval method. With the DOAS method, it is possible to retrieve ozone columns from GOME spectra in near real-time, i.e. within 3 hours after sensing. Near real-time ozone data are important for various applications, such as the assimilation of ozone in Numerical Weather Prediction (NWP) models [Stoffelen and Eskes, 1999; Struthers *et al.*, 2002], for monitoring the status of the ozone layer, and improving surface UV radiation forecasts [WMO, 2003].

As already mentioned, satellite ozone data is invaluable for the determination of long-term trends in ozone [e.g. WMO, 2003]. Although trend studies do usually not require near real-time data availability, they do require accurate ozone columns. For the ozone trend studies of the World Meteorological Organization (WMO), the satellite instruments should be able to detect a change of 1% in the ozone column over a period of 10 years [WMO, 2003]. The accuracy and calibration of the instruments is of particular importance when ozone data from two (or more) different instruments are merged, in order to construct a continuous time record. For example, GOME ozone columns can be used to bridge the 1995-1996 gap in the long time record of TOMS total ozone.

1.6 Ozone in the tropical troposphere

The tropics encompass approximately the geographical area between the tropic of Cancer and the tropic of Capricorn ($\sim 23^{\circ}\text{N} - 23^{\circ}\text{S}$). The tropical atmosphere covers about 60% of the Earth's atmosphere by volume. Probably the most characteristic meteorological feature of the tropics is the Inter Tropical Convergence Zone (ITCZ). The ITCZ is a zonally oriented band of deep convective clouds that migrates between the winter and summer solstice with the sun. The convective systems in the ITCZ are caused by convergence of air near the surface by the trade winds, in combination with a strong heating of the surface.

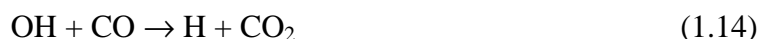
Ozone in the tropical troposphere plays various important roles. The intense UV radiation and high humidity in the tropics stimulate the formation of the hydroxyl radical (OH) by the photolysis of ozone (at wavelengths shorter than 315 nm):



OH is the most important oxidant in the troposphere because it reacts with virtually all trace gases, such as CO, CH₄ and other hydrocarbons. Since OH limits the residence time of many atmospheric pollutants, it is sometimes called the ‘cleaning agent’ of the atmosphere.

The tropopause, which separates the troposphere from the stratosphere, is higher (~17 km) and colder in the tropics, than at mid- and high latitudes. Since the radiative forcing by ozone is directly proportional to the temperature contrast between the radiation absorbed and the radiation emitted, ozone is most efficient as a greenhouse gas in the cold tropical upper troposphere [Lacis *et al.*, 1990; IPCC, 2001].

The tropics are also characterized by large emissions of nitrogen oxides (NO_x), carbon monoxide (CO) and hydrocarbons, both from natural and anthropogenic sources. Ozone that is formed over regions where large amounts of these ozone precursors are emitted, can be transported over great distances and affects areas far from the source [e.g. Thompson *et al.*, 2001]. The chemical production of ozone can be illustrated by the sunlight driven reaction cycle of NO_x and CO. First, CO is oxidized by the OH radical, leading to the formation of the peroxy radical HO₂:



where *M* is either an oxygen or nitrogen molecule. In the presence of NO_x, the peroxy radicals react with NO leading to the formation of NO₂:



And ozone is formed after the photolysis of NO₂:



The ozone production becomes apparent by calculating the net result of reactions (1.14) – (1.18):



The CO molecule in this reaction cycle can be substituted by other ozone precursors, such as methane (CH₄) and formaldehyde (HCHO).

Natural emissions of non-methane hydrocarbons (NMHC) from tropical forest and savannas are very large, but rather uncertain. Estimates of the magnitude of the biogenic NMHC emissions indicate that over half of the total NMHC emissions are from natural sources [Guenther *et al.*, 1995]. Large amounts of NO_x are produced by lightning: between 2 and 20 Tg N yr⁻¹ globally, of which more than 70% in the tropics [e.g. Price *et al.*, 1997; Huntrieser *et al.*, 1998]. NO_x is also released by natural savannah burning and by the tropical soil. However, the most important source of ozone precursors are the anthropogenic emissions by biomass burnings [Hao *et al.*, 1990; Crutzen and Andreae, 1990]. Approximately 500

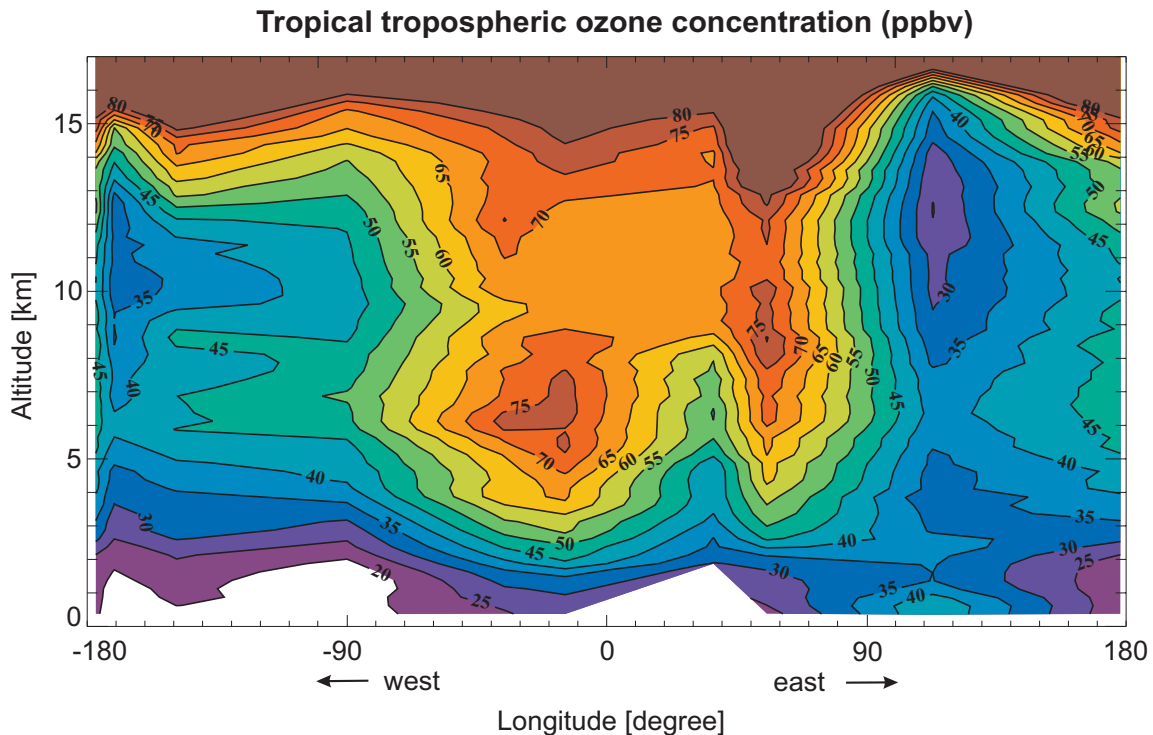


Figure 1.6 Tropospheric ozone distribution in the southern Tropics (0° – 20° S) for September – November, determined from ozonesonde observations in 1998–2000. The ozone concentration is given in parts per billion (ppb). Clearly visible are the enhanced ozone concentrations over the Atlantic and the low values over the Pacific. Reproduced from Thompson *et al.* [2003b].

million hectares of land are burned globally every year. Large amounts of ozone precursors, such as CO , NO_x , CH_4 and other hydrocarbons are released over Africa and South America during the so-called biomass burnings seasons. Most burnings during these dry periods occur for shifting cultivation, deforestation and clearing of agricultural waste. Recent emission estimates indicate that the amount of carbon released to the atmosphere is $3\text{--}4 \text{ Pg C yr}^{-1}$ [Hao and Liu, 1994; Van der Werf *et al.*, 2003]. The biomass burning seasons are usually well defined, with large-scale fires over southern Africa and South America in September and October and over northern Africa in December and January. However, there is also considerable inter-annual variability in the magnitude and location of the fires. For example, in 1997, tropical rainforests were burned in Indonesia and Brazil due to the extreme El Niño–Southern Oscillation (ENSO) conditions [Siebert *et al.*, 2001]. This resulted in ozone plumes that extended as far as India [Thompson *et al.*, 2001].

Observations of tropical tropospheric ozone are carried out by several ozonesonde sites, mainly in Southern Tropics. Since the start of the Southern Hemisphere Additional Ozone Sounding (SHADOZ) program in 1998, the number of tropical ozonesonde sites has increased considerably, with 11 sites on the Southern Hemisphere, and one site, Paramaribo, on the Northern Hemisphere [Thompson *et al.*, 2003a; Fortuin *et al.*, 2003; Peters *et al.*, 2002b]. The SHADOZ sites fill an important gap in the global monitoring network, and provide valuable information about the variability in tropical tropospheric ozone [Thompson *et al.*, 2003b]

(Figure 1.6). However, the spatial coverage of the tropical ozonesonde sites is still limited, especially on the Northern Hemisphere.

Satellite observations offer the possibility to measure the distribution of tropospheric ozone over large areas and to study its large-scale temporal and spatial variability. The first satellite pictures of the tropospheric ozone column in the tropics were produced by *Fishman et al.* [1990], and clearly showed enhanced ozone concentrations over the South Atlantic near the coast of Africa during the biomass burning season. Fishman et al. developed the concept of deriving a tropospheric ozone column with a residual method, by subtracting a stratospheric ozone column, measured by SAGE, from the total ozone column, measured by TOMS. More recent satellite studies used specific characteristics of the tropical atmosphere to distinguish tropospheric from stratospheric ozone [e.g. *Hudson and Thompson*, 1998; *Ziemke et al.*, 1998]. In the tropics, the tropospheric ozone column generally shows a maximum over the Atlantic Ocean and a minimum over the Pacific (Figure 1.6), while the stratospheric ozone column is nearly invariant with longitude [*Thompson et al.*, 2003a,b]. This ‘zonal wave one pattern’ in the tropical tropospheric ozone can be attributed to a complex interaction of biomass burning, lightning NO_x emissions and large-scale transport, [e.g. *Krishnamurti et al.*, 1993, 1996; *Thompson et al.*, 1996; *Chatfield et al.*, 1998; *Edwards et al.*, 2003].

In this thesis, the convective-cloud-differential (CCD) is used to determine the tropical tropospheric ozone column (TTOC) from satellite observations [*Ziemke et al.*, 1998; *Ziemke and Chandra*, 1999]. The CCD method uses total ozone measurements over highly reflecting, high-altitude clouds in the ITCZ to obtain an above-cloud stratospheric ozone amount. In certain regions, such as the tropical western Pacific, these bright clouds are mostly associated with strong convection and cloud tops in the upper troposphere. The TTOC is derived at cloud-free pixels by subtracting the stratospheric ozone amount from the total ozone column, assuming a zonally invariant stratospheric column.

1.7 Global chemistry transport models

Numerical models are useful tools to study the distribution of ozone and other trace gases in the tropics. Models can provide information about dynamical and chemical processes in the tropical atmosphere that cannot be easily measured. On the other hand, by comparing observed and modelled ozone fields, deficiencies in the model are recognized and shortcomings in the knowledge of atmospheric processes can be identified. Especially the comparison between satellite measurements and models can be useful, since the spatial scales of the satellite and model ozone fields are often comparable [e.g. *Peters et al.*, 2002a]. In a numerical model, all relevant atmospheric processes, the emissions and removal of trace gases and the chemical transformations in the atmosphere need to be integrated. Two types of models are commonly used: three-dimensional global chemistry models (CTMs) and global circulation models with chemistry (GCMs). Global circulation models solve the basic equations of motion, conservation of mass, and conservation of energy. Although GCMs are the most comprehensive, and are, for instance, able to calculate the climate effects of future greenhouse gas increases [e.g. *Sigmond et al.*, 2003], the high complexity and demand for computer resources reduce the flexibility.

Global chemistry models use prescribed meteorological fields, which reduces the required computer resources and increases the flexibility. CTMs give a good description of the observed state of the atmosphere, because they can use analysed meteorology of NWP models. In this thesis, the three-dimensional global chemistry model TM3 (Tracer Model version 3) is used to interpret the observed variability in the measured TTOC [Lelieveld and Dentener, 2000 and references therein; Van Velthoven and Kelder, 1996]. TM3 has a horizontal resolution of $2.5^\circ \times 2.5^\circ$, with 31 vertical layers and uses meteorological fields from the ECMWF operational weather model. The model has been employed in many atmospheric studies [e.g. Prather *et al.*, 2001; Jeuken *et al.*, 1999; Dentener *et al.*, 2003].

1.8 Thesis outline

The first topic of this thesis is the near real-time retrieval of total ozone columns from Global Ozone Monitoring Experiment (GOME) observations. This theme was instigated by the growing demand for global ozone observations and ozone forecasts from satellite instruments. For example, satellite ozone data are invaluable for monitoring the status of the ozone layer, e.g. during the development of the yearly Antarctic ozone hole, for ozone trend studies and for improving regional and global forecast of surface UV radiation. For some application, such as the assimilation of satellite ozone observations in Numerical Weather Prediction (NWP) models, the data can only be used if they are available in near real-time.

The important role of the tropical atmosphere and the new possibilities of GOME have initiated the second topic of this thesis: the variability in tropical tropospheric ozone. With the GOME instrument, it is possible to improve the existing convective-cloud-differential (CCD) method to derive a tropical tropospheric ozone column from satellite observations. Analysis of the GOME–TTOCs, with the aid of the TM3 model, helps to understand the tropical ozone distribution and the processes responsible for the variability in tropical tropospheric ozone.

In this thesis, the following questions are addressed:

1. *Can ozone columns be retrieved from GOME observations in near real-time, with the required quality for use in Numerical Weather Prediction models?*
2. *How well do the GOME ozone columns agree with ground-based observations, and can the accuracy of the GOME ozone columns be improved further?*
3. *What is the influence of low stratospheric temperature on observations of ozone mini-holes from the ground and from space?*
4. *Can the existing retrieval methods of tropospheric ozone columns in the tropics be improved with GOME observations?*
5. *How to interpret the observed variability of ozone in the tropical troposphere?*

In Chapter 2, the first two questions are addressed by presenting a Fast Delivery system for the retrieval of near real-time ozone columns from GOME data. With the DOAS retrieval technique, it is possible to have the ozone data available within 3 hours after the GOME observation. The quality of the near real-time satellite ozone data has been established by a pseudo-global validation with ground-based measurements. This chapter has been published in the *International Journal of Remote Sensing*, Vol. 24, in 2003 [Valks et al., 2003a].

The third question is addressed in Chapter 3. An ozone mini-hole with total ozone values less than 200 DU passed over north-western Europe on November 30, and December 1, 1999. The total ozone values were measured from the ground, with a Brewer Spectrophotometer at De Bilt and an ozonesonde, and from space with the GOME instrument. In this chapter, the ground-based and GOME measurements are described and the accuracy of the measurements are discussed. Since the recorded stratospheric temperatures were very low during this low-ozone event, the sensitivity of the retrieved ozone amount to the atmospheric temperature is of particular importance. This chapter has been published in *Geophysical Research Letters*, Vol. 27, in 2000 [Allaart et al., 2000]. The author contributed to the analysis of the GOME observations.

The last two questions are addressed in Chapter 4, where the variability in tropical tropospheric ozone has been analysed using GOME observations and the TM3 chemistry transport model. The CCD method to derive tropical tropospheric ozone columns (TTOC) from TOMS data [Ziemke et al., 1998; Ziemke and Chandra, 1999], has been improved by using GOME ozone columns and GOME cloud measurements. Monthly mean values of the tropospheric ozone columns below 200 hPa have been determined on a 2.5° latitude by 2.5° longitude grid between 20°N and 20°S. The GOME-TTOCs have been validated with ozonesonde measurements from the SHADOZ network, also including the site Paramaribo (6°N, 55°W) in the northern tropics. The GOME-TTOCs and the TM3 model have been used to untangle the intriguing relation of the South Atlantic TTOC maximum to biomass burning emissions, lightning NO_x emissions and large scale transport. The variability of the TTOC in the northern tropics has been examined as well. This chapter has been published in the *Journal of Geophysical Research*, Vol. 108, in 2003 [Valks et al., 2003b].

Chapter 5 focuses on the second question. The validation of the Fast Delivery (FD) ozone columns, as described in Chapter 2, has raised some issues for further improvements of the DOAS total ozone algorithm. The most important issue is the solar zenith angle and latitudinal dependence of the FD ozone columns. Therefore, an improved GOME total ozone algorithm called TOGOMI (Total Ozone algorithm for Gome using the OMI algorithm), has been developed. The new algorithm is based on the total ozone algorithm developed for the Ozone Monitoring Instrument (OMI), to be launched on EOS-Aura in 2004 [Veeffkind and de Haan, 2002; De Haan, 2003]. The main improvements of the new algorithm are: (1) a new DOAS fit-equation that accounts for inelastic scattering, (2) the use of an empirical DOAS method to account for the wavelength dependence of the air mass factor, and (3) the use of a slant column dependent air mass factor to account for atmospheric variability. In this Chapter, the improved DOAS algorithm is described, and the TOGOMI ozone columns are compared with the Fast Delivery ozone columns and with ground-based measurements. This chapter will be submitted for publication in a scientific journal.

Chapter 6 presents the main conclusions of this thesis and an outlook to further research.

Chapter 2

A Fast Delivery System for the retrieval of near-real time ozone columns from GOME data^{*}

Abstract

A Fast Delivery (FD) system has been developed to provide GOME total ozone columns within 3 hours after observation. This meets the growing demand for near-real time ozone products for applications as the assimilation of ozone in Numerical Weather Prediction (NWP) models, monitoring the status of the ozone layer and improving surface UV radiation forecasts. The FD system uses only a small part of the raw GOME data that are available in near-real time. The FD level 0-to-1 and level 1-to-2 processors are based on algorithms as used within the off-line ESA/DLR GOME Data Processor (GDP). However, several changes in the algorithms have been made to improve the retrieval of the ozone columns: (1) the use of effective ozone absorption cross-sections based on ECMWF temperature forecast in the ozone slant column fit, (2) the use of the DAK radiative transfer model and the Fortuin and Kelder ozone climatology for the air mass factor calculations and (3) the use of the FRESCO cloud algorithm. The accuracy of the FD ozone columns has been determined by a pseudo-global validation study involving ground-based total ozone observations from about 15 NDSC sites. There is a reasonable general agreement with the ground-based measurements (within 5% for low- and mid-latitudes, within -10 to +5% for high latitudes) and the level of quality meets the requirements for near-real time applications.

^{*}This chapter has been published as: P. J. M. Valks, A. J. M. Piters, J. C. Lambert, C. Zehner and H. Kelder, *Int. J. Remote Sensing*, Vol. 24, 423-436, 2003.

2.1 Introduction

There is a growing demand for global ozone measurements from satellite instruments for various purposes. For example, an interesting recent application is the assimilation of satellite ozone observations in Numerical Weather Prediction models. This is expected to give a better description of the stratospheric dynamics, the temperatures and the radiation and heating in the NWP model [Stoffelen and Eskes, 1999; Hólm, 2000 pers. comm.]. Satellite ozone data are also used for monitoring the status of the ozone layer (e.g. during the development of the yearly Antarctic ozone hole), and to improve – in combination with data assimilation - the regional and global forecasts of surface UV radiation (the derivation of surface UV from satellite measurements is described in Ziemke *et al.* [2000] and references therein). Another application is the use of satellite ozone data for planning and support of ground-based atmospheric (chemistry) experiments during measurement campaigns. Recent examples are the THESEO and SOLVE campaigns that took place in the 1999-2000 winter in the Arctic [Newman *et al.*, 2002]. For this kind of applications, satellite ozone observations are especially useful when they are available in near-real time (NRT), i.e. within 3 hours after observation. However, the usability of NRT satellite ozone data depends on the accuracy of the data and the accuracy requirements of the particular application. Therefore, it is necessary to establish the quality of NRT satellite ozone data by a validation with other (independent) ozone measurements.

In this paper, a Fast Delivery system is described which retrieves ozone columns in near-real time from radiation measurements by the Global Ozone Monitoring Experiment (GOME) onboard the European Space Agency's (ESA) Second European Remote Sensing (ERS-2) satellite. Because of the near-real time constraint, the FD system uses only a small part of the raw GOME data that are available in near-real time. Several aspects of the FD system are described. In the first part of the paper, an overview is given of the GOME instrument, the data transfer from the satellite to the FD system, and the operational processing of the raw GOME data. Since the near-real time constraint is an important facet of the FD system, the various time delays in the processing chain are explained as well. The second part of the paper focuses on the total ozone retrieval algorithm and the validation of the FD ozone columns. The retrieval algorithm consists of a conversion of the raw GOME data into calibrated reflectance spectra (level 0-to-1 processing) and the calculation of total ozone columns from the calibrated spectra (level 1-to-2 processing). To establish the quality of the ozone columns, the FD ozone columns have been validated with ground-based measurements. The results of this pseudo-global validation are described and the accuracy of the FD ozone columns is assessed. The paper ends with our concluding remarks.

2.2 The Fast Delivery system

2.2.1 GOME instrument

The GOME instrument is a passive four-channel spectrometer that measures the direct solar irradiance and the solar radiance reflected by the Earth's atmosphere and surface in the UV/VIS spectral range (240 to 790 nm). GOME scans the Earth's surface in the nadir direction (across-track scan angle 32°) with a spatial resolution of 40 x 320 km² and a global coverage within 3 days. Total ozone columns are retrieved from the ratio of the Earthshine and Sunshine spectra, utilising the characteristic ozone spectral absorption features in a part of the Huggins ozone absorption band (325 to 335 nm) [ESA, 1995; Burrows *et al.*, 1999a].

2.2.2 Data transport

The raw GOME science data, containing the readouts of the detector array for every 1.5 seconds GOME measurement, is stored on-board on tape recorders. During periods of ground station visibility, typically once every orbit (100 minutes), the recorded data is downlinked to one of the four ESA ground stations. The main ground station at Kiruna in Sweden receives the data from 10 out of 14 orbits; the data from the other four orbits are transmitted to the ground stations Gatineau, Prince Albert (both in Canada) and Maspalomas (Spain). At the ground stations, the raw GOME science data, the orbit information and the instrument housekeeping data are extracted in so-called EGOC products. Each EGOC product contains the data for one (1.5 seconds) GOME measurement (8484 bytes). Over a 24-hour period, about 57,600 EGOC products are generated, giving a total daily data volume of 488 Mbytes. The EGOCs are put on tapes and sent to the ESA Processing and Archiving Facility (D-PAF) at DLR in Oberpfaffenhofen, Germany, for further processing.

This process of data collection at the ground-stations, physical transport of tapes and processing of the raw data to ozone column values at D-PAF takes several days. To be able to retrieve ozone columns in near-real time, the so-called Extracted GOME Instrument Header (EGOI) data are used. EGOIs are created at the ESA ground-stations from the downlinked satellite data in a similar way as EGOCs and contain orbit information, instrument housekeeping data and samples of the raw science data. These samples contain parts of the readouts of the detector arrays in the spectral range 272 to 777 nm for every GOME measurement. About 15% (1284 bytes) of the total amount of raw data is put in an EGOI. Normally three to four EGOI files are generated for each orbit and about 1300 GOME measurements are grouped in one EGOI file. After creation at the ground stations, the EGOI files are sent to ESA's data exploitation centre (ESRIN) in Frascati, Italy, via direct ground link. At ESRIN they are mainly used for instrument monitoring purposes. The EGOI files are also transferred to the FD system at KNMI (by Internet/FTP), where they are used for the retrieval of the total ozone columns.

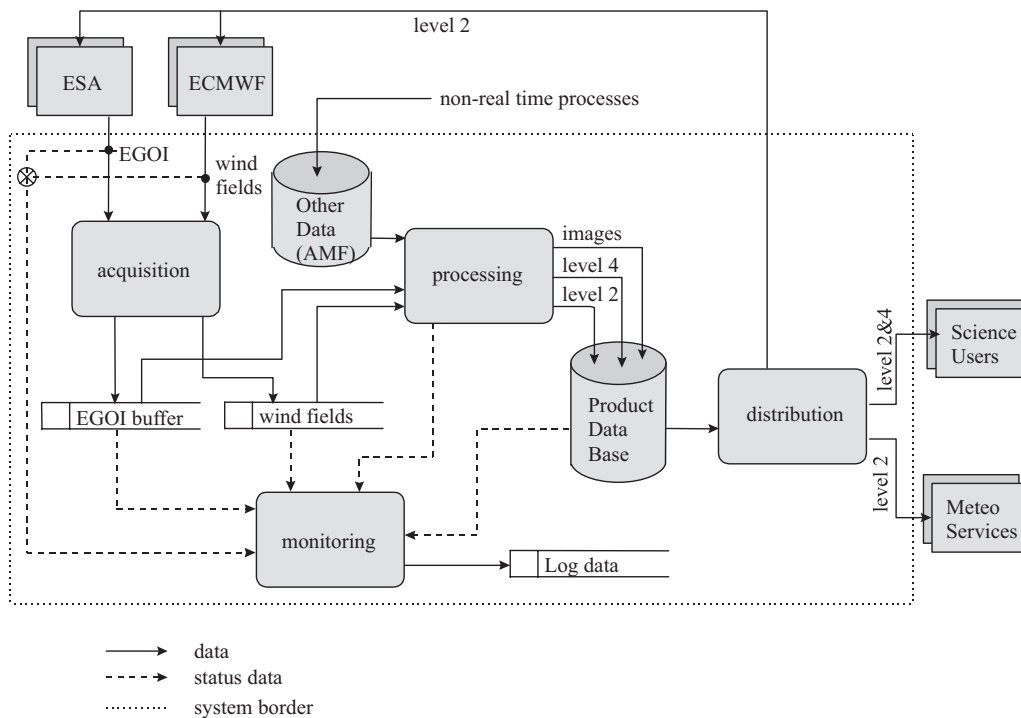


Figure 2.1 The Fast Delivery system performs the following three functions: acquisition, processing, distribution and monitoring (see text). The input and output for these functions and their place in the system are shown in the flow chart.

2.2.3 Operational Environment

The FD system performs the following three main functions: data acquisition, data processing and data distribution. The input and output for these functions and their place in the system are shown in Figure 2.1. The acquisition function takes care of the (Internet/FTP) transport of EGOI files from ESA/ESRIN to the processing environment at KNMI. The processing function consists of a level 0-1 processor, a level 1-2 processor and a level 2-4 processor. The EGOI files and auxiliary data (stored within the processing environment) are input for the level 0-1 processor. The output of the level 0-1 processor (calibrated reflectance) is input for the level 1-2 processor (together with auxiliary data). The output of the level 1-2 processor are level 2 data files containing geo-locations, observation times and ozone vertical columns with uncertainties. The level 0-1 and 1-2 processors are described in more detail in the next section. In the level 2-to-4 processing, the ozone columns are assimilated in a three-dimensional tracer transport model and a (level 4) global ozone field is calculated [Jeuken *et al.*, 1999; Eskes *et al.*, 2001]. The performance of the data acquisition and processing functions is checked by a monitoring function. At the end, the distribution function takes care of the distribution of the level 2 and 4 data to the end-users (by Internet/FTP) and to the Fast Delivery Internet/WWW site, where they are made available for the general public.

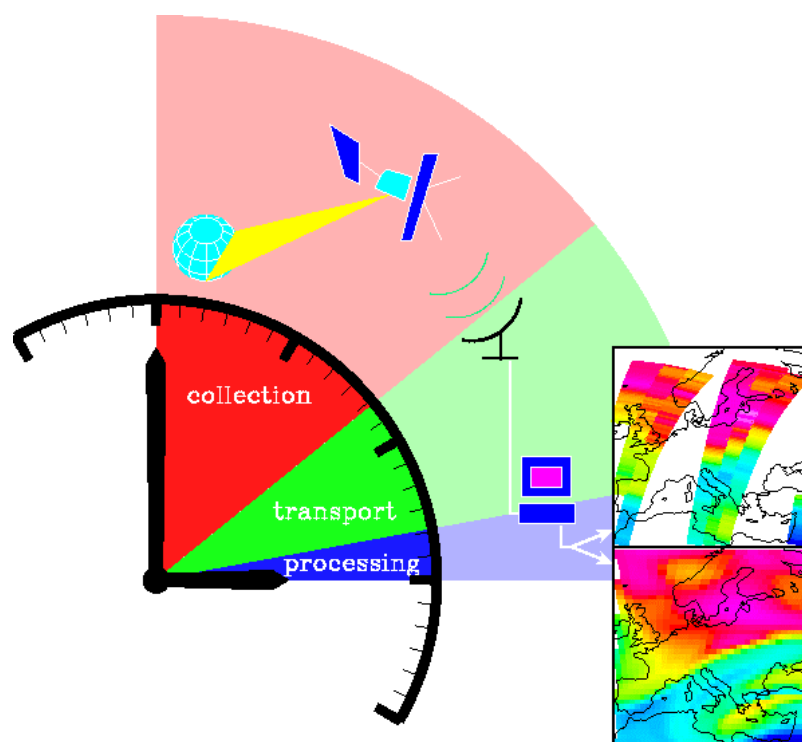


Figure 2.2 Raw GOME data is downlinked to the ESA ground stations once every orbit, resulting in a time delay between the GOME observation and the reception at the ground station of 100 minutes at maximum. The collection of the raw data at the ground-stations, the creation of the EGOI files and the transfer of these files to KNMI, via ESRIN, takes about 75 min. The processing of the EGOI data to level 2 ozone columns and the distribution of the level 2 data to the end-users only takes a few minutes.

2.2.4 Time delays

The near-real time constraint is an important aspect of the FD system, which means that the period between the actual GOME measurement and the delivery of the total ozone columns to the end-users must be less than 3 hours. The time delays in the data transport and processing chain is visualised in Figure 2.2. Since the raw GOME data are downlinked to the ESA ground stations ones every orbit, the time delay between the GOME observation and the reception at the ground station can be 100 minutes at maximum. The collection of the raw data at the ground-stations, the creation of the EGOI files and the transfer of these files to KNMI, via ESRIN, takes about 75 min. The processing of the EGOI data to the level-2 ozone data and the distribution of the level 2 data to the end-users takes only a few minutes. Generally more than 93% of the ozone columns are available and distributed to the end-users within 3 hours after observation. Figure 2.3 shows an example of the retrieved ozone columns for a single day (30 November 1999).

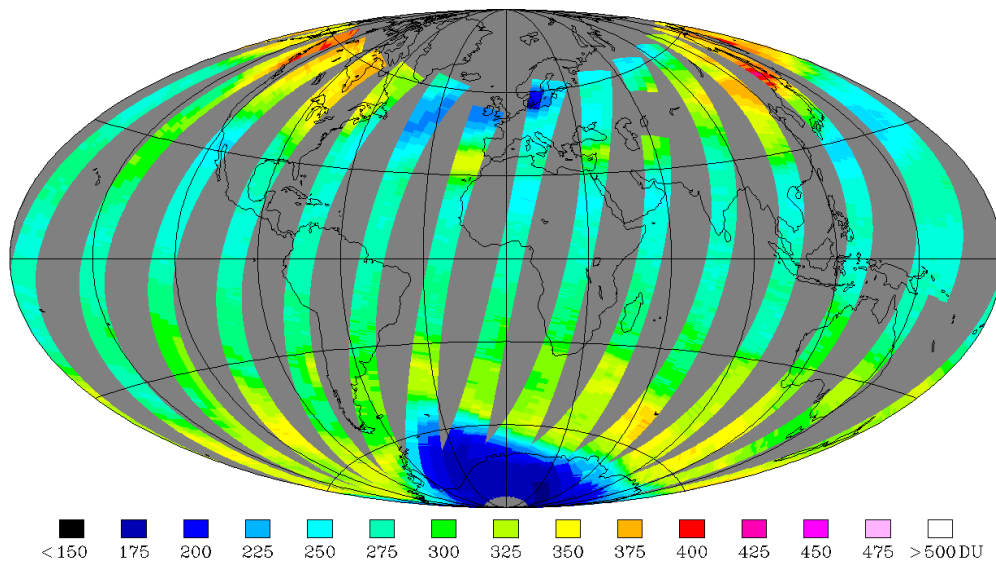


Figure 2.3 Fast Delivery total ozone columns for 30 November, 1999. Clearly visible are the very low ozone values above Europe and the remainder of the Antarctic ozone hole.

2.3 Total ozone retrieval algorithm

The retrieval of total ozone columns from the raw GOME data is done in two steps. In the level 0-to-1 processing, the readouts of the detector array are converted to calibrated reflectance spectra and in the level 1-to-2 processing the total ozone columns are retrieved from the calibrated spectra. The level 0-to-1 and level 1-to-2 processors used in the Fast Delivery system are based on the off-line ESA/DLR GOME Data Processor (GDP), operated by the D-PAF at DLR [Spurr *et al.*, 2002; Aberle *et al.*, 2002]. However, there are several important differences between the FD and off-line GDP processors. In this section, an overview of the FD level 0-1 and level 1-2 processors is given and the main differences between the FD and off-line level 1-2 processors are explained.

2.3.1 Level 0-1 processor

The level 0-to-1 processing consists of two parts: a radiometric calibration and a wavelength calibration. In the radiometric calibration, the raw detector signals are corrected for leakage current, straylight, Peltier noise and the pixel-to-pixel variability. In addition, a polarisation correction is carried out because the optics of the instrument are sensitive to the polarisation of the Earthshine radiation [Schutgens and Stammes, 2002]. Finally, a wavelength calibration is performed on the Earthshine and Sunshine spectra by using a high-resolution reference solar spectrum [Caspar and Chance, 1997], and the reflectance spectra (ratio of the Earthshine and Sunshine spectra) are calculated. A more detailed description of the FD level 0-1 processor and the differences with the off-line GDP processor can be found in Piters *et al.* [2001].

2.3.2 Level 1-2 processor

The first step in the retrieval of the total ozone column from the calibrated reflectance spectra is the calculation of the ozone slant column density. This is the total amount of ozone per cm^2 along the average optical path through the atmosphere and is determined by the Differential Optical Absorption Spectroscopy (DOAS) method [Platt, 1994]. The DOAS algorithm used in the FD processor consists of a least squares fitting of the ozone absorption cross-section, a Ring spectrum and a third order polynomial, to the ratio of the measured Earthshine and Sunshine spectra:

$$\tau(\lambda) = N_s \cdot \sigma_{\text{O}_3}(\lambda) + c_{\text{ring}} \cdot \sigma_{\text{ring}}(\lambda) + P_3(\lambda) \quad (2.1)$$

where $\tau(\lambda)$ denotes the slant optical thickness: $\tau(\lambda) = -\ln[I_e(\lambda)/I_s(\lambda)]$, with $I_e(\lambda)$ the Earthshine spectrum and $I_s(\lambda)$ the Sunshine spectrum. The wavelength λ ranges from 325 to 335 nm, where $\tau(\lambda)$ shows characteristic ozone absorption features of the Huggins band. N_s is the slant column density and $\sigma_{\text{O}_3}(\lambda)$ is the ozone absorption cross-section. To account for the Ring effect (the filling-in of solar Fraunhofer lines in the earthshine spectrum), a theoretical Ring spectrum $\sigma_{\text{ring}}(\lambda)$, convolved with the GOME slit function, is included in the fit [Chance and Spurr, 1997]. $P_3(\lambda)$ is a third order polynomial that is subtracted from the slant optical thickness to remove the slowly varying spectral structures resulting from Rayleigh and aerosol scattering and reflections at the ground surface.

The use of accurate ozone absorption cross-sections and the handling of the temperature dependence of the ozone cross-sections in the DOAS algorithm are very important for an accurate determination of the ozone slant column density. In the FD processor, the GOME Flight-Model (FM) ozone absorption cross-sections are used, which were measured prior to launch with the GOME spectrometer [Burrows *et al.*, 1999b]. To account for the temperature dependence, an effective ozone absorption cross-section is calculated daily, using the 24-hour temperature forecast from the ECMWF model:

$$\sigma_{\text{O}_3, \text{eff}}(\lambda) = \frac{\int \rho(z) \cdot \sigma_{\text{O}_3}(T(z), \lambda) \cdot dz}{\int \rho(z) \cdot dz} \quad (2.2)$$

where $\rho(z)$ is the ozone concentration at altitude z , here determined from an ozone profile climatology from Fortuin and Kelder [1998], and $\int \rho(z) \cdot dz$ is the corresponding vertical ozone column. $T(z)$ is the ECMWF temperature at altitude z (the new ECMWF model provides temperatures for 60 vertical levels with equally-distributed levels in the middle stratosphere with 1.5 km spacing, as described by Untch and Simmons [1998]), and $\sigma_{\text{O}_3}(T(z), \lambda)$ is the temperature dependent ozone absorption cross-section. The resulting effective cross-section $\sigma_{\text{O}_3, \text{eff}}(\lambda)$ is used in Eq. (2.1) to calculate the ozone slant column density. To account for spectral calibration errors in the GOME-FM ozone absorption cross-

sections, a wavelength shift is applied on the cross-sections. The value of the wavelength shift is allowed to vary in the fitting. Information on the quality of the fit is derived from the variance in the ozone slant column density. The estimated uncertainty in the ozone slant column density mostly falls within the 1% to 2.5% range.

In order to determine the ozone column accurately, the cloud fraction and cloud top pressure need to be determined. Furthermore, GOME can only measure the ozone column above the cloud top. To provide the end-users a total ozone column in the presence of clouds, a climatological ozone column below the cloud top (the so-called ghost vertical column) is added to the retrieved ozone column. In the FD processor, the cloud fraction and cloud top pressure are retrieved with the Fast Retrieval Scheme for Cloud Observables (FRESCO) algorithm [Koelemeijer *et al.*, 2001], using the reflectivities in a part of the oxygen absorption A-band (758-766 nm).

To convert the ozone slant column density into a vertical ozone column, the air mass factor is needed. Air mass factors are calculated with a radiative transfer model and contain the scattering and absorption processes that define the average optical path of photons in the atmosphere. For the FD processor, the air mass factors have been calculated with a pseudo-spherical version of the Doubling Adding model DAK [De Haan *et al.*, 1987]. A look-up table has been generated for different viewing scenarios (solar and satellite viewing angles), surface heights and albedos, and ozone- and temperature profiles. The dependence of the air mass factor on the ozone profile is of particular importance (as presented in the last section of this paper). For the air mass factor calculations in the FD processor, ozone profiles from the Fortuin and Kelder [1998] climatology are used. This climatology includes monthly ozone profiles for 10° latitude bands, determined from ground-based and satellite ozone profile measurements. The air mass factor is obtained by interpolation of the look-up table, with the solar and viewing angles taken from the level-1 data and the surface parameters from a monthly climatology. For the interpolation between the climatological ozone profiles, the latitude and time corresponding to the GOME measurement are used.

An additional complication is that in the DOAS spectral fitting window (325-335 nm), the air mass factor is wavelength dependent [Marquard *et al.*, 2000]. In the standard DOAS retrieval method, as used in the FD processor, the wavelength dependence is neglected and only one air mass factor is used. By calculating the air mass factor at 325 nm, where the ozone absorption is largest, the error due to this approximation is minimised [Burrows *et al.*, 1999a].

In the last step, the vertical ozone column is calculated. For cloud-free situations, the vertical ozone column N_v can simply be calculated by dividing the slant column density by the appropriate air mass factor ($N_v = N_s / M$). However, in the presence of clouds, two air mass factors are needed: one down to the ground surface (M_{clear}) and one down to the cloud top (M_{cloudy}). The latter is obtained from the air mass factor look-up table, using the determined cloud top height and a cloud albedo of 0.8, which corresponds to a highly reflecting cloud [Koelemeijer *et al.*, 2001]. The vertical ozone column is then given by:

$$N_v = \frac{N_s + f \cdot N_g \cdot M_{cloudy}}{M} \quad (2.3)$$

where the total air mass factor M is given by: $M = f \cdot M_{cloudy} + (1-f)M_{clear}$. The ghost vertical column N_g is determined by integrating the appropriate climatological *Fortuin and Kelder* [1998] ozone profile from the surface to the cloud top pressure. The cloud fraction f and the cloud top pressure have been determined with the FRESCO cloud algorithm.

2.3.3 FD versus off-line GDP ozone columns

As already noted, the level 1-to-2 algorithms of the current FD processor (version 3) and off-line ESA/DLR GOME Data Processor (version 2.7) are quite similar: both processors use the DOAS retrieval method. However, there are several important differences between the two processors. The main modifications applied in the FD level 1-2 processor are: (1) the use of an effective ozone absorption cross-section based on ECMWF temperature forecasts in the slant column fit, (2) the use of a pseudo-spherical version of the DAK radiative transfer model and the use of the *Fortuin and Kelder* [1998] ozone climatology for the air mass factor calculations and (3) the use of the FRESCO cloud algorithm. Due to these modifications, the FD and GDP ozone columns differ considerably. As illustrated in Figure 2.4, differences range from less than 1% to more than 10%, depending on location, cloud cover condition, solar zenith angle and season. It is therefore necessary to establish the quality of the FD ozone columns by validation with ground-based ozone measurements. The results of this validation are described in the next section.

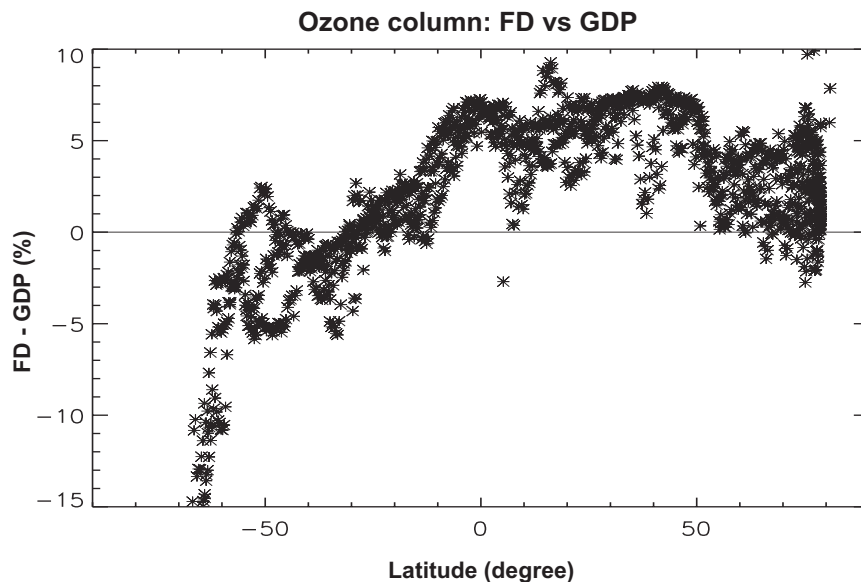


Figure 2.4 Relative difference between the FD (version 3) and off-line GDP (version 2.7) ozone columns for three GOME orbits of 16 August 1998.

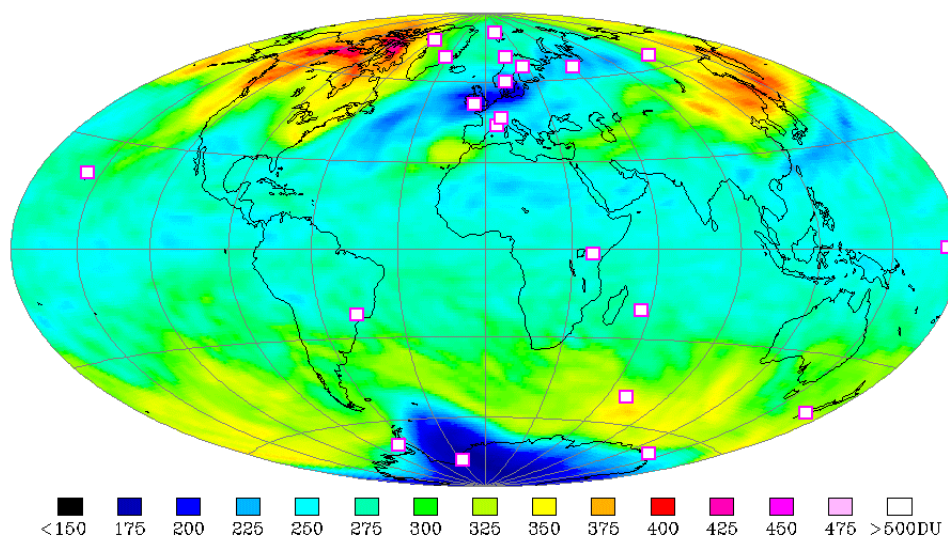


Figure 2.5 Locations of the ground-based measurement sites used for the validation of the FD ozone columns. This pseudo-global validation relies on comparisons with correlative ground-based measurements from about 15 zenith-sky UV-visible spectrometers affiliated with the NDSC and from associated Dobson and Brewer spectrophotometers. As an example, the assimilated global ozone field for 30 November 1999 is plotted as well.

2.4 Ground-based validation

Relying on the use of independent sources of information, validation is the process through which uncertainties and scientific usability of a data product are assessed. Furthermore, the development of any satellite data product is an iterative process in which validation plays the crucial role as a diagnostic tool. In the case of the FD ozone columns, the accuracy and geophysical consistency have been investigated through comparisons with well-controlled and documented ground-based correlative measurements, associated with the international Network for the Detection of Stratospheric Change (NDSC, see *Lambert et al.* [1999]) and, where needed, from other sources such as the Norwegian ozone monitoring network [*Hansen et al.*, 1999] and the World Ozone and UV Radiation Data Centre (WOUDC, see *WMO* [1995]). Similar ground-based comparisons have been performed for the off-line ESA/DLR GOME Data Processor (version 2.7) and for the Earth Probe Total Ozone Mapping Spectrometer (EP/TOMS) version 7 [*Lambert et al.*, 1999, 2000, and reference therein].

A detailed description of the complete validation effort falls beyond the scope of this paper. This section aims at outlining the major validation results for the FD processor, involving correlative total ozone data collected from about 15 zenith-sky UV-visible spectrometers affiliated with the NDSC and from associated Dobson and Brewer spectrophotometers, operating at stations highlighted in Figure 2.5. At each site, coincident FD and ground-based ozone columns have been compared for the years 1998 and 1999, and several parameters have been investigated, such as the dependence on the latitude, the season, the solar zenith angle of the GOME measurement, the ozone column, and the cloud fraction. The comparison method relies on the complementarity between the UV-visible and UV

measurement techniques used at the various ground sites, in terms of air mass and of uncertainties [Lambert *et al.*, 1999]. UV and UV-visible ground-based data agree within a few percent, the discrepancies being attributed to well known effects such as the temperature dependence of the UV absorption cross-sections and the atmospheric profile shape dependence of the zenith-sky air mass factor [Van Roozendael *et al.*, 1998].

Some of the ground-based validation results are illustrated in Figure 2.6, where the yearly mean relative differences between the three satellite ozone processors (GOME/FD, off-line GOME GDP, and EP/TOMS) and correlative ground-based total ozone are depicted as a function of latitude. Main features of the FD ozone columns in relation to the other satellite ozone data, as revealed from Figure 2.6, are as follows:

- The comparisons performed with independent ground-based techniques yield consistent results within the accuracy limit of the ground-based sensors, that is, a few percent. Apparent differences between nearly collocated ground-based instruments can be attributed to the aforementioned effects (temperature dependence of the UV absorption cross-sections and the atmospheric profile shape dependence of the zenith-sky air mass factor) which are not yet taken into account in the ground-based data as available from NDSC and WOUDC databases.

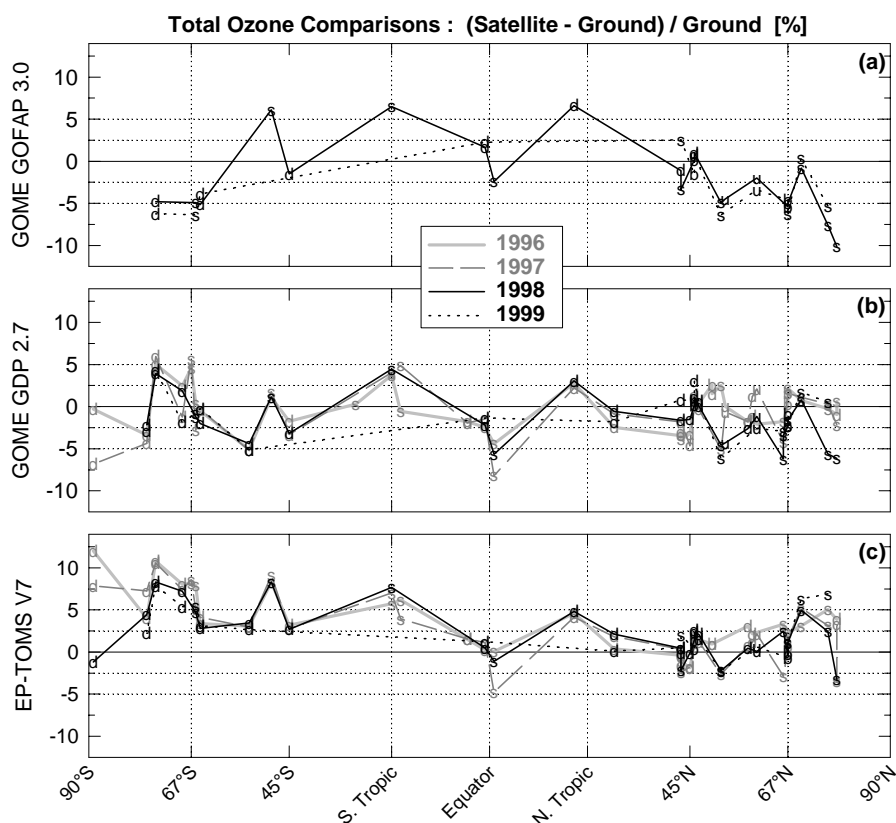


Figure 2.6 Yearly mean relative differences between satellite ozone columns ((a) GOME/FD version 3, (b) off-line GOME/GDP version 2.7 and (c) EP/TOMS V7) and ground-based total ozone as a function of latitude. The ground-based instruments are denoted by: S=SAOZ, U=other UV-visible, d=Dobson, b=Brewer. The 2.5% and 5% difference levels are indicated.

- At mid-latitudes, the yearly mean agreement between GOME (both FD and off-line GDP) and the ground generally falls within $\pm 5\%$. FD reports slightly lower values than GDP. This underestimation increases with the latitude.
- At high latitudes, the yearly mean agreement between GOME and the ground varies within the 0 to -10% range for FD and within the +6 to -7% range for GDP. FD reports systematically lower ozone values than GDP. More pronounced than in the middle latitudes, this underestimation can reach 5% beyond the polar circles.
- The overall agreement between EP/TOMS and the ground is similar to that reported previously [Lambert *et al.*, 1999, 2000]. In particular, it is interesting to note that the already reported bias between Northern and Southern EP/TOMS data from mid-1996 to mid-1998 persists through 1998 and 1999.
- At the tropics, the three satellite ozone processors overestimate the ground-based values by about 5% on a yearly average. The agreement is better around the Equator.
- Except near the poles, the year-to-year variation of the differences is weak, within a few percent.

Further ground-based validation concludes to the following main features of the FD ozone columns (not shown in Figure 2.6):

- Qualitatively, the three satellite ozone processors studied here and the ground-based networks capture the ozone field and its short-term variations similarly.
- After removal of the average difference as a function of time, the dispersion (1σ) of satellite data with respect to ground-based observations is similar for the three satellite processors. It varies from $\pm 2-3\%$ in the tropics and in summertime mid-latitudes, to 5% in wintertime mid-latitudes, and up to $\pm 10\%$ at high latitudes in winter and also at low sun elevation. This behaviour correlates with that of the natural variability of atmospheric ozone.
- The uncertainty in the ozone column in the presence of clouds is 0.9 to 1.5% higher than for a cloud free situation. This is mainly due to the large uncertainty in the (climatological) ghost column.
- At middle and high latitudes, GOME processors (both FD and GDP) are affected by fictitious seasonal variations in the ozone columns of a few percent. Such seasonal variations are significantly reduced with EP/TOMS. The FD-induced seasonal signatures are smaller than those introduced by the off-line GDP. This is likely due to the use in the FD processor of (1) a monthly varying ozone profile database [Fortuin and Kelder, 1998] relying on real measurements rather than on modelling results, and (2) the use of effective ozone absorption cross-sections based on ECMWF temperature forecasts.
- In the (sub)-tropics, the aforementioned 5% overestimation of ground-based values by the three satellite ozone processors exhibits a small seasonal variation of a few percent.
- At high latitudes, a solar zenith angle (SZA) dependent difference appears. The monthly mean agreement varies within the -10% to +5% range for the FD ozone columns and the -10% to +10% range for the GDP ozone columns.
- In polar summer, the SZA dependence generates an additional bias between GDP data of ascending and descending orbits. This bias is reduced with the FD processor, and hardly existing with EP-TOMS.

- The FD processor has a tendency to underestimate winter ozone values at high latitudes. It is worth noting that the amplitude of this underestimation is comparable to the already reported bias between Northern and Southern EP/TOMS data [*Lambert et al.*, 2000].

2.5 Concluding remarks

The Fast Delivery system described in this paper, retrieves total ozone columns in near-real time (i.e. within 3 hours after observation) from radiation measurements by the GOME satellite instrument. The FD ozone columns are used in an increasing number of applications such as assimilation of satellite ozone data in Numerical Weather Prediction models, for monitoring the status of the ozone layer, and to improve the forecast of surface UV radiation.

The FD processor is based on the off-line ESA/DLR GOME Data Processor: both processors use the DOAS retrieval method. However, the FD processor uses only a small part of the raw GOME data that is available in near-real time, and several changes in the level 0-to-1 and level 1-to-2 algorithms have been made to improve the retrieval of the ozone columns. The main modifications in the level 1-to-2 processor are: (1) the use of an effective ozone absorption cross-section based on ECMWF temperature forecasts in the slant column fit, (2) the use of the DAK radiative transfer model and the Fortuin and Kelder ozone climatology for the air mass factor calculations, and (3) the use of the FRESCO cloud algorithm.

The quality of the FD ozone columns has been established by a pseudo-global validation with correlative ground-based measurements from about 15 sites, associated with the international NDSC network. From this validation, it can be concluded that the FD processor gives a consistent picture of the ozone field. The near-real time ozone columns are in reasonable agreement with the ground-based measurements (within 5% for low- and mid-latitudes, within -10 to +5% for high latitudes) and capture temporal and spatial structures of the ozone field similarly. The level of quality meets the requirements for the discussed near-real time applications [*Stoffelen and Eskes*, 1999; *Hólm*, 2000 pers. comm.] and is comparable to that of the off-line GOME Data Processor or the EP/TOMS ozone sensor. Nevertheless, validation has raised some issues for future improvements in the FD processor. An important issue is the SZA/latitudinal dependence of the ozone columns, which is attributed to two effects: the current treatment of the atmospheric profile shape effect in the air mass factors, and the partial unsuitability of the particular spectral analysis when the atmosphere becomes optically thick [*Marquard et al.*, 2000]. In the current version of the FD system, the air mass factors are determined from a static climatology of monthly ozone profiles, which may differ significantly from the actual, highly variable ozone profiles. This deterministic approach cannot allow for atmospheric variability and can increase the error in the retrieved ozone column by about 5-10%, especially for high solar zenith angles where the sensitivity to the ozone profile shape is the highest. This error may be reduced to a few percent by adopting an iterative approach based on an ozone profile climatology with higher degree of freedom, e.g. classified by latitude/column [*Wellemeier et al.*, 1997; *Spurr*, 1999] or by latitude / season / tropopause height [*De Mazière et al.*, 1999].

Acknowledgements

This work would not have been possible without the helpful discussions with many colleagues within the GOME community. Special thanks goes to all people involved in developing the ESA/DLR GOME Data Processor, of which the algorithms served as a basis of our Fast Delivery processor. The ground-based data used in this publication was obtained as part of the Network for the Detection of Stratospheric Change (NDSC) and from the World Ozone and Ultraviolet Radiation Data Centre (WOUDC), two major contributors to the WMO's Global Atmospheric Watch programme. Fruitful discussions with instrument operators and with G. Hansen (NILU) and D. Ionov (SPbSU) are gratefully acknowledged.

Chapter 3

Ozone mini-hole observed over Europe, influence of low stratospheric temperature on observations^{*}

Abstract

A region of extreme low ozone values passed over North-western Europe during November 30, and December 1, 1999. The total ozone values were measured from the ground, with a Brewer Spectrophotometer, and from space with the GOME and TOMS satellite instruments. The ozone sonde measurement and the retrieved GOME ozone profile have shown that the main reduction in the ozone column occurred between the ozone maximum (22 km) and the tropopause. The low temperatures found in the stratosphere during this event have significant consequences for the ozone retrieval algorithm, both for satellite retrievals and for the Brewer measurements.

^{*}This chapter has been published as: M. Allaart, P. Valks, R. van der A, A. Piters, H. Kelder and P. van Velthoven, *Geophys. Res. Lett.*, Vol. 27, 4089-4092, 2000.

3.1 Introduction

Ozone mini-holes occur regularly throughout the mid-latitudes of both hemispheres [James, 1998]. These are relatively short-lived phenomena that are caused by horizontal and vertical advection in the middle atmosphere [McKenna *et al.*, 1989; Fiedler *et al.*, 1993; Vaughan and Timmis, 1998], this in sharp contrast to the Antarctic ozone-hole that is caused by chemical destruction of ozone. The reported increase in the number of mini-hole events may account for up to a third of the published ozone trend during spring [Reid *et al.*, 2000].

On rare occasions the column integrated amount of ozone (“total ozone”) above the Northern Hemisphere drops below 180 DU. Three such events can be identified in the “Total Ozone Mapping Spectrometer” (TOMS) [McPeters *et al.*, 1998] instrument’s total ozone database (1978-2000).

The ozone mini-hole of November 30, and December 1, 1999 passed over the station *De Bilt*, allowing accurate ground-based measurements. Here we will present these observations, the results from a balloon-borne ozone sonde, the total ozone measurements and the ozone profile deduced from the Global Ozone Monitoring Experiment (GOME) satellite instrument.

As the ozone absorption cross-section in part of the ultra-violet is temperature dependent, and the recorded stratospheric temperatures were very low during this event, we have put some emphasis on the sensitivity of the retrieved ozone amounts to temperature.

3.2 Ground-based observations

Observations

The low ozone values were measured with the Brewer spectrophotometer #100 operated by the Royal Netherlands Meteorological Institute (KNMI) in *De Bilt*, The Netherlands (“Brewer”) at 52.1° North, 5.13° East. Regular observations at this site have started in 1994. The Brewer measures the extinction of ultraviolet sunlight, from which the total ozone value is computed. The Brewer performs ozone measurements on a regular basis (a few times per hour). Here we will only discuss the “Direct Sun” observations, as they are the most accurate. Direct Sun measurements are made in groups of five consecutive measurements. In Table 3.1 average values and Root-Mean-Square differences are listed. The solar zenith angle (SZA) is also indicated.

The weather conditions during the observations were not optimal. On November 30, there was an unbroken layer of high (7 km) stratus cloud that became too thick to allow Direct Sun observations in the second half of the day. During both days there were some scattered cumulus and/or stratocumulus clouds.

Table 3.1 Brewer total ozone measurements at De Bilt (52.1°N, 5.1°E) on 30 November and 1 December 1999. The total ozone value corrected for the effects of low stratospheric temperature is also listed.

| <i>30 November 1999</i> | | | |
|-------------------------|-----------------|----------------------|-------------------|
| Time | SZA (degree) | Brewer Ozone (DU) | Corrected (DU) |
| 10:49 | 74.2 | 205.4±1.9 | 209.7 |
| 10:57 | 74.0 | 205.6±0.4 | 209.9 |
| 11:51 | 73.9 | 198.4±1.4 | 202.5 |
| 12:44 | 75.6 | 197.8±1.3 | 201.9 |
| 12:54 | 76.1 | 197.7±2.3 | 201.8 |
| Daily average: | | 202.5 | 206.7 |

| <i>1 December 1999</i> | | | |
|------------------------|-----------------|----------------------|-------------------|
| Time | SZA (degree) | Brewer Ozone (DU) | Corrected (DU) |
| 10:46 | 74.4 | 206.2±2.0 | 210.5 |
| 10:54 | 74.2 | 206.2±0.7 | 210.5 |
| 11:16 | 73.9 | 208.2±1.2 | 212.5 |
| 11:27 | 73.9 | 207.8±0.9 | 212.1 |
| 11:30 | 73.9 | 207.8±0.8 | 212.1 |
| 11:41 | 73.9 | 209.4±0.5 | 213.7 |
| 11:52 | 74.1 | 211.0±0.7 | 215.4 |
| 12:03 | 74.3 | 209.2±0.7 | 213.5 |
| 12:16 | 74.6 | 209.6±1.0 | 213.9 |
| 12:24 | 74.9 | 209.4±0.6 | 213.7 |
| 12:34 | 75.3 | 209.0±1.7 | 213.3 |
| 12:46 | 75.8 | 209.7±1.0 | 214.0 |
| Daily average: | | 208.6 | 212.9 |

Accuracy of the measurements

The Brewer instrument is properly maintained, and has been regularly compared to a travelling standard, most recently in July 1999. During this and previous calibrations only small (~1%) systematic errors were found. Stability checks with an internal standard lamp give no indication of a deterioration of the instrument since then.

Typical errors of this instrument are on the order of 2% [Wauben and Kuik, 1998]. In general, errors increase with the Solar Zenith Angle (SZA). Measurements with SZA larger than 80° give unreliable ozone readings.

Special attention should be given to the temperature dependence of the ozone cross-section. The standard Brewer ozone retrieval software does not use actual stratospheric temperatures, nor a seasonal temperature climatology. Only one temperature value, -46.3°C, is assumed and is present implicitly in one of the calibration coefficients.

Within reasonable approximation the Brewer temperature dependence can be expressed as [Van Roozendaal *et al.*, 1998]:

$$DU_{corr} = \frac{DU}{1 + \alpha(T - T_0)} \quad (3.1)$$

where DU_{corr} is the corrected total ozone value, DU is the output from the standard Brewer ozone retrieval software, $T_0 = -46.3^\circ\text{C}$ and $\alpha = 0.0013/^\circ\text{C}$. The actual temperature can be measured with an ozone sonde.

Ozone sonde measurement

On December 1, at 12:00 UT, an ozone sonde was launched from *De Bilt*. The observed temperature and ozone profiles are shown in Figure 3.1. The tropopause was found at 11.5 km altitude (210 hPa), with a temperature of -57°C. Immediately above the tropopause the temperature dropped further to a minimum value of -80.4°C at 22.9 km (31.6 hPa). Such low temperatures are only rarely observed over *De Bilt*. The ozone sensor failed at 21 km (41 hPa), but by comparing this profile with the normal profile for this time of year, it is clear that the main difference lies in the lower ozone mixing ratios between the tropopause and the ozone maximum.

To simplify the discussion on the temperature sensitivity of optical instruments, we constructed the “ozone temperature” of the atmosphere, T^* , defined as:

$$T^* = \frac{\int T \cdot \rho_{\text{O}_3} \cdot dz}{\int \rho_{\text{O}_3} \cdot dz} \quad (3.2)$$

As both T and ρ_{O_3} are measured with the ozone sonde, T^* can be computed for each ozone sonde in our archive. T^* is around -46°C in summer, and typically between -55° and -65°C in winter. On first of December 1999, a value of -62°C was computed. This was caused by a combination of a very cold stratosphere, and a relatively warm troposphere. We conclude that the values shown in Table 3.1 should be increased by 2.1% to give the correct total ozone values.

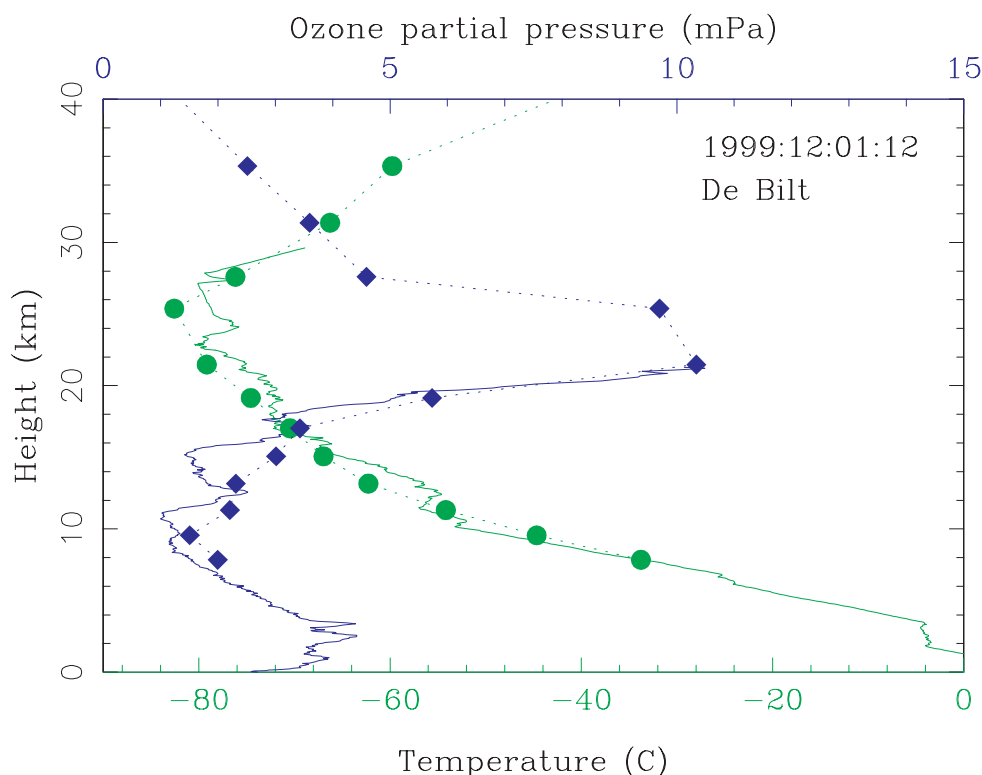


Figure 3.1 Ozone sonde and GOME profiles. The black and grey lines represent the ozone partial pressure and temperature as measured with the ozone sonde, respectively. Black diamonds (connected by dots) show retrieved GOME ozone profile, while the grey circles (connected by dots) show ECMWF temperature profile used for the retrieval.

3.3 Satellite observations

The unusual low ozone values over North-western Europe were also measured by the GOME satellite instrument. GOME is a passive imaging spectrometer on-board the European Space Agency's (ESA) Second European Remote Sensing (ERS-2) satellite and measures the solar irradiance and the earth-shine radiance in the UV/VIS spectral range 240-790 nm [Burrows *et al.*, 1999a]. GOME scans the earth surface in the nadir direction (across-track scan angle $\pm 32^\circ$) with a ground pixel of $40 \times 320 \text{ km}^2$, resulting in a global coverage within 3 days. Total ozone data are retrieved from the ratio of the earth-shine and sunshine spectra utilising the characteristic ozone spectral absorption features in a part of the Huggins band (325-335 nm). The retrieval algorithm used in this study [Valks *et al.*, 2003a] is an improved version of that used in ESA/DLR GOME Data Processor v. 2.7 [Spurr *et al.*, 2002]. Figure 3.2 shows the retrieved GOME total ozone values for November 30, and December 1, 1999. Clearly visible are the very low ozone values found over the North Atlantic ocean and North-western Europe.

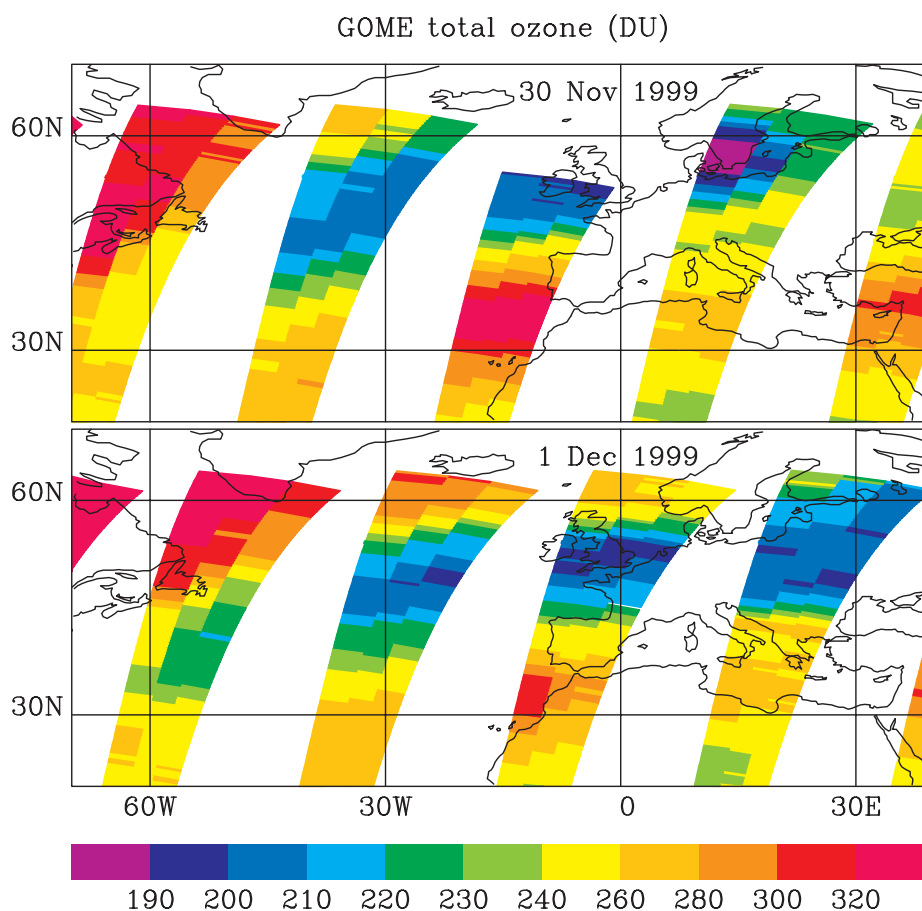


Figure 3.2 GOME total ozone maps for 30 November and 1 December 1999. Values as low as 185 DU are seen over Europe.

GOME temperature dependence

The effect of the very low temperatures in the stratosphere, coinciding with the low ozone values over Europe, on the retrieval of GOME total ozone values have been analysed as well. In the GOME retrieval algorithms, usually climatological temperature profiles are used to determine the ozone temperature T^* and the resulting ozone cross-sections [Burrows *et al.*, 1999b]. This results in an error in the retrieved total ozone values if the actual temperature profile deviates from the climatological temperature profile. To minimise this error, we use 24h forecast temperature profiles from the 50-level ECMWF (European Centre for Medium-Range Weather Forecasts) model [Untch and Simmons, 1998] in the latest version of our GOME retrieval algorithm. From these temperature profiles, daily global ozone temperature fields and corresponding ozone cross-sections are calculated. For the ozone mini-hole area over Europe, the ozone temperatures calculated with the ECMWF temperature profiles are about 10°C lower than the ozone temperatures calculated with climatological temperature profiles. In Table 3.2, we show that the use of ECMWF ozone temperatures in the retrieval algorithm causes a significant decrease in total ozone to 185 DU (-4.1%). For comparison, the TOMS total ozone value for this location is also shown.

Table 3.2 Total ozone values for the GOME ground pixel above Denmark (pixel centre: 56.6°N, 13.4°E) for 30 November 1999. The two GOME values are retrieved with a climatological ozone temperature (T^*) and with an ozone temperature derived from 24h temperature forecast of the 50-level ECMWF model. For comparison, the TOMS total ozone value for this location is also shown.

| Instrument | Ozone temperature | Total ozone |
|------------|----------------------|-------------|
| GOME | climatological -53°C | 193 DU |
| GOME | ECMWF -64°C | 185 DU |
| TOMS | | 175 DU |

It is interesting to note that GOME's sensitivity to T^* is larger and of opposite sign compared to that of the Brewer instrument. This is caused mainly by the difference in wavelength bands used (325-335 nm, 310-320 nm respectively). The temperature dependence of the ozone absorption increases with wavelength in this region of the UV.

Retrieved ozone profile from GOME observations

On 1 December 11.17 UT, GOME observed the region with low ozone over *De Bilt*. The steep rise of ozone absorption in the wavelength range from 340 to 260 nm, offers the possibility of inferring height-resolved information on the ozone concentration [Munro *et al.*, 1998, Chance *et al.*, 1997; Hoogen *et al.*, 1999; Van der A *et al.*, 2002]. Part of this spectrum has been used for the column retrieval as mentioned before. The observed radiances with the lowest wavelengths, necessary for profile retrieval, are acquired with longer observation times. Therefore, the retrieved ozone profile is an average for a ground pixel of 960 by 100 km² (This is 7.5 times the size of the ground pixel for total ozone retrieval.) The ground pixel considered is located over parts of the Netherlands, England and Scotland (pixel centre: 51.03° N, 1.17° W). The ozone profile retrieval is performed with the optimal estimation method [Rodgers, 1990], where the information of the observation is combined with *a priori* information. This method is used on a linearisation of the forward model utilising an iterative process to account for the non-linearity. For each iteration step the forward model is linearised by a weighting function, which is the derivative of the radiances to the ozone concentration at a number of altitudes. For the forward calculation the radiative transfer model MODTRAN 3.7 [Berk *et al.*, 1989] is used. For each iteration, an optimal estimate profile is calculated from the profile of the former iteration step, the weighting function and the measured radiances. As *a priori* ozone profile the ozone sonde measurement, extended with climatological values [Fortuin and Kelder, 1998] in the upper stratosphere, has been used. The retrieved profile is shown in Figure 3.1, where the profile from GOME complements the missing profile information of the sonde in the upper stratosphere. The deviations in the troposphere are explained by the difference in co-location and the lower

accuracy of the retrieved profile in the troposphere. Due to the low solar zenith angle (73.3°) at the time of the measurement, the accuracy is lower than usual. The accuracy in the troposphere is about 50%, while the accuracy in the stratosphere is better than 15%.

3.4 Conclusions

Total ozone values well below 200 DU were recorded over Western Europe during November 30, and December 1, 1999. The main reduction in the ozone occurred between the tropopause and the ozone maximum (22 km).

The absorption cross-section of ozone in the ultra-violet is temperature dependent. As the stratosphere was very cold, the standard ozone retrieval software for the Brewer spectrophotometer produces total ozone values which are 4.2 DU or 2.1% too low. The GOME instrument has the opposite sensitivity to the atmospheric temperature. If the ECMWF temperatures are used instead of the climatological ones, the GOME retrieved total ozone values are lower by 8 DU or 4%.

In using the Brewer network for calibration or validation of other ozone measuring systems (e.g. satellite instruments) it is essential to take into account the sensitivity of both instruments to the stratospheric temperature.

Acknowledgements

Parts of this work have been funded by the ESA Data User Programme (GOFAP).

Chapter 4

Variability in tropical tropospheric ozone: Analysis with GOME observations and a global model^{*}

Abstract

Tropical tropospheric ozone columns (TTOCs) have been determined with a convective-cloud-differential (CCD) method, using ozone column and cloud measurements from the Global Ozone Monitoring Experiment (GOME) instrument. GOME cloud top pressures, derived with the Fast Retrieval Scheme for Clouds from the Oxygen A-band (FRESCO) method, indicate that most convective cloud top levels are between 300 and 500 hPa, and do not extend to the tropical tropopause. The new GOME-CCD method takes this tropical transition layer below the tropopause into account, and uses above-cloud and clear-sky ozone column measurements to derive a monthly-mean TTOC below 200 hPa. Validation of the GOME-TTOCs with 7 Southern Hemisphere ADditional OZonesondes (SHADOZ) sites shows good agreement, with an RMS difference of about 5 DU. In the northern tropics, the GOME-TTOC compares most of the time well with in-situ measurements at Paramaribo (6°N,55°W) and Abidjan (5°N,4°W). Analysis of the GOME-TTOCs for 2000 and 2001, with the aid of the chemistry-transport model TM3, illustrates that the variability in the TTOC depends on a complex interaction of several processes, including biomass burning, lightning, and large-scale transport. The much larger extent of the South-Atlantic TTOC maximum in September-October 2001 compared to September-October 2000, can be attributed to differences in large-scale transport. An exceptional situation in the northern tropics occurred during the biomass burning season December 2001-January 2002, when there were almost no fires over northern Africa. This resulted in strongly reduced TTOCs over the Atlantic between the equator and 10°N.

^{*} This chapter has been published as: P. J. M. Valks, R. B. A. Koelemeijer, M. van Weele, P. van Velthoven, J. P. F. Fortuin, and H. Kelder, *J. Geophys. Res.*, Vol. 108, 4328, 2003.

4.1 Introduction

Ozone in the tropical troposphere plays various important roles. It is the primary source of hydroxyl radicals, which act as detergents of the troposphere, initiating almost all oxidation processes in the tropics. Near the surface, excessive amounts of ozone are toxic to ecosystems, animals and man. Upper tropospheric ozone acts as a greenhouse gas by absorbing long-wave terrestrial radiation.

Compared to ground-based measurements of tropospheric ozone, which give accurate data for limited time and space, observations from space platforms offer the possibility to measure the distribution of tropospheric ozone over large areas and to study its large-scale temporal and spatial variability. This is of great importance, since ozone that is formed over regions where large amounts of ozone precursors are emitted, can be transported over great distances and affects areas far from the source.

Fishman and co-workers [Fishman *et al.*, 1990] developed the concept of deriving a tropospheric ozone column with a residual method, by using total ozone measurements from the Total Ozone Mapping Spectrometer (TOMS) and subtracting a stratospheric ozone column derived from Stratospheric Aerosol and Gas Experiment (SAGE) measurements. One of the main findings of this tropospheric ozone residual (TOR) technique was the occurrence of enhanced ozone concentrations over the South Atlantic near the coast of Africa during the biomass burning season. As the eruption of Mount Pinatubo in June 1991 prevented the use of SAGE data to quantify the amount of ozone in the stratosphere, later studies used Solar Backscattered Ultraviolet (SBUV) data [Fishman *et al.*, 1996] and data from the Upper Atmosphere Research Satellite (UARS) microwave limb sounder (MLS) and halogen occultation experiment (HALOE) [Ziemke *et al.*, 1998]. A limitation of the residual technique is that stratospheric ozone measurements from the independent sensor may be uncertain in the lower stratosphere, giving large uncertainties in the tropospheric column amounts [Fishman and Balok, 1999]. Therefore, two new methods have been developed to distinguish tropospheric from stratospheric ozone. Both methods use TOMS data and are limited to the tropical latitudes.

With the modified-residual (MR) method [Kim *et al.*, 1996; Hudson and Thompson, 1998; Thompson and Hudson, 1999], tropical tropospheric ozone columns (TTOCs) are derived by combining TOMS total ozone with ground-based ozonesonde measurements across the tropical South Atlantic. The residual technique is based on the assumption that in the tropics, the stratospheric ozone column is nearly invariant with longitude; therefore the variations in the total ozone column can largely be attributed to variations in the tropospheric ozone column. The convective-cloud-differential (CCD) method [Ziemke *et al.*, 1998; Ziemke and Chandra, 1999] uses TOMS total ozone measurements over bright, high-altitude clouds in the tropical western Pacific to obtain an above-cloud stratospheric ozone amount. In this region, bright clouds are often associated with strong convective outflows and cloud tops in the upper troposphere. The TTOC is derived at cloud-free pixels by subtracting the stratospheric ozone amount from TOMS total ozone, assuming again a zonally invariant stratospheric column. Because cloud height information is not measured by TOMS, the primary assumption in the CCD method is that the high-reflectivity clouds often have cloud tops at the tropopause. However, as noted in the aforementioned papers, a difficulty with the

CCD method is that most convective cloud tops do not extend up to the tropical tropopause (which lies around 100 hPa), but to the bottom of a so-called tropical transition layer, several kilometres below the tropopause [Highwood and Hoskins, 1998; Folkins *et al.*, 1999].

In this paper, an improved CCD method for the tropics is presented that uses total ozone and cloud measurements from the Global Ozone Monitoring Experiment (GOME) instrument. GOME, aboard the European Space Agency's (ESA) Second European Remote Sensing Satellite (ERS-2), is the first of a new generation of UV/VIS/NIR remote sensing instruments, that improves the capabilities to observe ozone and other important species such as NO₂, SO₂, HCHO and BrO in the troposphere. Several papers have been published with first scientific results on tropospheric NO₂ [Leue *et al.*, 1999; Richter and Burrows, 2002; Velders *et al.*, 2001], BrO [Wagner and Platt, 1998; Richter *et al.*, 1998; Van Roozendael *et al.*, 2002a] and SO₂ [Eisinger and Burrows, 1998]. Studies on GOME tropospheric ozone and NO₂ in the tropics have focussed on the derivation of excess vertical columns stemming from pollution, by subtracting vertical columns of ozone and NO₂ from a clean air region (e.g. the Pacific) [Burrows *et al.*, 1999a]. Here, we use GOME measurements of cloud fraction and cloud top pressure to improve the original CCD method. The GOME instrument is able to determine these cloud properties by using measurements in the near-infrared wavelength region. By combining the cloud information with GOME ozone column measurements, monthly-mean values of the tropospheric ozone columns below 200 hPa have been determined. The GOME-TTOCs have been calculated on a 2.5° latitude by 5° longitude grid between 20°N and 20°S. The whole GOME period from July 1995 to the end of 2001 is covered. We validate the GOME-TTOCs with ozonesonde measurements from the SHADOZ (Southern Hemisphere Additional OZonesondes) network [Thompson *et al.*, 2003a], also including the site Paramaribo (6°N,55°W) in the northern tropics.

The validated GOME-TTOCs for the years 2000 and 2001, and the chemistry-transport model TM3, are used to untangle the intriguing relation of the South-Atlantic TTOC maximum to biomass burning emissions, lightning NO_x emissions, and large-scale transport [Krishnamurti *et al.*, 1993, 1996; Thompson *et al.*, 1996; Chatfield *et al.*, 1998; Jacob *et al.*, 1996; Pickering *et al.*, 1996; Martin *et al.*, 2002a]. We examine the variability of the TTOC in the northern tropics as well, and focus on the northern-Atlantic region during the unusual biomass burning season December 2001-January 2002.

In Section 4.2, an overview of the GOME instrument is given and the GOME total ozone and cloud algorithms are described. Section 4.3 focuses on the GOME-CCD method and the uncertainties in the retrieved tropospheric ozone columns. In Section 4.4, the TM3 chemistry-transport model is described and possible causes for the variations in the TTOC are examined for the years 2000 and 2001. The paper ends with conclusions and a future outlook.

4.2 GOME measurements

The GOME instrument is a passive four-channel spectrometer and measures the direct solar irradiance and the solar radiance reflected by the Earth atmosphere and surface in the UV/VIS/NIR spectral range 240 to 790 nm. GOME scans the Earth surface in the nadir direction (across-track scan angle 32°) with a spatial resolution of 40x320 km² and a global

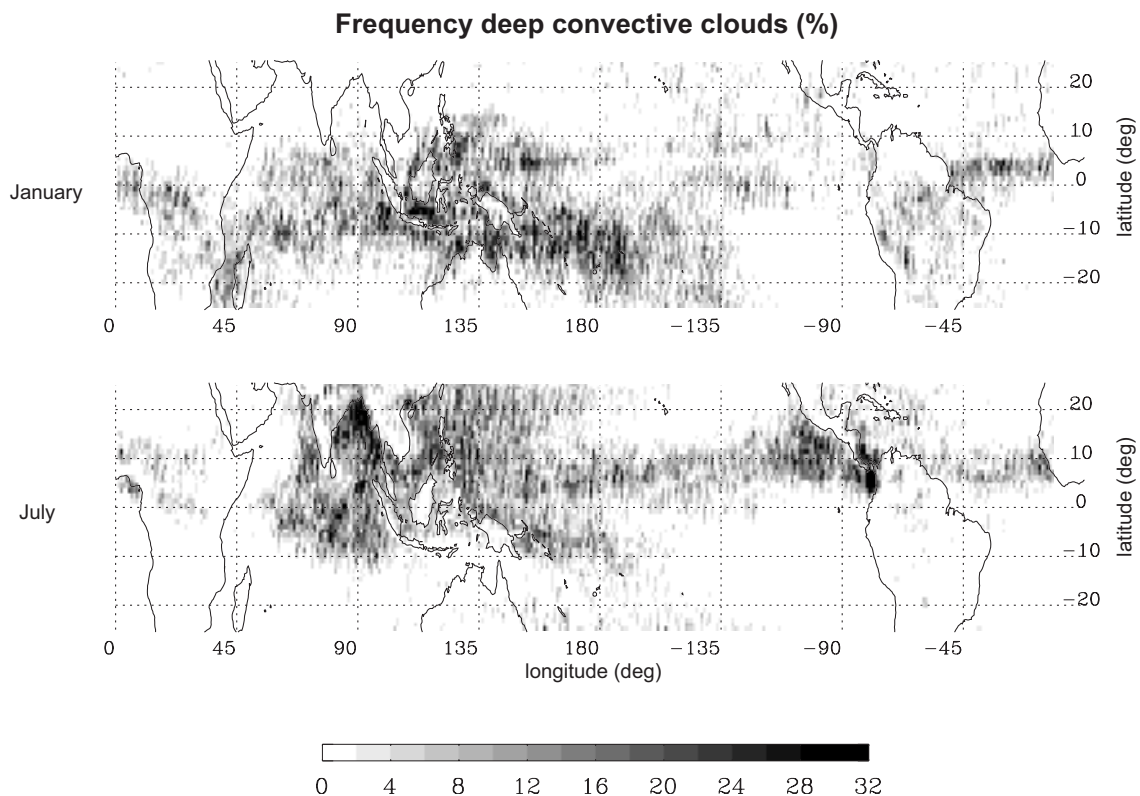


Figure 4.1 Frequency of occurrence of deep-convective clouds as derived from GOME oxygen A band measurements using the FRESCO method. Results are shown for (top) January and (bottom) July, averaged for the years 1998-2000. Clouds are classified as deep convective if their tops are above the 400 hPa level and their effective cloud fraction exceeds 0.6.

coverage within 3 days [Burrows *et al.*, 1999a].

The measurements that are needed to derive a TTOC with the GOME-CCD method are: total ozone column, cloud fraction and cloud top pressure. The first step in the retrieval of these GOME products is the conversion of the raw GOME data into calibrated reflectance spectra (level 0-to-1 processing). The level 0-1 processor used for this study is based on the algorithm used by the off-line ESA/DLR GOME Data Processor (GDP) [Aberle *et al.*, 2002]. However, several changes in the algorithms have been made to improve the level-1 quality, mainly with respect to the wavelength calibration and degradation correction [Schutgens and Stammes, 2002; Van der A *et al.*, 2002, Van Geffen and Van Oss, 2003]. In the second step (level 1-to-2 processing), the cloud properties and total ozone columns are retrieved from the calibrated reflectance spectra, as described below.

4.2.1 FRESCO cloud algorithm

The cloud fraction and cloud top pressure are derived using the Fast Retrieval Scheme for Clouds from the Oxygen A-band (FRESCO) method [Koelemeijer *et al.*, 2001, 2002]. The retrieval is based on a non-linear least squares fitting of the reflectivity spectrum measured by

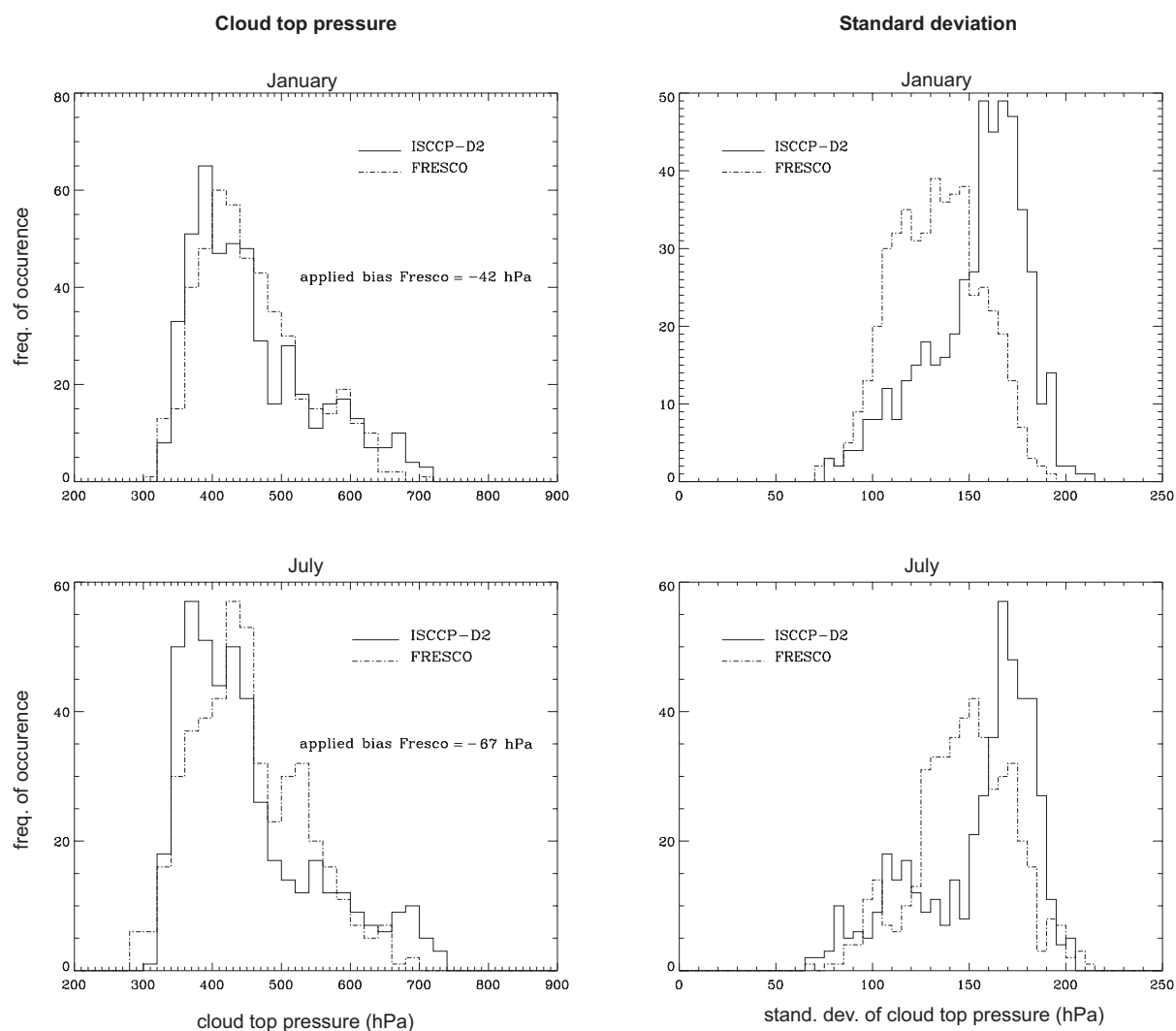


Figure 4.2 Histograms of (left) FRESKO and ISCCP-D2 cloud top pressures and (right) temporal standard deviations for the area 12.5°S - $12.5^{\circ}\text{N}/70^{\circ}\text{E}$ - 170°W . Results are shown for (top) January and (bottom) July. The cloud top pressure measurements have been spatially averaged on a 2.5° by 2.5° grid, and then the number of grid cells has been counted as a function of cloud top pressure/standard deviation for 20/10 hPa bins. The FRESKO data is from 1995 (July) and 1997 (January); the ISCCP-D2 data are averaged over the period 1984-1993.

GOME to a simulated spectrum in the range 758-766 nm, and solving for cloud fraction and cloud top pressure. The cloud fraction is derived assuming a cloud albedo of 0.8, corresponding to an optically thick cloud, and this should therefore be regarded as an effective cloud fraction. Our cloud albedo choice has been optimised for ozone air mass factor calculations in the UV and does not significantly influence retrieved cloud top pressures over the oceans, but gives rise to a small positive pressure bias with thin clouds over land [Koelemeijer *et al.*, 2002].

The above-cited studies about FRESKO were focussed on mid-latitude cloud systems as well as global cloud systems on a monthly-averaged basis. Here, we focus on deep-convective clouds in the tropics. Figure 4.1 shows maps of frequency of occurrence of deep-convective

clouds as derived from FRESCO, for January (top) and July (bottom). To obtain the figure, we classified clouds as deep convective if their tops are above the 400 hPa level and their effective cloud fraction exceeds 0.6. The patterns in Figure 4.1 show the structure of the intertropical convergence zone (ITCZ) and the seasonal migration of the ITCZ. The eastern part of the tropical Indian ocean and western part of the tropical Pacific have the highest frequency of deep-convective clouds. Particularly apparent are the large latitudinal shifts over South America, Africa and the South-Asian subcontinent. These patterns agree well with the monthly-averaged ISCCP (International Satellite Cloud Climatology Project) D2 data [Rossow *et al.*, 1993; Rossow and Schiffer, 1999] and the HRC (High Reflectivity Cloud) dataset, constructed from daily visible and infrared satellite mosaics [Waliser and Gautier, 1993; Garcia, 1985].

The left panels of Figure 4.2 show the frequency distributions of cloud top pressures over the tropical Indian ocean and western Pacific as derived by FRESCO for January (top left) and July (bottom left). For comparison, the frequency distributions of the ISCCP-D2 cloud top pressures are shown as well. The right panels show the corresponding standard deviations. The FRESCO derived cloud top pressures histograms were shifted upwards by -42 hPa (January) and -67 hPa (July) to give the same mean as the ISCCP-D2 data. This bias in FRESCO cloud top pressures is consistent with the previous FRESCO studies [Koelemeijer *et al.*, 2001, 2002] and is due to neglecting the absorption by oxygen within and below the cloud. No shift was applied to the FRESCO standard deviation histograms. Figure 4.2 indicates that the monthly-mean pressures of tropical convective cloud tops are between 300 and 500 hPa in the highly convective areas over the Indian ocean and western Pacific. These cloud tops are several hundred hPa below the tropopause, which lies around 100 hPa in the tropics. This is in agreement with other studies that suggest that most convective cloud tops do not extend up to the tropopause, but to the bottom of the tropical transition layer [Highwood and Hoskins, 1998; Folkins *et al.*, 1999], several kilometres below the tropopause. Figure 4.2 shows that although the standard deviation histograms of ISCCP have a larger skewness than those of FRESCO, the standard deviations have similar magnitudes. We conclude that tropical cloud top pressures derived from FRESCO in this region are biased by about 50 hPa on average, and show standard deviations comparable to ISCCP-D2. For the GOME-CCD method, we have corrected the FRESCO cloud top pressure for this bias.

4.2.2 GOME total ozone

GOME total ozone columns are retrieved from the ratio of the Earthshine and Sunshine spectra, utilizing the characteristic ozone spectral absorption features in a part of the Huggins ozone absorption band (325-335 nm). The total ozone algorithm used for this study is based on the algorithm used in the GDP level 1-2 processor [Spurr *et al.*, 2002], but changes in the algorithm have been made to improve the retrieval of the ozone columns [Valks *et al.*, 2003a].

The first step in the total ozone algorithm is the calculation of the ozone slant column density. This is the total amount of ozone per cm^2 along the average optical path through the atmosphere, and is determined by the Differential Optical Absorption Spectroscopy (DOAS) method [Platt, 1994]. The DOAS algorithm consists of a least-squares fitting of the ozone absorption cross-section, a Ring spectrum and a third-order polynomial. The Ring spectrum

accounts for the Ring effect (the filling-in of solar Fraunhofer lines in the Earthshine spectrum), and the polynomial removes the slowly varying spectral structures resulting from Rayleigh and aerosol scattering and reflections at the ground surface. To account for the temperature dependence of the ozone absorption cross-sections, an effective ozone absorption cross-section is calculated daily, using temperature profiles from the European Centre for Medium-Range Weather Forecasts (ECMWF) model.

To convert the ozone slant column density into a vertical ozone column, the so-called air mass factor is needed. The air mass factors have been calculated with a pseudo-spherical version of the Doubling Adding model DAK [Stammes, 2000 and references therein], which describes the scattering and absorption processes that affects the average optical path of photons in the atmosphere. The air mass factor depends on the viewing scenario (solar and satellite viewing angle), surface height and albedo (derived from the *Herman and Celarier* [1997] and *Koелеmeijer et al.*, [2003] databases), cloud properties, and the ozone and temperature profiles. In the air mass factor calculations, absorption inside and below clouds is not accounted for. However, the resulting error in the retrieved ozone column is minimized by making the same approximation in the cloud top pressure retrieval with the FRESCO algorithm, such that the absorption by ozone is normalized to that of oxygen. The effect of aerosols has also not explicitly be taken into account, but if significant aerosol scattering occur in clear-sky conditions, the aerosol layer will be detected as a thin cloud layer and as such be taken into account.

The dependence of the air mass factor on the ozone profile is of particular importance. Here, *a priori* ozone profiles from the *Fortuin and Kelder* [1998] climatology have been used. This climatology includes monthly ozone profiles for 10° latitude bands, determined from ground-based ozone profile measurements. For cloud-free situations, the vertical ozone column N_v can simply be calculated by dividing the slant column density N_s by the appropriate clear-sky air mass factor ($N_v = N_s / M_{clear}$). However, in the presence of clouds, two air mass factors are needed: one down to the ground surface (M_{clear}) and one down to the cloud top (M_{cloudy}). The vertical ozone column is then given by:

$$N_v = \frac{N_s + w \cdot N_g \cdot M_{cloudy}}{M} \quad (4.1)$$

where the total air mass factor $M = w \cdot M_{cloudy} + (1-w)M_{clear}$. The weighting factor w is the fraction of the photons that originates from the cloudy part of the pixel ($w = f \cdot I_{cloudy} / I$) [Martin *et al.*, 2002b]. The cloud fraction f and the cloud top pressure have been determined with the FRESCO cloud algorithm, as described above. In the total ozone algorithm, the amount of ozone below the cloud top is called the ghost vertical column (N_g), which cannot be detected by GOME and is derived from an ozone profile climatology. For the GOME-CCD method, this ghost column correction is not included, because the ozone column above the cloud top ($N_{cloud-top}$) is used:

$$N_{cloud-top} = \frac{N_s}{M_{cloudy}} \quad (4.2)$$

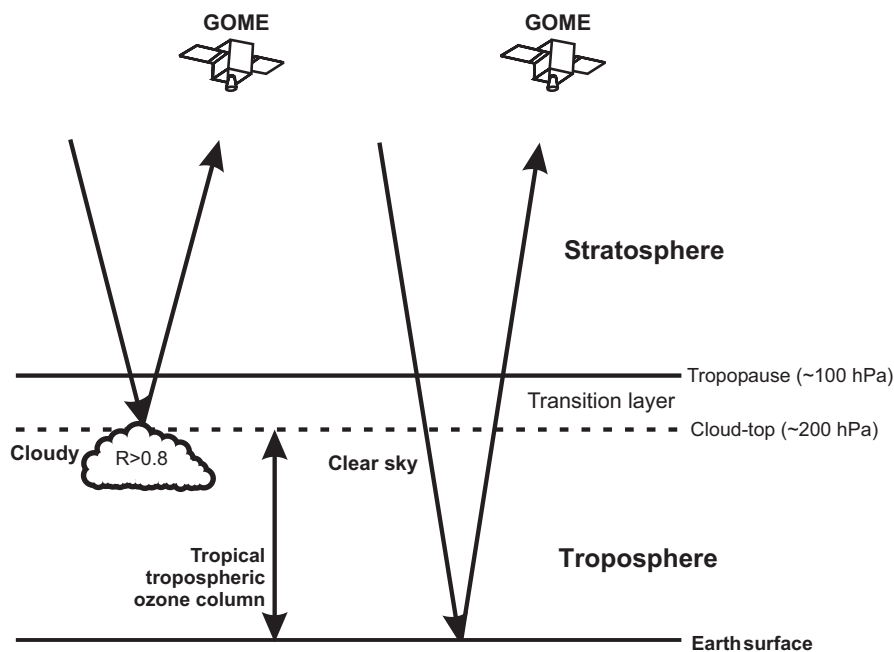


Figure 4.3 Schematic illustration of the GOME-CCD technique for the tropics. Cloudy GOME measurements with cloud fraction ≥ 0.8 and cloud top pressure ≤ 350 hPa, which are used to determine the above-cloud ozone column, are shown on the left. Cloud-free GOME measurements (cloud fraction ≤ 0.1) are shown on the right. The result is a tropical tropospheric ozone column below 200 hPa.

4.3 Tropical tropospheric ozone from GOME

4.3.1 GOME-CCD method

Figure 4.3 shows a schematic illustration of the GOME-CCD technique. In the first step, cloudy GOME measurements with cloud fraction $f \geq 0.8$ and cloud top pressure $p_c \leq 350$ hPa are used to determine the above-cloud ozone column (including the ozone column in the stratosphere and the tropical transition layer), as shown on the left of Figure 4.3. The cloudy GOME pixels are selected from tropical measurements over the highly convective eastern Indian Ocean and the western Pacific ($70^\circ\text{E} - 170^\circ\text{W}$), where the greatest frequency of high level clouds is found. As explained in Section 4.2.1, average pressures of tropical convective cloud tops are between 300 and 500 hPa. For the individual GOME measurements, the cloud top hardly ever exceeds 200 hPa. To be able to calculate a useful tropospheric ozone column, the above-cloud ozone column is calculated for a fixed pressure level of 200 hPa. To that end, a small correction has been made for the difference between the cloud-top level and the 200 hPa level (typically 0-2 DU), assuming a constant ozone volume mixing ratio. After this correction, the ozone columns above 200 hPa are monthly averaged for 2.5° latitude bands between 20°N and 20°S . Hereby, it is assumed that the ozone column above 200 hPa is independent of longitude in a given latitude band. This assumption and the error associated with it is discussed in Section 4.3.2.

The number of cloudy GOME pixels with $f \geq 0.8$ and $p_c \leq 350$ hPa varies between 150-

400 per month for each (2.5 degree) latitude band. Although this number is only about 1% of all the GOME measurements, it is sufficiently large to provide an adequate statistical mean for the ozone column above 200 hPa. Because of the seasonal migration of the ITCZ, the region of tropical air shows a seasonal displacement as well. Periodically, sub-tropical air is present in the outer latitude bands (20-15°N or 15-20°S), resulting in a small number of deep-convective cloud tops and an increased zonal variation in the derived ozone column above 200 hPa. In those cases, the northern or southern boundary for the GOME-CCD analysis is limited to lower latitudes.

In the second step, cloud-free GOME measurements ($f \leq 0.1$) are used to determine the total ozone column, as shown on the right of Figure 4.3. In the case of cloud-free pixels, GOME is able to detect both ozone in the stratosphere and in the troposphere. About half of the total number of GOME measurements in the tropics are cloud-free. In the case of cloud-free measurements, an efficiency correction is made for the reduced sensitivity of GOME for ozone in the lower troposphere. A description of the GOME efficiency correction is given in the Appendix (Section 4.6). The retrieval efficiency of GOME for the TTOC below 200 hPa is usually higher than 90 percent. After the efficiency correction, the total ozone columns are monthly averaged on a 2.5 by 5 degree grid. In a last step, the ozone column above 200 hPa is subtracted from the gridded total ozone values, resulting in the monthly-averaged TTOC below 200 hPa.

4.3.2 Zonal variations in the ozone column above 200 hPa

The assumption made in the GOME-CCD method is that the ozone column above 200 hPa is independent of longitude in the tropics. In previous tropical tropospheric ozone studies [Thompson and Hudson, 1999; Ziemke and Chandra, 1999 and references therein], the assumption of a zonally invariant stratospheric ozone column (above ~100 hPa) has been examined. In these studies ozone data from the HALOE and MLS satellite instruments have been used to analyse the tropical stratospheric ozone column. They indicate that although the stratospheric ozone column is relatively invariant, the zonal variability is still of the order of 5-10 DU. HALOE stratospheric ozone columns show a zonal variability of about 5 DU. However, the interpretation of HALOE data is hampered by the relatively large error in the HALOE mixing ratio in the lower stratosphere (for example 18% at 40 hPa and 30% at 100 hPa), resulting in an error of 5-9 DU in the stratospheric column measurements from HALOE. Comparisons of the stratospheric ozone column derived with the MR method with integrated MLS ozone from 1 to 100 mbar, show differences of up to 15 DU. However, MLS ozone below the 46 hPa level is neither very precise, resulting in an error in the stratospheric column that may exceed 10 DU.

The ozone column above 200 hPa contains both stratospheric ozone and ozone in the tropical transition layer below the tropopause. Because of the errors in the HALOE and MLS ozone data below 100 hPa, it is even more problematic to use the data of these satellites to analyse the assumption of a zonally invariant ozone column above 200 hPa, as used in the GOME-CCD method. Therefore, in this study comparisons have been made with 0-200 hPa ozone columns based on ozonesonde data from the SHADOZ network. Sonde measurements between the surface and the 200 hPa level were integrated and subtracted from GOME total

ozone measurements to derive the ozone column above 200 hPa. The ozone column above 200 hPa is not derived directly from the sondes because of potential inaccuracies from extrapolating ozone above the sonde burst altitude [Thompson *et al.*, 2003a]. Figure 4.4a shows a comparison for the ozonesonde site American Samoa (14°S,171°W). The monthly-mean 0-200 hPa ozone column based on sonde measurements is plotted against the monthly-mean 0-200 hPa ozone column derived with the GOME-CCD method for the latitude band 12.5-15°S. The agreement is generally good with an RMS difference of 4.4 DU, although the variability in the sonde measurements is larger than variability in the zonally averaged GOME-CCD values. The comparison for Nairobi (1°S,37°E), in the latitude band 0-2.5°S is shown in Figure 4.4b, here there is a bias of 3.2 DU (underestimation by the 0-200 hPa ozone column derived with the GOME-CCD method) and a RMS difference of 4.7 DU. Comparisons for the other 6 equatorial SHADOZ sites show a comparable agreement: the biases are within the +/- 3 DU range and the RMS differences at the sonde sites lie between 4 and 7 DU. This shows that the assumption that the monthly-mean ozone column above 200 hPa (including both ozone in the stratosphere and the tropical transition layer) is invariant with longitude has sufficient validity to derive a TTOC that contains information about the tropospheric ozone variability.

4.3.3 The tropical tropospheric ozone column below 200 hPa

With the GOME-CCD method, monthly-averaged ozone columns below 200 hPa have been calculated on a 2.5 by 5 degree grid for the tropical region (usually between 20°N and 20°S) from July 1995 (to present). The images and data are available on the Internet at <http://www.temis.nl/>.

We have assessed the accuracy of the GOME-CCD method by comparing the TTOCs with tropical ozonesonde measurements from the SHADOZ network [Thompson *et al.*, 2003a]. Measurements have been used from 7 sites: American Samoa (14°S,171°W), San Cristóbal (1°S,90°W), Natal (5°S,35°W), Ascension (8°S,14°W), Nairobi (1°S,37°E), Malindi (3°S,40°E), and Watukosek (8°S,113°E), and from one site in the northern tropics: Paramaribo (6°N, 55°W). For most sites, ozonesonde measurements are available throughout the period July 1998 – December 2001. For the comparison, the ozonesonde profiles have been integrated from the ground to the 200 hPa pressure level and then the monthly mean and standard deviation were calculated. At most stations, there were between 3 to 5 ozonesonde measurements each month. A detailed description of the tropospheric ozone variability for these stations is given in Thompson *et al.* [2003b].

Figure 4.4 (opposite) Ozone columns above 200 hPa for American Samoa and Nairobi for the period July 1998 to December 2001. Ozonesonde measurements between the surface and the 200 hPa level are integrated and subtracted from GOME total ozone measurements (asterisks). The diamonds denote the ozone column above 200 hPa derived with the GOME-CCD method for the latitude band (top) 12.5-15°S and (bottom) 0-2.5°S. The bias and RMS difference between the two datasets are shown as well.

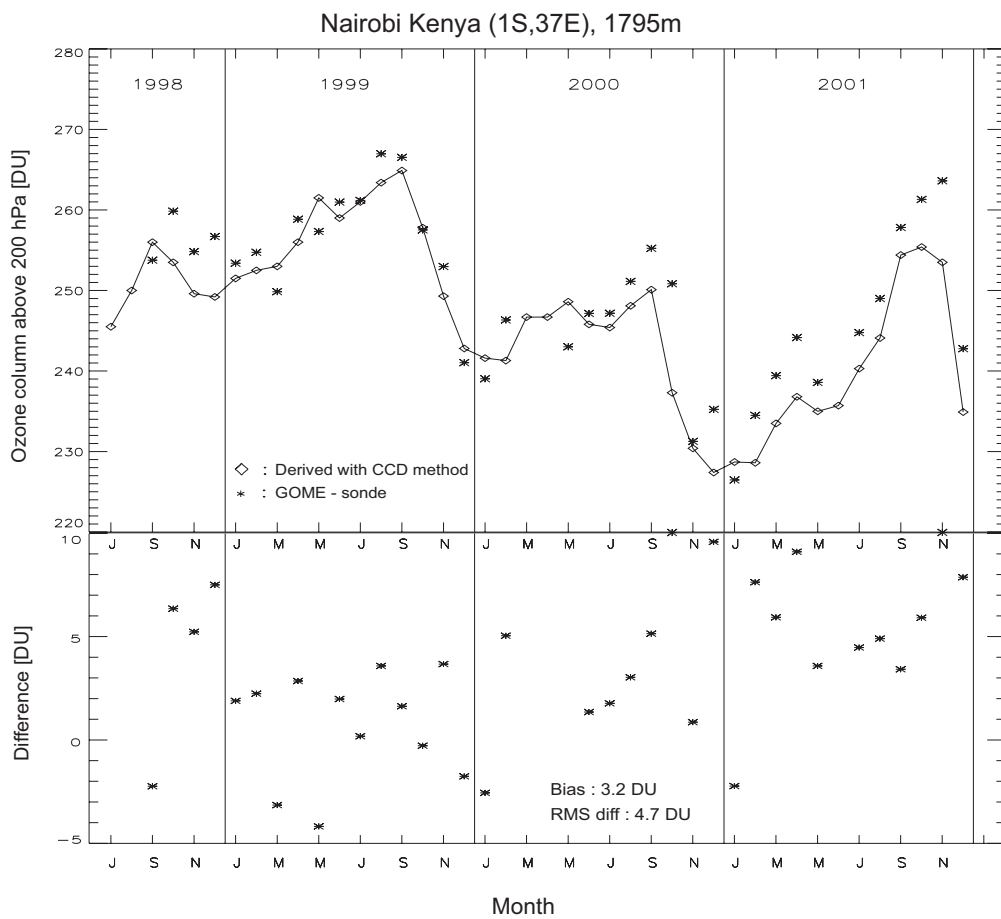
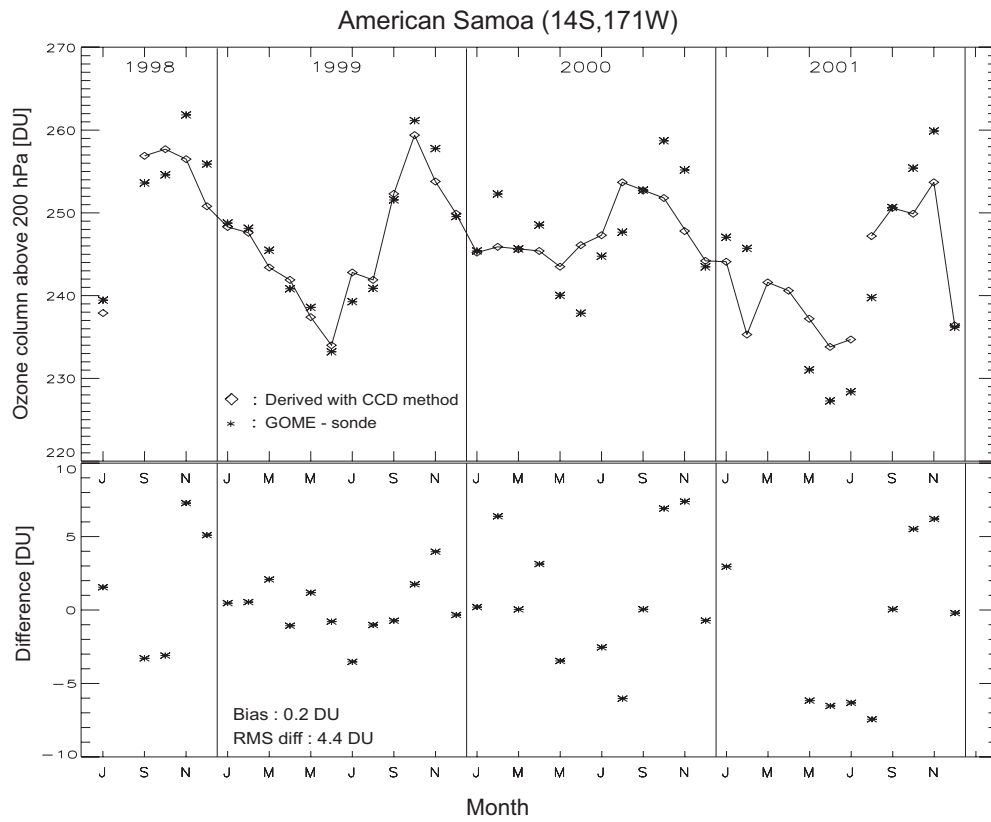


Figure 4.5a shows the comparison for the Brazilian station Natal for the period July 1998 – December 2001. There is good agreement between the GOME-TTOC values and sonde measurements, with an RMS difference of only 4.2 DU (correlation coefficient is 0.77). There is a strong yearly increase in tropospheric ozone during the biomass burning season, starting in June/July and ending in October/November. The comparison for American Samoa is shown in Figure 4.5b. Above Samoa over the Pacific Ocean, the tropospheric ozone columns are usually very low, with values of less than 20 DU, due to deep convection of ozone poor air. The slight increase in the TTOC between September and November is ozone rich air transported from African biomass burning areas [Thompson *et al.*, 2003b].

Figure 4.5c shows the comparison for the northern tropical station, Paramaribo. Here, the seasonal variation in the tropospheric ozone column is explained by the migration of the ITCZ over Paramaribo, twice a year, between December-February and April-August [Peters *et al.*, 2002b]. In both wet seasons, the tropospheric ozone columns are fairly low, due to convection of humid and ozone poor air. The increase in the tropospheric ozone values during the long dry season (August-December) is present in both the GOME-TTOCs and the sonde measurements. Note that the GOME-CCD method captures this seasonal variation better than the TOMS-TTOC products [Peters *et al.*, 2002b].

Table 4.1 lists the monthly and yearly-averaged GOME-TTOCs at the 8 ozonesonde locations, and the RMS difference between the GOME and sonde TTOCs. For all sites, the RMS difference is between 4 and 6 DU, in accordance with the estimated uncertainty in the monthly-mean ozone column above 200 hPa (see Section 4.3.2).

Although the number of tropical ozonesonde sites has increased considerably with the SHADOZ network, the coverage in the tropics is still limited, especially on the Northern Hemisphere. The temporal and geographical variability of the tropospheric ozone column is large and there is usually only one sonde measurement each week. The uncertainty in the monthly-averaged TTOC from sondes can therefore be quite large, as can be seen from the occasionally large 1σ intervals in Figure 4.5. A complication for the interpretation of the TTOC with ozonesondes, is the fact that GOME has a relatively large GOME ground pixel ($40 \times 320 \text{ km}^2$), while the ozonesondes are point measurements. The use of chemistry-transport models to support the interpretation of the TTOC is most obvious, since the spatial scales of the satellite and model ozone fields are comparable. For example, the GEOS-CHEM and TM3 models have recently been used in TOMS-TTOC interpretation studies [Martin *et al.*, 2002a; Peters *et al.*, 2002a]. Here, we use the TM3 model to interpret observed variability in the GOME-TTOC.

Figure 4.5 (opposite) Tropospheric ozone columns (below 200 hPa) for Natal, American Samoa and Paramaribo for the period July 1998 – December 2001. The asterisks denote the integrated ozonesonde measurements with 1σ error bars (if there was only one sonde measurements in a particular month, the error bar is omitted). The diamonds denote the TTOCs derived with the GOME-CCD method. For Natal, the TTOCs calculated with TM3 chemistry transport model (squares) are also shown for the years 2000 and 2001 (see Section 4.4.2).

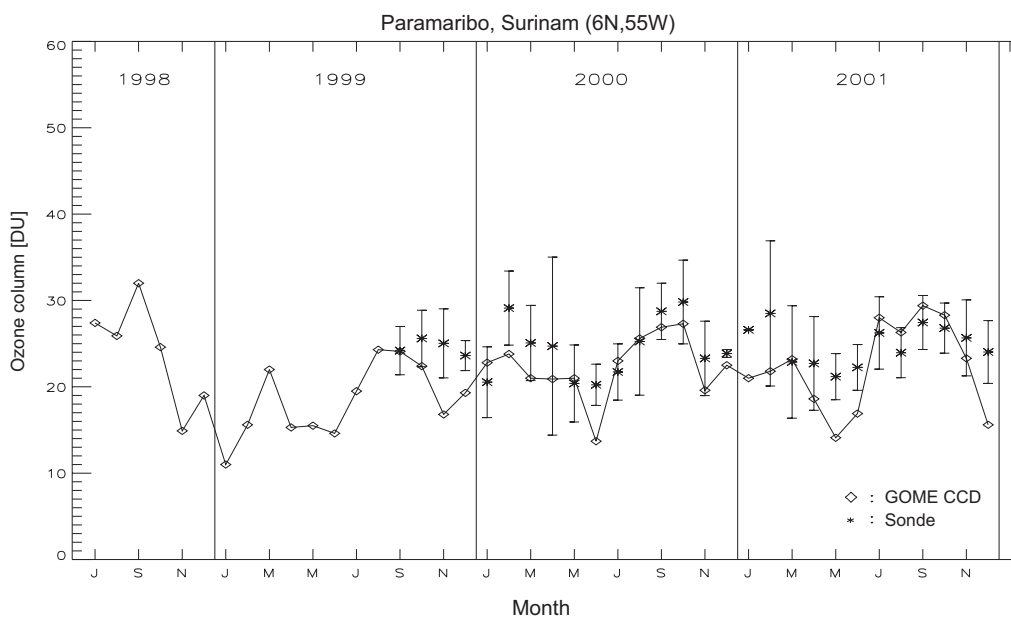
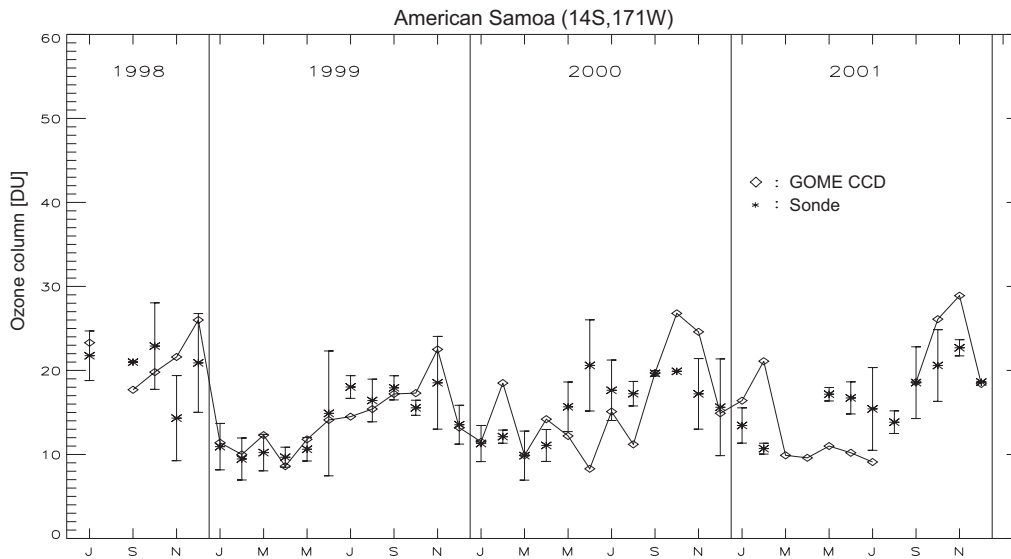
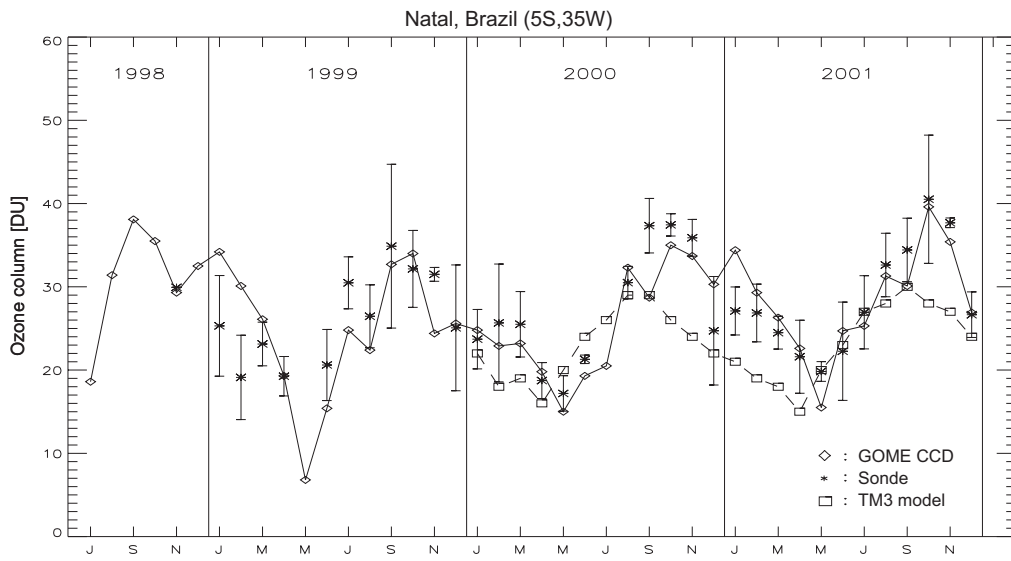


Table 4.1 Monthly and yearly averaged GOME-TTOC at eight SHADOZ ozonesonde sites, based on three year of GOME data (1999-2001)^a. All values are in DU.

| Ozonesonde site | Jan | Feb | Mar | Apr | May | Jun | Jul | Aug | Sep | Oct | Nov | Dec | Year | RMS |
|----------------------------|------|------|------|------|------|------|------|------|------|------|------|------|------|-----|
| Samoa (14°S, 171°W) | 13.1 | 16.5 | 10.7 | 10.8 | 11.7 | 10.9 | 12.9 | 11.0 | 18.5 | 23.4 | 25.3 | 15.5 | 15.0 | 4.7 |
| San Cristóbal (1°S, 90°W) | 16.9 | 17.0 | 15.9 | 14.2 | 10.3 | 12.5 | 14.8 | 24.7 | 20.3 | 13.1 | 15.5 | 14.1 | 15.7 | 4.0 |
| Paramaribo (6°N, 55°W) | 21.9 | 22.8 | 22.1 | 19.8 | 17.5 | 15.3 | 25.5 | 26.0 | 28.1 | 27.8 | 21.5 | 19.0 | 22.3 | 4.1 |
| Natal (5°S, 35°W) | 31.1 | 27.4 | 25.2 | 20.6 | 12.4 | 19.8 | 23.5 | 28.7 | 30.5 | 36.2 | 31.2 | 27.6 | 26.2 | 4.2 |
| Ascension Isl. (8°S, 14°W) | 30.4 | 30.1 | 28.2 | 25.9 | 20.4 | 21.1 | 23.1 | 29.4 | 29.4 | 32.8 | 27.2 | 29.1 | 27.3 | 5.7 |
| Nairobi (1°S, 37°E) | 18.2 | 23.9 | 21.3 | 28.3 | 22.9 | 25.6 | 25.5 | 26.5 | 26.1 | 29.1 | 28.6 | 27.3 | 25.3 | 5.3 |
| Malindi (3°S, 40°E) | 19.9 | 21.8 | 18.0 | 25.1 | 24.3 | 23.5 | 23.9 | 27.1 | 24.3 | 30.1 | 28.4 | 26.8 | 24.4 | 5.2 |
| WatuKosek (8°S, 113°E) | 11.5 | 13.6 | 11.3 | 11.6 | 12.5 | 11.9 | 11.8 | 13.2 | 15.3 | 17.0 | 14.2 | 18.5 | 13.5 | 5.2 |

^aThe last column denotes the RMS difference between the collocated GOME-TTOC and the TTOC calculated from the ozonesonde measurements.

4.4 TTOC variability examined with the GOME-CCD method and the TM3 model

There are pronounced differences between the GOME-TTOC distributions in 2000 and 2001, both in the southern- and northern tropics. Therefore, we focus on the TTOC distributions in these years, and use the TM3 chemistry-transport model to interpret the differences.

4.4.1 The TM3 chemistry-transport model

TM3 (Tracer Model version 3) is a widely used global off-line chemistry-transport model. Recent model validation studies, in particular of the global 3-D distributions of tropospheric ozone and methane are documented in *Peters et al.* [2002a], *Dentener et al.* [2003], *Prather et al.* [2001] and *Lelieveld and Dentener* [2000].

In this study, TM3 is applied at its presently highest horizontal resolution of 2.5°x2.5°, with 31 vertical layers. The model uses meteorological fields from the ECMWF operational weather model for the years 2000-2001. These fields include global distributions for horizontal wind, surface pressure, temperature, humidity, liquid water content, ice water content, cloud cover, large scale and convective precipitation, and boundary layer parameters. Stratospheric boundary conditions for ozone are applied by relaxation of stratospheric ozone at levels above 50 hPa towards TOMS zonal monthly-mean ozone columns. The vertical distribution of ozone above 50 hPa is taken from the *Fortuin and Kelder* [1998] climatology. *Lelieveld and Dentener* [2000] showed that this technique resulted in realistic values for atmospheric ozone columns. The calculated net ozone flux from the stratosphere is about 600 Tg using ECMWF operational meteorological data for the year 2000.

The model includes full HO_x-NO_x-SO_x-CO-CH₄-NMHC chemistry, as described by *Houweling et al.* [1998]. In total 38 gaseous constituents are considered, of which 23 tracers are transported, and 110 gas phase reactions. Photolysis rates are calculated based on the

parameterisation by *Landgraf and Crutzen* [1998], accounting for overhead ozone column, cloud scattering, and surface reflection following *Krol and van Weele* [1997]. The yearly anthropogenic emissions of NO_x , CO and NMHC are taken from the historical emission database developed by *Van Aardenne et al.* [2001], which is based on the Emission Database for Global Atmospheric Research (EDGAR) inventory [*Olivier et al.*, 1996]. The emissions for 2000-2001 are obtained by extrapolation of the 1990 emissions using statistics from *Marland et al.* [2000], similar to what has been done for the year 2000 runs in the OxComp model intercomparison, organised in preparation of the Intergovernmental Panel on Climate Change (IPCC) Third Assessment Report [*Prather et al.*, 2001]. Isoprene emissions (~ 400 Tg(C)/yr, including monoterpenes) are daylight dependent and based on *Guenther et al.* [1995]. Agricultural and natural soil NO_x emissions (~ 5.5 Tg(N)/yr) are monthly varied and based on *Yienger and Levy* [1995]. For the temporal distribution of the biomass emissions, the model relies on the *Hao and Liu* [1994] fire calendar, which contains monthly fractions of annual amounts of biomass burned on a $5^\circ \times 5^\circ$ resolution. Important to note is that the biomass emissions data do not resolve inter-annual variability. The yearly totals remain the same (~ 7 Tg(N)/yr), while the emissions maximize in August and September (0.77 and 0.61 Tg(N), respectively). The NO_x production resulting from lightning discharges is coupled to the convective precipitation in the model [*Meijer et al.*, 2001]. The total NO_x emission from lightning in the model is about 5 Tg(N)/yr, but varies slightly from year to year, due to the coupling to convective precipitation (in the tropics the interannual variation in the total lightning emission is about 5%).

4.4.2 Southern Tropics

Figure 4.6 shows the observed monthly-averaged TTOC for October 2000 and October 2001, derived with the GOME-CCD method. In the month October, the zonal wave-one pattern in the southern tropics is very pronounced, showing a maximum in tropospheric ozone over the Atlantic Ocean and a minimum over the Pacific Ocean. In 2001, maximum GOME-TTOC values of 40-45 DU are found over a large area over Africa and the southern Atlantic, while minimum values of 10 DU or less are found over the Pacific. Several studies have suggested that the South-Atlantic TTOC maximum can be attributed to a complex interaction of biomass burning, lightning and large-scale transport [*Krishnamurti et al.*, 1993, 1996; *Thompson et al.*, 1996; *Chatfield et al.*, 1998, *Jacob et al.*, 1996; *Pickering et al.*, 1996, *Martin et al.*, 2002a]. The large-scale ozone increases over the southern Atlantic occur primarily in the middle and upper tropical troposphere. An interesting phenomenon is the difference between the South-Atlantic TTOC maximum in 2000 and 2001 (Figure 4.6). In 2000, the maximum in TTOC over the southern Atlantic was much less pronounced than in 2001, with maximum GOME-TTOC values of 30-40 DU.

To find out if there are any differences between the biomass burning emissions in 2000 and 2001, monthly global fire maps from the ATSR (Along-Trace Scanning Radiometer) satellite instrument have been examined [*Arino et al.*, 2001]. These global fire maps are available from the ATSR World Fire Atlas at <http://shark1.esrin.esa.int/iona/FIRE/AF/ATSR/>. Surprisingly, the ATSR fire maps show that the African and South American fires in the

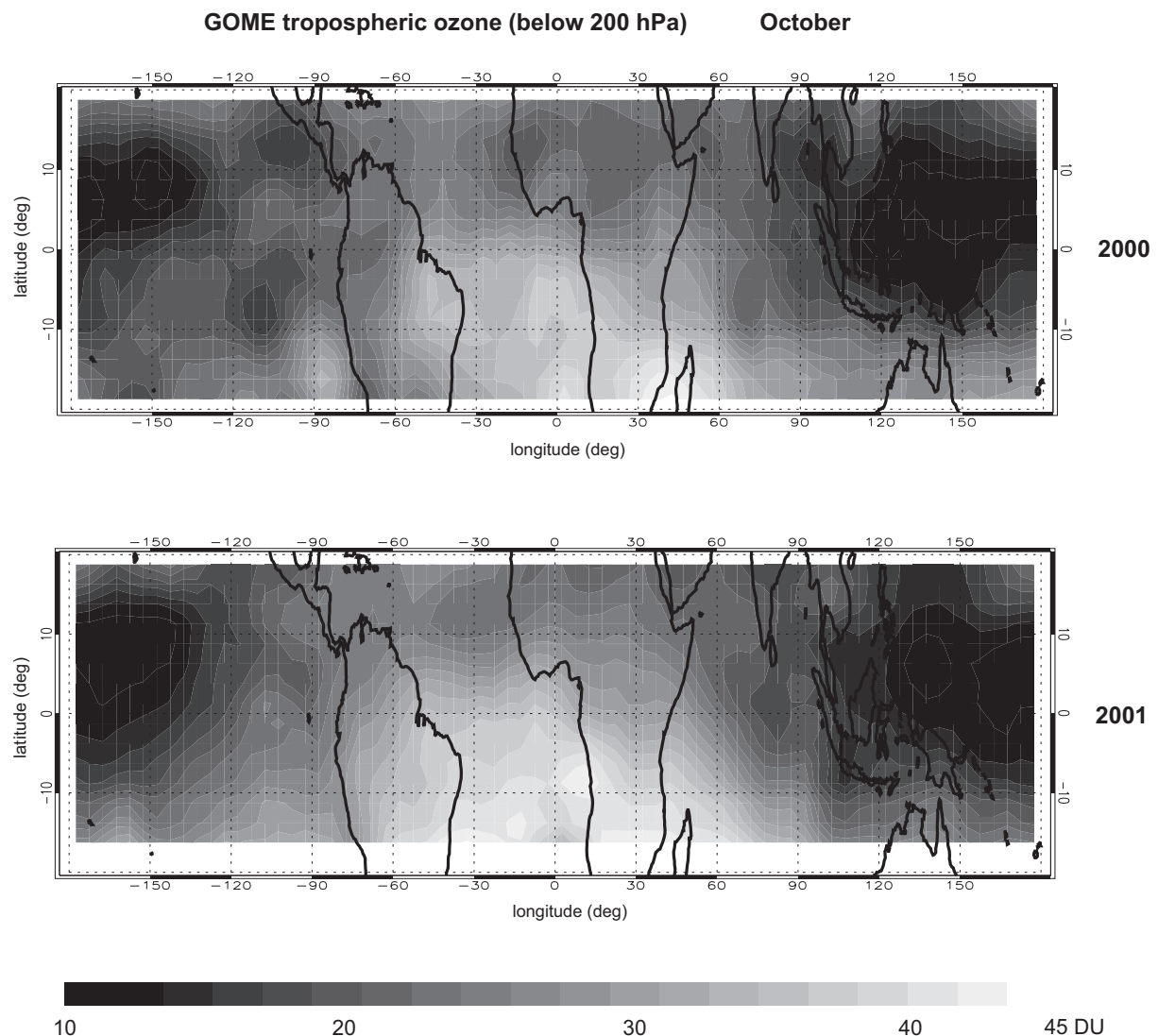


Figure 4.6 Tropical tropospheric ozone columns (below 200 hPa) derived with the GOME-CCD method for (top) October 2000 and (bottom) October 2001.

period August-October are less widespread in 2001 than in 2000. This indicates that other processes such as transport and lightning must play a major role in the development of the South-Atlantic TTOC maximum.

The modelled TTOC for October 2001 (Figure 4.7) shows a similar general pattern as the GOME-TTOC, but there are distinct differences in the absolute values. The modelled maximum values over the southern Atlantic are 7-12 DU smaller than the GOME observations. A gradient is present in the modelled TTOC between Africa and South America, while there is a broader maximum in the GOME observations. In contrast, the minimum TTOC values over the Pacific agree quite well. The TTOC model results for Natal (Figure 4.5a) show that the seasonal variation of the modelled TTOC over the southern Atlantic is similar to that of the GOME and ozonesonde observations. However, the TTOC values in the TM3 model are lower in most months. A widespread underestimation of the TTOC in the TM3 model over the tropical Atlantic was also found by *Peters et al.* [2002a]. They concluded

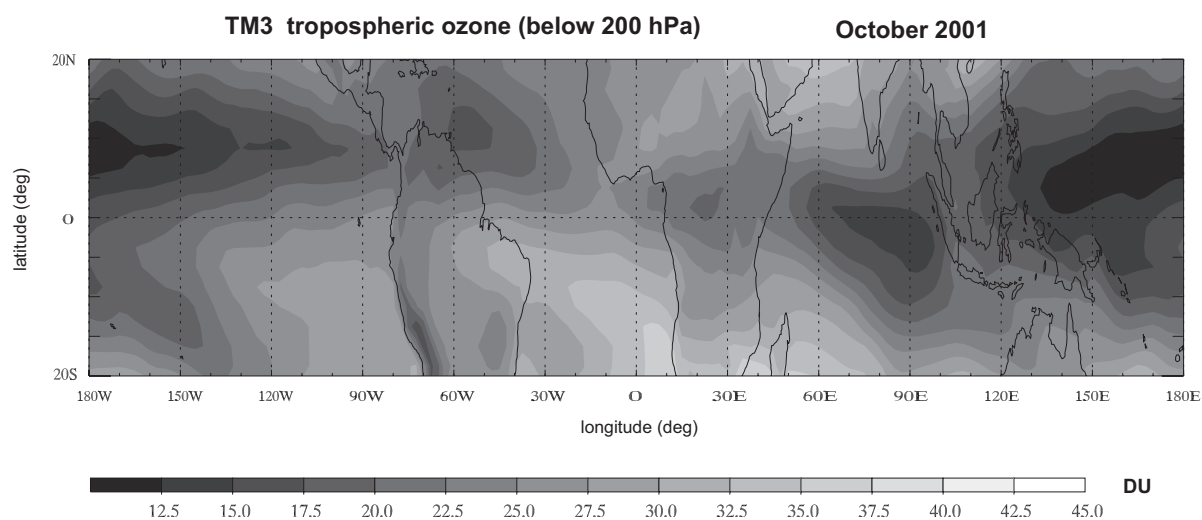


Figure 4.7 *Tropical tropospheric ozone columns (below 200 hPa) calculated with the TM3 model for October 2001.*

that systematic improvements in the model can be achieved with a better representation of biomass burning emissions (e.g. including inter-annual variability), but that it is unlikely that this is the only factor responsible for the observed differences.

In the month September, the (modelled) ozone production over the southern Atlantic is largest and the ozone plume is formed. The observed difference between the TTOCs in September 2001 and September 2000 is shown in Figure 4.8 (top panel), together with the modelled difference (lower panel). In 2001, the GOME-TTOCs are higher over eastern Africa and the western Indian Ocean, and over the tropical Atlantic between the equator and 10°S, as compared to 2000. The largest differences in the TTOC are found over eastern Africa and the western Indian Ocean, where the GOME-TTOCs are 10-15 DU higher in September 2001. The pattern of the modelled differences is similar to that of the GOME-TTOC, with the largest differences over eastern Africa and western Indian Ocean. The maximum differences (7-9 DU) over this region are smaller than in the GOME-TTOC observations.

The effect of lightning emissions and large-scale transport on the TTOC distributions in September 2000 and September 2001 has been studied with the TM3 model. Figure 4.9a shows the difference between the TM3 base run and a run in which the lightning emissions during September were switched-off. Hence, this figure illustrates the geographical pattern of the lightning perturbation to the TTOC in September 2001. The largest lightning perturbations are found over the tropical Atlantic and the south-east Pacific. The lightning perturbation figures are quite similar for other months, with maximum enhancements over the same tropical regions. The magnitude of the lightning perturbations is comparable to that of the biomass burning perturbations (Figure 4.9b shows the difference between the TM3 base run and a run in which all biomass burning emissions (NO_x , SO_2 , CO , CH_4 , NMHCs and NH_3) were switched off during September), however, the biomass burning perturbations are more concentrated over the continents near the source regions.

Since the NO_x emission from lightning varies slightly from year to year in the model, we have also compared the lightning perturbations in September 2000 and 2001. The lightning perturbations to the TTOC is slightly larger in September 2001 over eastern tropical Africa

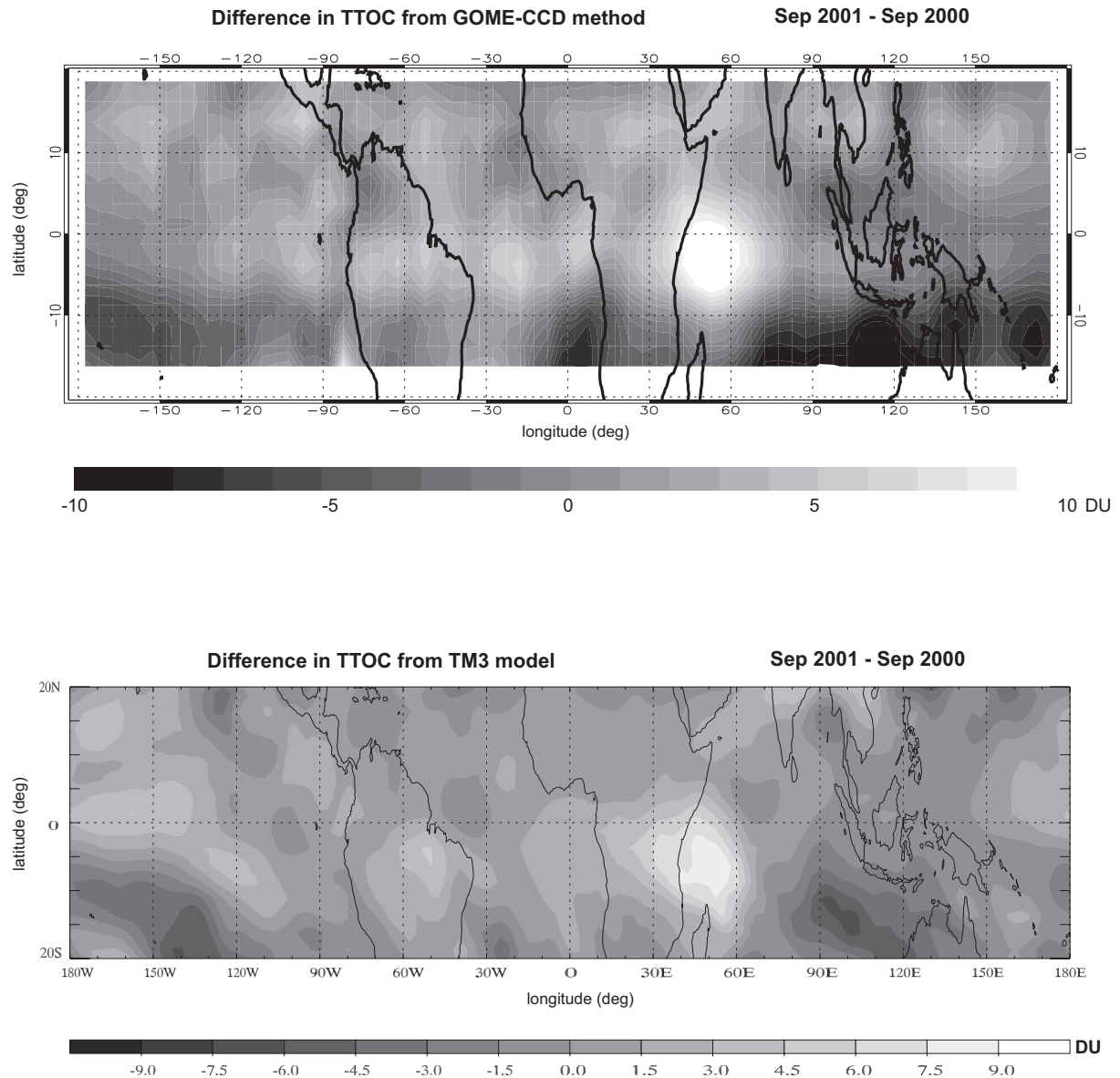


Figure 4.8 Difference between the TTOC (below 200 hPa) in September 2001 and 2000: (top) difference in the TTOC derived with the GOME-CCD method and (bottom) difference in the TTOC calculated with the TM3 model.

and South America (1-2 DU), but this can not explain the much larger differences observed in the TTOC, as shown in Figure 4.8.

The ECMWF wind fields used in the TM3 model indicate that the difference between the TTOC distributions in September 2000 and September 2001 can be explained by differences in transport in the middle troposphere (500-300 hPa). Both in 2000 and 2001, there are no ENSO (El Niño-Southern Oscillation) influences on the large-scale circulation, and a normal Walker (east-west) circulation is present in the tropical atmosphere. However, in September 2001 there is a stronger south-north transport of ozone rich air over eastern Africa (south of the ITCZ), and the Walker circulation is more pronounced than in September 2000. This

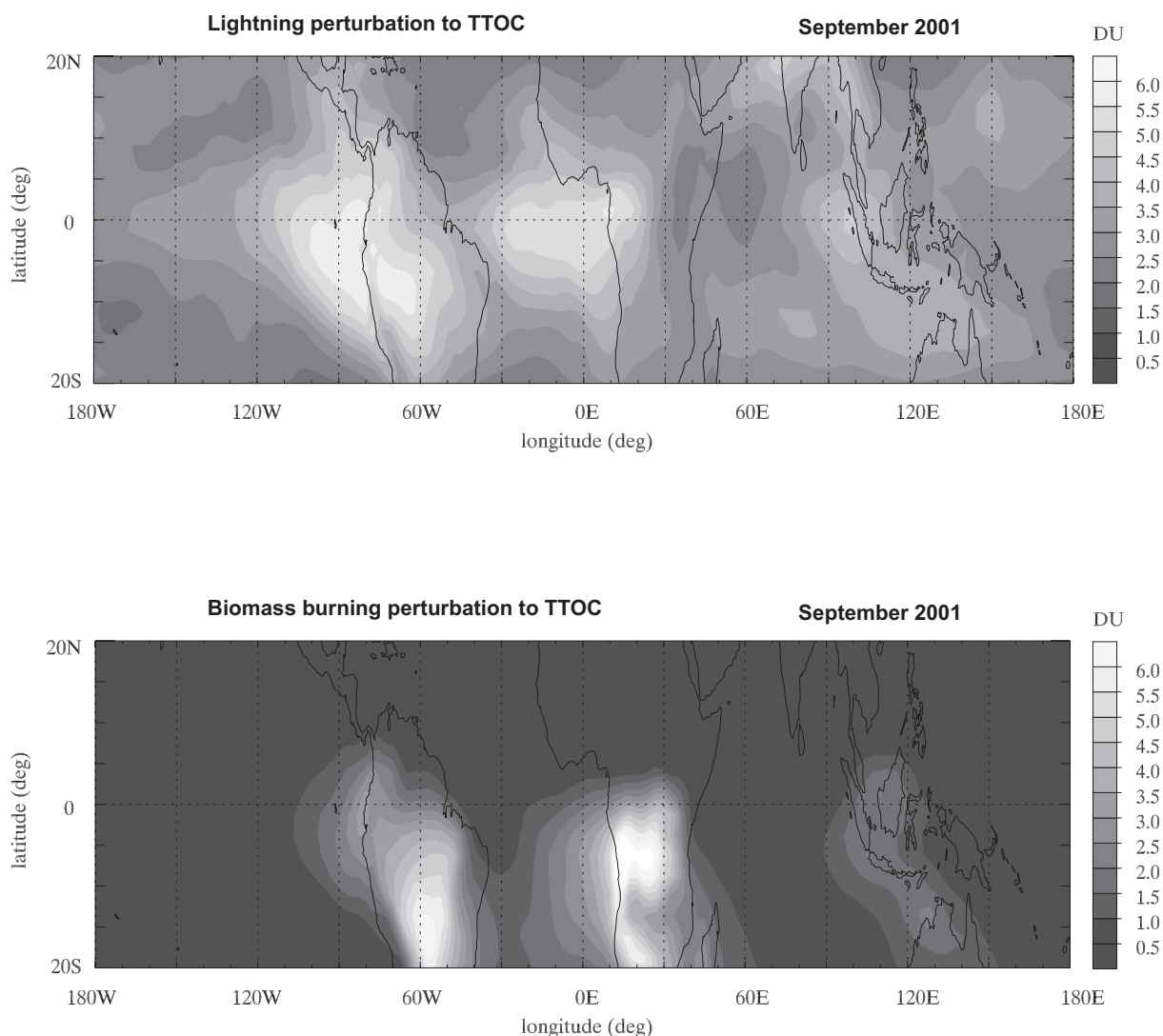


Figure 4.9 Geographical pattern of the perturbations by (top) the September lightning NO_x emissions and (bottom) biomass burning emissions to the TTOC. The perturbations are calculated with the TM3 model for September 2001.

resulted in subsidence over the southern tropical Atlantic and the western Indian ocean. These conditions are favourable for high TTOC values over these regions, and can at least partly explain the observed differences between the South-Atlantic TTOC maximum in September-October 2000 and September-October 2001. That the differences in the GOME-TTOCs are more pronounced than in the modelled TTOCs can have various causes. Potential differences arise from the uncertainty in the lightning NO_x production in the model, the calculated stratosphere-troposphere exchange in the sub-tropics and subsequent transport to the tropics, and the spatial distribution and magnitude of the biomass emissions, as discussed by *Peters et al.* [2002a].

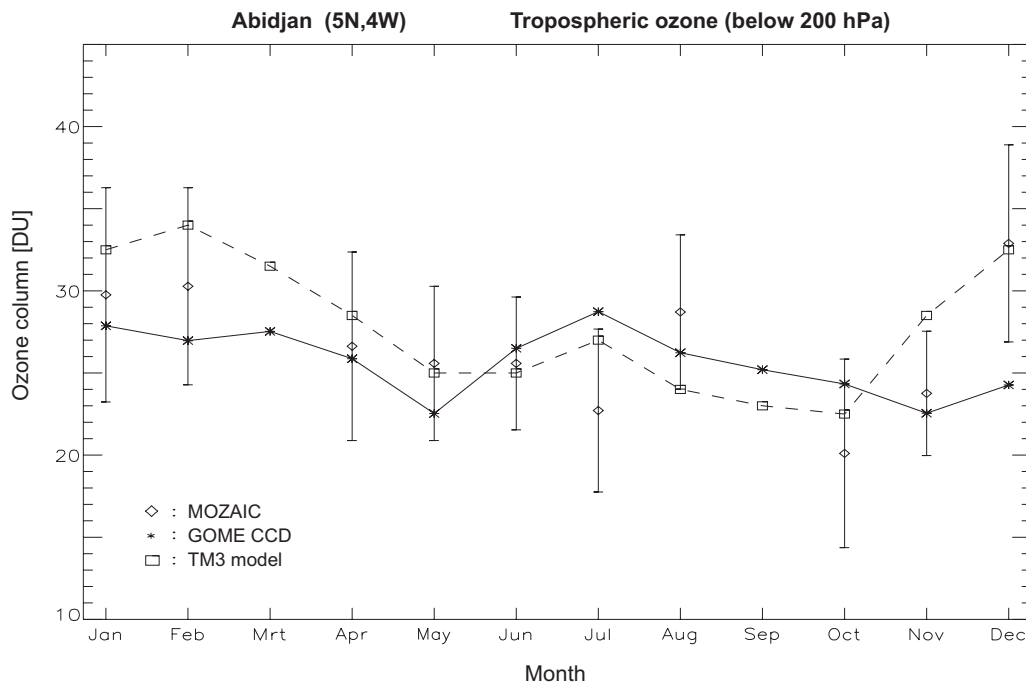


Figure 4.10 Seasonal variation in the tropospheric ozone column (below 200 hPa) for Abidjan. The diamonds denote MOZAIC aircraft measurements with error bars (standard deviation). The asterisks denote the TTOCs derived with the GOME-CCD method and the squares are the TM3 model results. The GOME and TM3 data are from 2000-2001; the MOZAIC data are from 1997-2000.

4.4.3 Northern Tropics

The second analysis focuses on sub-Saharan northern Africa and the northern tropical Atlantic. The TTOC over these regions are influenced by large-scale biomass burnings over Africa during the northern biomass season in December-February. These fires are very apparent in the ATSR World Fire Atlas. Aircraft measurements from the MOZAIC program [Marenco *et al.*, 1998] and studies with global tropospheric chemistry models [Martin *et al.*, 2002a; Peters *et al.*, 2002a] found enhanced ozone concentrations over these regions during the biomass burning season. In the northern tropics, the increases in ozone concentrations during the biomass burning season occur mainly in the lower troposphere, while the largest increases over the southern Atlantic occur in the middle troposphere. This is confirmed by the TM3 model results (not shown). The low altitude of the ozone variability hampers UV satellite measurements (e.g. from GOME and TOMS) to detect this variability to its full extent (see Appendix in Section 4.6).

The TTOCs derived with the TOMS-CCD and MR methods do not show a clear enhancement in tropospheric ozone during the northern biomass burning season [Thompson *et al.*, 2000; Martin *et al.*, 2002a]. Although the TOMS-CCD data have been improved by Martin *et al.* with an efficiency correction for ozone changes in the lower troposphere, the seasonal cycle of the TTOC values for northern Africa still do not compare well with MOZAIC aircraft measurements. This can be seen from Figure 7 in Martin *et al.* [2002a] for

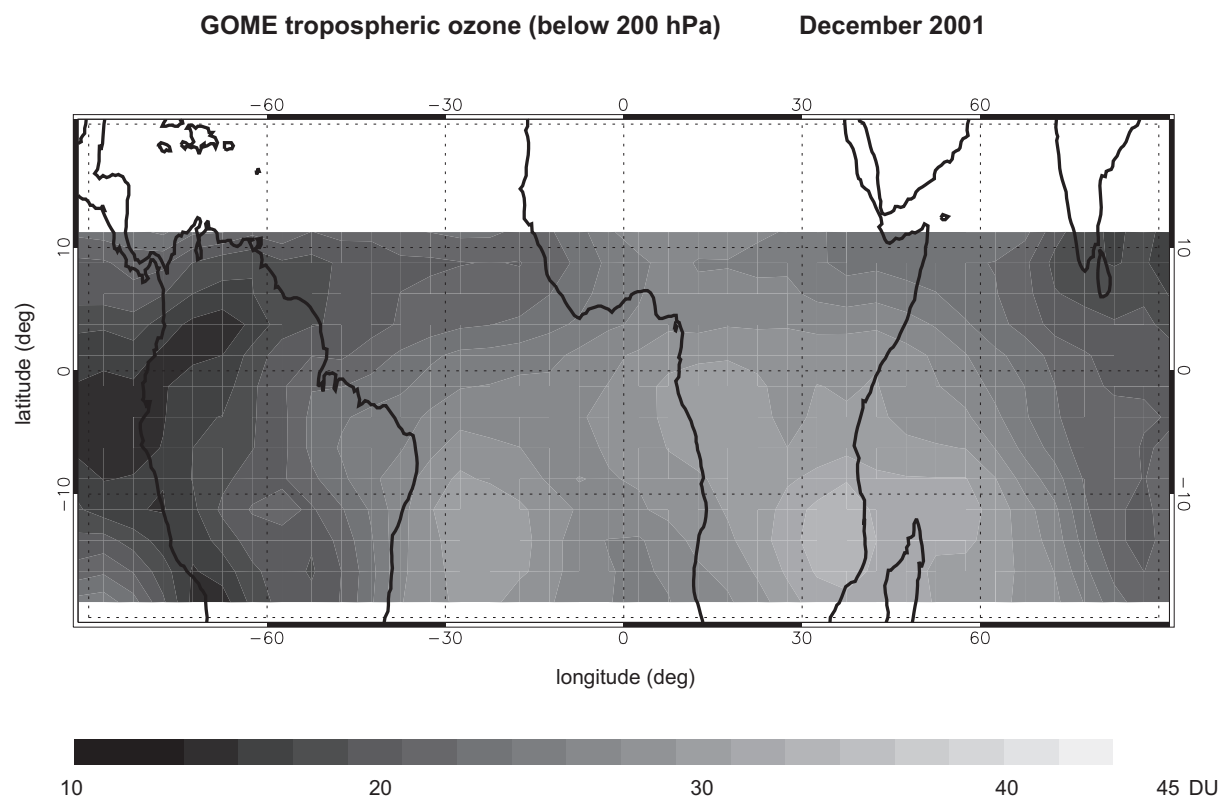


Figure 4.11 Tropospheric ozone columns (below 200 hPa) derived with the GOME-CCD method for December 2001. (The coverage of the TTOC field is limited to 20°S–10°N because there were only a small number of above-cloud GOME measurements north of 10°N).

the African site Abidjan (5°N,4°W). A similar comparison of the MOZAIC observations for Abidjan with the GOME-TTOCs and the TM3 model is shown in Figure 4.10. The overall agreement of the GOME-TTOCs with the MOZAIC observations is quite satisfactory and notably better than the TTOCs from the TOMS-CCD method. The GOME-TTOCs do not overestimate tropospheric ozone over northern Africa between June and October. However, there is a TTOC maximum between December-February in the MOZAIC observations, which is not captured by the GOME-CCD method. Note that the seasonal variation is much smaller than over the southern Atlantic (e.g. compared to Natal in Figure 4.5a). Furthermore, the uncertainty in the GOME-TTOCs is about 5 DU, which is relatively large compared to the observed seasonal variation in the MOZAIC measurements.

An interesting and exceptional situation in the northern tropics occurred during the biomass burning season December 2001-January 2002. In both months, there were almost no fires over northern Africa. This is an unusual phenomenon that has not occurred during the last decade (derived from AVHRR and ATSR World Fire Atlas data). The absence of biomass burnings has a large effect on the TTOC as can be seen in Figure 4.11, which shows the GOME-TTOCs for December 2001. The TTOCs over the Atlantic between the equator and 10°N are small, with values of 20 DU or less. The easterly trade winds in the lower troposphere (apparent in the ECMWF wind fields for this month) transport the air from sub-Saharan northern Africa over the Atlantic. Since this air was relatively clean of ozone

precursors in December 2001, the TTOCs are further reduced to about 20 DU by the chemical destruction over the ocean. Under normal conditions, the TTOC values over this region would be between 25-30 DU, as can also be seen from the average TTOCs for Abidjan (Figure 4.10).

4.5 Conclusions and future outlook

We have developed a convective-cloud-differential (CCD) method based on Global Ozone Monitoring Experiment (GOME) ozone column and cloud measurements. The cloud fractions and cloud top pressures derived with the GOME-FRESCO algorithm, indicate that most tropical convective cloud tops are between 300 and 500 hPa, and do not extend up to the tropopause. The GOME-CCD method takes this tropical transition layer below the tropopause into account, and uses the FRESCO cloud top pressures and GOME ozone column measurements to derive a tropical tropospheric ozone column (TTOC) below 200 hPa. Comparisons with ozonesonde measurements from the SHADOZ network show that the assumption of the GOME-CCD method of a zonally invariant ozone column above 200 hPa, including both ozone in the stratosphere and the transition layer, has good validity in the tropics.

Monthly-averaged TTOCs (below 200 hPa) have been calculated for the period July 1995-December 2001 on a 2.5° latitude by 5° degree longitude grid. Validation of the GOME-TTOCs with 7 SHADOZ ozonesonde sites show good agreement, with an RMS difference of about 5 DU. In the northern tropics, comparisons have been made with ozonesonde measurements at Paramaribo (6°N,55°W) and with MOZAIC aircraft observations at Abidjan (5°N,4°W). At these sites, the GOME-TTOCs also compare favourably with in-situ measurements. The GOME-TTOCs do not show the occasionally strong deviations seen in the TOMS-TTOC products. The seasonal variation at the northern tropical site Paramaribo is captured reasonably well.

For the GOME and TOMS instruments, the low sensitivity for ozone changes in the lower most troposphere forms a fundamental limitation in detecting lower tropospheric ozone from space. This is especially of importance for the northern tropics, where the increases in ozone concentrations during the biomass burning season occur mainly in the lower troposphere.

Analysis of the GOME-TTOCs for the years 2000 and 2001, with the aid of the chemistry-transport model TM3, illustrates that the variability in the TTOC depends on a complex interaction of several processes, including biomass burning, lightning, and large-scale transport. It is intriguing that the extent of the African and South American fires was less widespread during the biomass burning period in September-October 2001 compared to the same period in 2000, while the TTOC maximum over the southern Atlantic was much more pronounced in 2001. TM3 model results show that this can be explained by the difference in transport between the two years: in September 2001 there was a stronger south-north transport of ozone rich air over eastern Africa (south of the ITCZ) and the Walker circulation was more pronounced than in September 2000, resulting in high TTOC values over the southern Atlantic and eastern Africa.

An exceptional situation in the northern tropics occurred during the biomass burning

season December 2001-January 2002, when there were almost no fires over northern Africa. This resulted in strongly reduced TTOCs over the Atlantic between the equator and 10°N.

The analyses presented in this paper demonstrate the strength of the cloud-differential method to determine the tropical tropospheric ozone column. When the cloud-differential method is extended with a cloud slicing method, it is possible to retrieve ozone information for different tropospheric layers [Ziemke *et al.*, 2001]. Because of the large ground pixel of GOME (40x320 km²), the number of cloudy and clear sky measurements is generally too small to apply such a cloud slicing method. However, upcoming satellite instruments will greatly enhance the possibilities to retrieve information about the tropospheric ozone profile. The SCIAMACHY instrument, launched on ENVISAT in 2002, will provide collocated ozone and cloud data with a ground-pixel of 60x30 km² between 50°S and 50°N [Bovensmann *et al.*, 1999]. With SCIAMACHY, it is possible to continue and improve the present TTOC time series from the GOME and TOMS instruments. Furthermore, the small pixel size in the (sub)tropics and mid-latitudes allows the retrieval of tropospheric profile information with the cloud slicing method. Tropospheric ozone data derived with cloud-differentials techniques can also be used for comparisons with the more complex tropospheric residual methods, in which ozone columns measurements are combined with ozone profile measurements (e.g. from limb soundings). In the near future, we expect that the combination of satellite TTOC measurements with chemistry transport models like TM3 through data-assimilation techniques, may further improve our knowledge of the tropospheric ozone distribution.

4.6 Appendix: GOME retrieval efficiency

The ability of GOME and other nadir-looking UV spectrometers (e.g. TOMS), to detect ozone changes in the atmosphere depends on the height where the ozone concentration is changed, the surface albedo, the presence of clouds and aerosols, the viewing geometry and the wavelengths used in the retrieval algorithm. For the GOME ozone retrieval wavelengths, 325-335 nm, most of the radiance seen by the satellite instrument is scattered from the middle and lower troposphere or reflected from the Earth surface. The sensitivity of GOME for ozone changes in the tropical stratosphere and upper troposphere (above about 6 km) is therefore close to 100 percent. For the lower and middle troposphere the situation is different. For low surface albedos (< 0.1, e.g. vegetation and oceans), part of the radiance measured by GOME has not passed through the lower troposphere, and therefore the sensitivity for ozone changes in the lower part of the troposphere decreases to 30 percent or less near the ground. Over highly reflecting surfaces, such as clouds, the radiance reflected from this surface will dominate the scattered radiance, and the sensitivity for ozone changes above the reflecting surface will be close to 100 percent, or even a little bit higher due to multiple scattering.

In the GOME retrieval algorithm, the reduced sensitivity in the lower and middle troposphere for cloud-free situations is taken into account by the air mass factor. However, a systematic error is introduced in the retrieved ozone column, if the actual ozone profile in the atmosphere deviates from the *a priori* ozone profile (Fortuin and Kelder [1998] climatology) used in the air mass factor calculations. In that case, an additional correction for the reduced sensitivity needs to be made, which depends primarily on the surface albedo and the

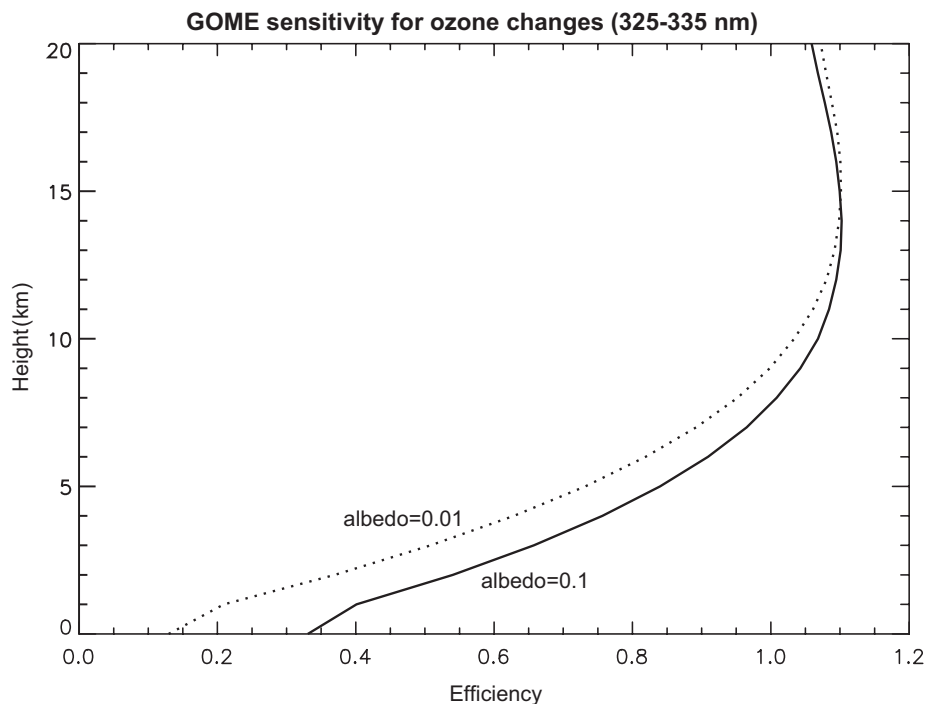


Figure 4.12 Sensitivity of the GOME instrument for ozone changes as a function of height. GOME uses the 325-335 nm wavelength region to measure the ozone column. Sensitivity profiles for two low surface albedos (0.01 and 0.1) for a typical low-latitude situation (solar zenith angle = 20°) are plotted.

difference between the actual ozone profile and the *a priori* ozone profiles used in the retrieval algorithm. How the sensitivity correction is applied for the GOME-CCD method is described below.

GOME sensitivity profiles in the 325-335 nm wavelength region have been calculated with the radiative transfer model DAK [Stammes, 2000 and references therein]. Figure 4.12 shows the sensitivity profile for two low surface albedos (0.1 and 0.01) for a typical low-latitude situation (solar zenith angle = 20°). The shape of the GOME sensitivity profile is similar to that of the TOMS instrument [Hudson *et al.*, 1995]. However, the sensitivity is slightly better due to use of the wavelength window 325-335 nm for the ozone column retrieval, which includes larger wavelengths than the main TOMS retrieval wavelength (317.5 nm). Figure 4.12 shows that the sensitivity for ozone changes in the lower and middle troposphere clearly depends of the surface albedo. Surface albedos as low as 0.01 are found over land surfaces (e.g. vegetation), while albedos of 0.1 can occur over the tropical oceans.

An exact correction for the reduced sensitivity in the lower troposphere requires information on the actual ozone profile in the troposphere. Although the GOME-CCD method does not provide ozone profile information, the estimate of the tropospheric ozone column can still be improved by using an efficiency factor ε :

$$TOC^{\text{improved}} - TOC^{\text{a-priori}} = \varepsilon (TOC^{\text{GOME}} - TOC^{\text{a-priori}}) \quad (4.3)$$

A look-up table of efficiency factors have been calculated using the GOME sensitivity profiles (Figure 4.12) and ozonesonde measurements from the SHADOZ network [Thompson *et al.*, 2003a], which serve as ‘true’ reference ozone profiles. The appropriate efficiency factor to be used in Eq. (4.3) is determined as a function on the surface albedo (derived from the Herman and Celarier [1997] and Koelemeijer *et al.* [2003] databases) and the difference between the retrieved GOME tropospheric ozone column and the *a priori* tropospheric ozone column ($TTOC^{GOME} - TTOC^{a-priori}$).

The retrieval efficiency for GOME tropospheric ozone columns below 200 hPa is generally higher than 90 percent. This relatively high efficiency is primarily due to the fact that in the GOME total ozone algorithm, *a priori* profiles from the Fortuin and Kelder [1998] ozone climatology are used. This climatology is based on actual ground-based and satellite ozone measurements and contains zonal mean ozone profiles for 10° latitude bands for each month of the year.

Acknowledgements

The research described in this paper has been performed within the framework of the TEMIS project, part of ESA’s Data User Programme. This work would not have been possible without the helpful discussions with many colleagues within the GOME community. We are grateful to ESA/ESRIN for providing the ATSR World Fire Atlas data and we thank the SHADOZ and MOZAIC communities for the availability of the ozone data. Finally, we would like to thank the reviewers for their constructive comments.

Chapter 5

Improved GOME total ozone columns: an empirical DOAS method that accounts for Raman scattering

Abstract

An improved total ozone algorithm for the Global Ozone Monitoring Experiment (GOME) instrument has been developed, which uses the Differential Optical Absorption Spectroscopy (DOAS) retrieval method. The new algorithm, TOGOMI, is based on the total ozone algorithm developed for the Ozone Monitoring Instrument (OMI), to be launched on EOS-Aura in 2004. The main improvements of the TOGOMI algorithm are: (1) a new DOAS fit-equation that properly accounts for inelastic Raman scattering, (2) the use of an empirical DOAS method to account for the wavelength dependence of the air mass factor, and (3) the use of a slant column dependent air mass factor to account for atmospheric variability. In addition, the new algorithm offers the possibility to use a 5 nm wide spectral fit window centred around 334.1 nm, to reduce the sensitivity to the ozone profile and atmospheric temperature. The new DOAS fit-equation results in 3-10% larger ozone slant columns compared to the slant columns retrieved with the common DOAS fit-equation. The largest differences are found for large solar zenith angles at high latitudes, due to the increase in Raman scattered light. The empirical air mass factor approach used in the TOGOMI algorithm, reduces the errors involved in the DOAS method when the atmosphere becomes optically thick at high solar zenith angles. The uncertainty in the air mass factor due to the natural ozone profile variability, is reduced by using a slant column dependent air mass factor, based on the ozone profile climatology from Logan, Labow & McPeters. A preliminary validation of the improved ozone columns with ground-based Brewer and Dobson measurements shows a very good agreement. The differences with the ground-based measurements are generally within 1-2%, and there are no seasonal dependent differences.

5.1 Introduction

For the ozone mini-hole and tropical tropospheric ozone studies described in Chapters 3 and 4, the GOME Fast Delivery (FD) ozone columns have been used. The FD total ozone algorithm is based on the ESA/DLR GOME Data Processor (GDP) version 2.7 [Spurr *et al.*, 2002], and uses the Differential Optical Absorption Spectroscopy (DOAS) retrieval method [Platt, 1994]. As described in Chapter 2, several changes in the algorithm has been made to improve the retrieval of the ozone columns: (1) the use of an effective ozone absorption cross-section based on ECMWF temperature forecasts in the slant column fit, (2) the use of the DAK radiative transfer model and the Fortuin and Kelder [1998] ozone climatology for the air mass factor calculations, and (3) the use of the FRESCO cloud algorithm [Koelemeijer *et al.*, 2001, 2002].

The pseudo-global validation of the FD ozone columns with ground-based measurements described in Section 2.4, shows that there is a reasonable agreement between the near-real time ozone columns and the ground-based measurements (within 5% for low- and mid-latitudes, within -10 to +5% for high latitudes). The level of quality is comparable to that of the GDP v2.7 or the EP-TOMS ozone sensor. Nevertheless, the validations of the FD and GDP v2.7 ozone columns have raised some issues for further improvements of the GOME-DOAS total ozone algorithm. An important issue is the solar zenith angle and latitudinal dependence of the ozone columns, which is mainly attributed to two effects: the treatment of the atmospheric profile shape effect in the air mass factors, and the partial unsuitability of the DOAS method when the atmosphere becomes optically thick [Marquard *et al.*, 2000].

In the FD and GDP v2.7 algorithms, the air mass factors are determined from a static climatology of (monthly) ozone profiles, which may differ significantly from the actual, highly variable ozone profiles. This deterministic approach cannot allow for atmospheric variability and can increase the error in the retrieved ozone column by about 5-10% at high solar zenith angles, where the sensitivity to the ozone profile shape is the highest. To reduce this error, an iterative approach has been implemented in the new GDP v3 algorithm [Spurr, 1999; Spurr *et al.*, 2002], using the TOMS v7 ozone profile climatology, classified by latitude and ozone column [McPeters *et al.*, 1998]. A validation of the GDP v3 ozone columns with ground-based measurements shows that this iterative approach resulted in significantly improved ozone columns, but that a solar zenith angle and seasonal dependent error persists [Lambert and Zehner, 2002].

To resolve the remaining limitations of the GDP v3 and FD algorithms, the improved GOME total ozone algorithm TOGOMI (Total Ozone algorithm for Gome using the OMI algorithm) has been developed. The new algorithm is based on the total ozone algorithm developed for the Ozone Monitoring Instrument (OMI), to be launched on EOS-Aura in 2004 [Veefkind and De Haan, 2002; De Haan, 2003]. The main improvements of this algorithm are: (1) a new DOAS fit-equation that accounts for inelastic Raman scattering, (2) the use of an empirical DOAS method to account for the wavelength dependence of the air mass factor, and (3) the use of a slant column dependent air mass factor to account for atmospheric variability. In addition, the new algorithm offers the possibility to use a smaller (5 nm) spectral fit window at longer wavelengths to reduce the sensitivity to the ozone profile and

atmospheric temperature. Improvements in the total ozone columns are also achieved by improving the calibration of the measured Earthshine and solar spectra.

In this Chapter, the new TOGOMI algorithm is described and the retrieved slant- and vertical columns are analysed. First, the improvements of the measured GOME (ir)radiance spectra are discussed in Section 5.2. In Section 5.3, the new DOAS fit-equation that accounts for inelastic scattering is described, and the fitted slant columns are analysed. Section 5.4 focuses on the ozone cross-sections, the atmospheric temperature dependence of the cross-sections and the spectral fit-window choice. The calculation of the empirical air mass factors is described in Section 5.5. In Section 5.6, the cloud correction and the vertical ozone column calculations are discussed. Section 5.7 contains comparisons with the FD and GDP ozone columns, and with ground-based measurements. The chapter ends with concluding remarks.

5.2 Improvement of the GOME (ir)radiance spectra

5.2.1 The GomeCal package

The TOGOMI algorithm uses the GOME Earthshine and solar spectra as produced by the GDP level 0-to-1 algorithm [Aberle *et al.*, 2002], but with several improvements. A wavelength re-calibration, an improved polarisation correction and a radiometric correction is applied to the GDP spectra, using the software package GomeCal [Van Geffen, 2002]. Of particular importance is the wavelength calibration of the GOME (ir)radiance spectra. Errors in the wavelength calibration can be a major source of error in DOAS retrievals (e.g. [Aliwell *et al.*, 2002] and [Van Roozendaal *et al.*, 2002b]). The standard wavelength calibration of the GDP uses spectral lines of an onboard PrCr/Ne hollow cathode lamp to correct for shifts in the wavelengths associated with the detector pixels, with respect to a pre-flight calibration (e.g. caused by temperature effects). This method is not accurate enough for DOAS algorithms. A new calibration method, developed by Van Geffen and Van Oss [2003], uses as reference spectrum a high-resolution solar spectrum, with irradiance values given at 0.01 nm intervals. This method provides a calibration accuracy of 0.001 nm or better above 290 nm, corresponding to about 1/100th of a detector pixel for the DOAS wavelength region 325-340 nm.

The GDP applies a polarisation correction to the Earth radiance spectra, based on a theoretical value at 300 nm, an assumed shape of the fractional polarization as a function of wavelength in the 300-350 nm range, and polarisation measurements in 100 nm wide windows around 350, 500 and 700 nm. This correction, however, is shown to lead to errors in the reflectance up to 10%, in particular in the UV range [Schutgens and Stammes, 2002]. GomeCal contains an improved polarisation correction developed by Schutgens and Stammes [2002] that is based on a parameterisation of the UV Earthshine polarisation between 290 and 330 nm, as function of solar zenith angle, viewing geometry, scene albedo and total ozone column.

Furthermore, it has been shown that the GOME instrument degrades, notably since 1998. This degradation is time and wavelength dependent, and the measured Earthshine radiances degrade differently from the solar irradiance spectra. In the GDP, the degradation of the

reflectance is not corrected for. Moreover, the interference of the Peltier cooler conduct signals on the detector signals causes an offset in the radiance (in the GOME instrument, Peltier elements are used for cooling the detector). For these reasons, a radiometric correction procedure was made by *Van der A et al.* [2002], consisting of three parts that can be applied independently in addition to the corrections of the GDP extractor: a radiometric calibration, a correction for the degradation of the instrument, and a correction to remove residual effects of the interference of the Peltier cooler signals.

5.2.2 Reduced effective spectral resolution

The DOAS ozone retrieval in the Huggins band (310-350 nm) is complicated by the undersampling of GOME and the uncertainty in the GOME slit function for this wavelength region. The spectral resolution is determined by the width and shape of the GOME slit. For the ozone fit-window range 325-340 nm, the slit is usually described as a Gauss-function with a FWHM (Full Width at Half Maximum) of 0.16 nm. Because the sampling distance in this wavelength region is about 0.12 nm, the GOME (ir)radiance spectra do not satisfy the Nyquist theorem and are undersampled. An additional complication is that for the 325-340 nm wavelength range, the GOME slit is asymmetric and that the FWHM varies between 0.16 and 0.21 nm [*Van Roozendael et al.*, 2002b]. The undersampling of GOME and the uncertainty in the slit function can be resolved by convolving the GOME (ir)radiance spectra with a wider slit-function, thereby reducing the effective spectral resolution. In case of DOAS ozone retrieval in the Huggins band, a slit function with a FWHM up to 0.6 nm can be used, without much loss of information [*Burrows et al.*, 2003]. An advantage of this procedure is that the effective slit function is known very accurately, as it is determined by the convolution with the wider slit-function. In the TOGOMI algorithm, the GOME (ir)radiance spectra are convolved with a flat-top Gaussian with a FWHM of 0.45 nm. This slit-function resembles the slit of the OMI instrument [*Dirksen and Dobber*, 2002]. The convolution with the OMI slit function has the additional advantage that these GOME spectra with reduced spectral resolution, can be used as ‘simulated’ OMI spectra.

5.3 DOAS slant column fit

5.3.1 Common DOAS fit-equation

As described in the Introduction of this thesis (Section 1.5), the first step in the retrieval of the total ozone column from the (re)calibrated GOME spectra is the calculation of the ozone slant column density. The commonly used DOAS fit-equation to calculate the ozone slant column is:

$$\frac{I^{meas}(\lambda)}{F_0^{meas}(\lambda)} = P(\lambda) \exp[-N_s \sigma(\lambda)] + c_R \frac{I_{Ring}(\lambda)}{F_0^{meas}(\lambda)} \quad (5.1)$$

where $I^{meas}(\lambda)$ and $F_0^{meas}(\lambda)$ are the measured radiance and irradiance, $I_{Ring}(\lambda)$ a so-called Ring spectrum (described in the next section), $\sigma(\lambda)$ the ozone absorption cross-section, $P(\lambda)$ a low-order polynomial (e.g. two- or third-order), c_R a Ring-effect scale factor, and N_s the fitted ozone slant column density. The DOAS fit Eq. (2.1) as used in the FD algorithm is a linearized version of Eq. (5.1). By taking the logarithm of I^{meas}/F_0^{meas} as the measurement, and by treating the Ring spectrum as a pseudo-absorption spectrum, the DOAS fit-equation becomes linear (ignoring higher order terms), and a simple least-squares solution for N_s can be found [Spurr *et al.*, 2002]. The ozone slant columns resulting from the (non-linear) DOAS fit Eq. (5.1) and the linear fit-equation used in the FD algorithm are very similar (within about 1%), if a differential Ring spectrum is used in Eq. (5.1). (Differential means that a low-order polynomial is fitted to the spectrum and then subtracted from the spectrum, so that the differential spectral fine structure remains.)

5.3.2 Accounting for Raman scattering

As explained in Section 1.5, the DOAS fit-equation describes the ozone absorption along the scattered light paths through the atmosphere reaching the GOME instrument, according to the Lambert-Beer attenuation law. A Ring spectrum is included in Eq. (5.1) to take into account that about 4% of all scattering events on air molecules is scattered inelastically. Nearly all of this inelastically scattered light is due to rotational Raman scattering on N_2 and O_2 molecules. Inelastic scattering on an air molecule results in a shift of the scattered photon wavelength with regard to the incoming photon wavelength. This associated energy shift equals the change in rotational energy of the scattering molecule. For incident light with a wavelength of 330 nm, shifts up to 2 nm occur. This is illustrated in Figure 5.1, where the Raman lines of N_2 and O_2 are plotted for the individual transitions, as a function of wavelength.

The most pronounced consequence of inelastic scattering is that the Fraunhofer lines in the Earthshine spectrum are shallower compared to the lines in the solar spectrum. The inclusion of a Ring spectrum $I_{Ring}(\lambda)$ into the DOAS fit-equation should take this filling in of solar Fraunhofer lines into account. The Ring spectrum, introduced in Eq. (5.1), is given by:

$$I_{Ring}(\lambda) = \sum_{k=1}^K \frac{\sigma_k(\lambda - \Delta\lambda_k)}{\sigma_0(\lambda)} F_0(\lambda - \Delta\lambda_k) \quad (5.2)$$

where λ is the wavelength of the incident light, $\Delta\lambda_k$ is the wavelength shift due to rotational Raman scattering, $\sigma_k(\lambda)$ is the Raman scattering cross-section for transition k , and $K = N_{N_2} + N_{O_2}$ is the total number of transitions that are taken into account. The elastic scattering component ($\Delta\lambda_k = 0$) is described by $\sigma_0(\lambda)$, the scattering cross-section of the Cabannes line [Young, 1980]. Ring spectra for the ozone fitting wavelength region have been calculated by Chance and Spurr [1997] and De Haan [2003]. Figure 5.2 shows the Ring spectrum and the ratio $I_{Ring}(\lambda)/F_0(\lambda)$ on the OMI spectral resolution. The Ring spectrum, being a scrambled solar spectrum, is rather smooth. The division by the solar spectrum

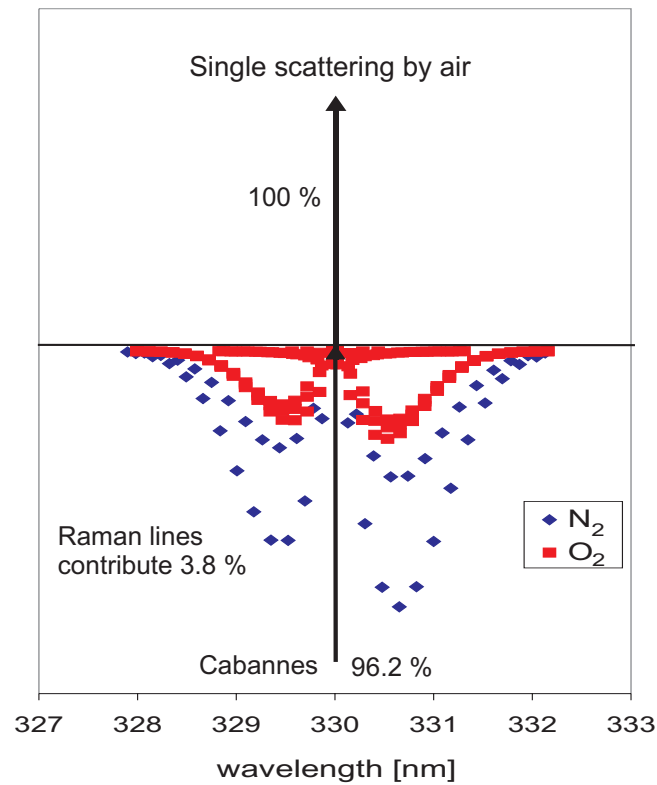


Figure 5.1 Schematic of the relative contribution of the individual Raman lines of N_2 and O_2 to single scattered light, as a function of wavelength. The incident wavelength is 330 nm. The Cabannes line at 330 nm (elastic scattering) contributes about 96% to single scattered light, while the 200 Raman lines contribute about 4%.

generates most of the spectral structure, as can be seen in the ratio $I_{Ring}(\lambda)/F_0(\lambda)$. In DOAS Eq. (5.1) usually a differential version of $I_{Ring}(\lambda)/F_0(\lambda)$ is used, together with a scale factor c_R . The inclusion of this Ring term into the DOAS equation results in strongly reduced fit-residuals and up to 10% higher ozone slant columns [De Haan, 2003; Van Roozendaal et al., 2002b].

The commonly used DOAS fit-equations (5.1) and (2.1) do not take into account that inelastic scattered light is also absorbed by ozone, just like elastic scattered light. This results in the filling-in of the ozone absorption features. An important assumption in the DOAS fit-equations (5.1) and (2.1) is that scattering does not change the spectral fine structures of the light. However, as explained above, inelastic scattering scrambles (a part of) the spectral fine structures. De Haan [2003] has developed a DOAS equation that properly accounts for inelastic Raman scattering, including the filling-in of the ozone absorption features. This improved DOAS equation includes an ozone absorption cross-section $\Delta\sigma_{inel}(\lambda)$ for inelastic scattering:

$$\frac{I^{meas}(\lambda)}{F_0^{meas}(\lambda)} = P_{el}(\lambda) \left(\exp[-N_s \sigma(\lambda)] + \frac{P_{inel}(\lambda)}{P_{el}(\lambda)} \frac{I_{Ring}(\lambda)}{F_0^{meas}(\lambda)} \exp[-N_s \Delta\sigma_{inel}(\lambda)] \right) \quad (5.3)$$

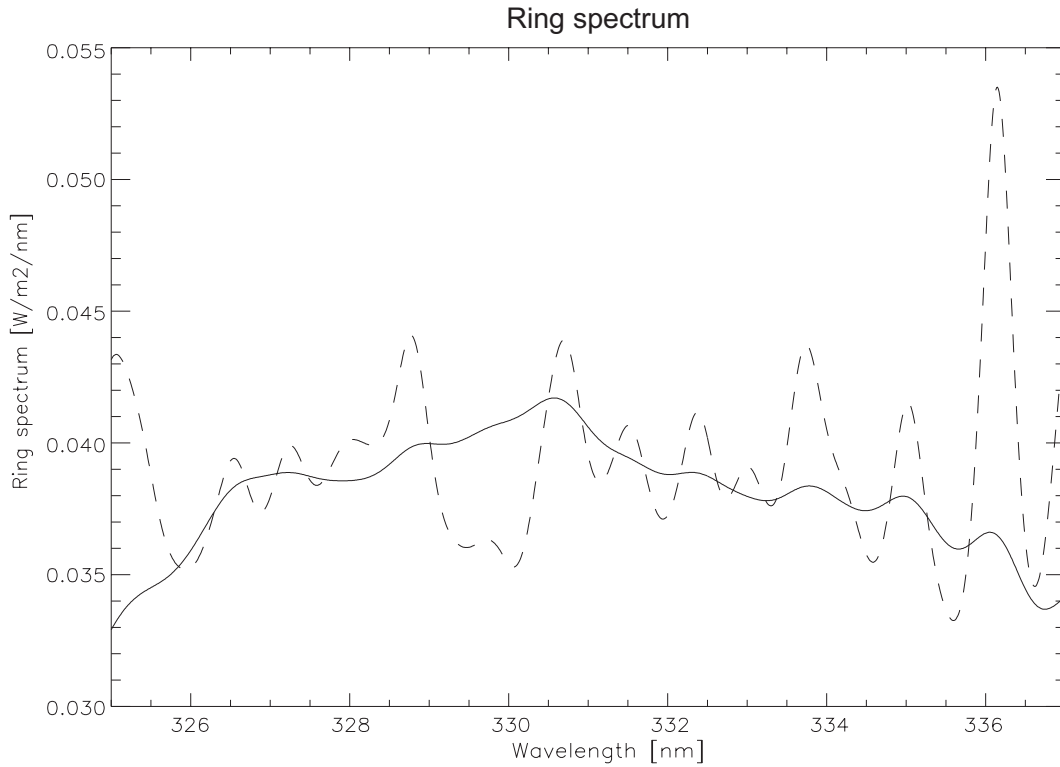


Figure 5.2 The Ring spectrum I_{Ring} (solid line) and the ratio I_{Ring}/F_0 (dotted line) calculated according to De Haan [2003] for the wavelength region 325–337 nm. The ratio is dimensionless, while I_{Ring} has the dimension $W m^{-2} nm^{-1}$. The OMI slit function was used (FWHM of 0.45 nm). The temperature of the scattering gas was 270 K.

where $\sigma(\lambda)$ is the common ozone absorption cross-section for elastic scattering (as used in Eq. (5.1)). Eq. (5.3) is based on two important assumptions: it is sufficient to consider only single inelastically scattered light, and the air mass factor for elastic and inelastic scattering is the same (see Section 5.5). The relative amount of twice or more inelastically scattered light is less than 0.1% [De Haan, 2003]. Therefore, the first assumption is justified. Because of the conservation of spectral fine structures upon (multiple) elastic scattering events, Eq. (5.3) can be applied to light that undergoes inelastic Raman scattering and zero, one, or more elastic scattering events. Multiple elastic scattering by aerosols, and the elastically reflecting surface contributes only to the smoothly varying polynomial $P_{el}(\lambda)$. The new DOAS equation uses a low-order polynomial $P_{inel}(\lambda)$, instead of a constant scale factor in front of the Ring spectrum, representing the change in the amount of Raman scattering over the fit-window.

The cross-section for inelastic scattering can be expressed in terms of a not-scrambled cross-section $\sigma_{ns}(\lambda)$ and a scrambled cross-section $\sigma_s(\lambda)$:

$$\Delta\sigma_{inel}(\lambda) = \frac{\mu_0\sigma_{ns}(\lambda) + \mu\sigma_s(\lambda)}{\mu + \mu_0} \quad (5.4)$$

where μ is the cosine of the viewing zenith angle and μ_0 the cosine of the solar zenith angle. Eq. 5.4 is based on a plane-parallel GOME viewing geometry, as illustrated in Figure 1.3. The scrambled cross-section $\sigma_s(\lambda)$ affects the light travelling from the sun to the scattering layer, while the not-scrambled cross-section $\sigma_{ns}(\lambda)$ affects the light scattered back to the GOME instrument. For GOME measurements with very high solar zenith angles ($\text{SZA} > 80^\circ$), the calculation of $\Delta\sigma_{inel}(\lambda)$ should be based on a curved atmosphere, as explained in *De Haan* [2003]. However, GOME measurements for these extreme geometries are not used in this study. In Eq. (5.4), the not-scrambled cross-section equals the cross-section for elastic scattering ($\sigma_{ns} = \sigma$). The scrambled cross-section is calculated by scrambling the cross-section and weighting with the scrambled solar spectrum:

$$\sigma_s(\lambda) = \frac{\sum_{k=1}^K \sigma_k(\lambda - \Delta\lambda_k) F_0(\lambda - \Delta\lambda_k) \sigma(\lambda - \Delta\lambda_k)}{\sum_{k=1}^K \sigma_k(\lambda - \Delta\lambda_k) F_0(\lambda - \Delta\lambda_k)} \quad (5.5)$$

Eq. (5.5) is derived assuming weak (or moderate) absorption, for strong absorption the scrambled cross-section also depends on the ozone column density and solar zenith angle.

5.3.3 Instrumental slit function

In the previous section, the spectral resolution of the GOME instrument was not taken into account. As described in Section 5.2.2., the effective spectral resolution of the GOME (ir)radiance spectra used in the DOAS slant column fit is about 0.45 nm. However, the incident solar irradiance varies strongly on a wavelength scale of a few hundreds of a nm in the Huggins band. The ozone absorption cross-sections also vary significantly over the wavelength range of the effective slit function (see Figure 1.4). Hence, the averaging that takes place over the wavelength range of the effective slit function should be taken into account in the DOAS fit. This effect, attributed to the spectral structures of the solar irradiance, is also known as the solar I_0 -effect.

A technique to correct for the solar I_0 -effect has been proposed by Johnston (see *Aliwell et al.* [2002]), by using an effective cross-section in the DOAS fit-equation. The effective cross-section for elastic scattered light is given by:

$$\sigma^{eff}(\lambda, N_s) = -\frac{1}{N_s} \ln \left(\frac{\int_{\lambda_{min}}^{\lambda_{max}} S(\lambda, \lambda') F_0(\lambda') \exp[-N_s \sigma(\lambda')] d\lambda'}{\int_{\lambda_{min}}^{\lambda_{max}} S(\lambda, \lambda') F_0(\lambda') d\lambda'} \right) \quad (5.6)$$

where $S(\lambda, \lambda')$ is the effective slit function, with $\int_{\lambda_{min}}^{\lambda_{max}} S(\lambda, \lambda') d\lambda' = 1$. The effective cross-section depends slightly on the ozone slant column, for which a climatological value is used in the TOGOMI algorithm. The use of an effective ozone cross-section has a small impact on

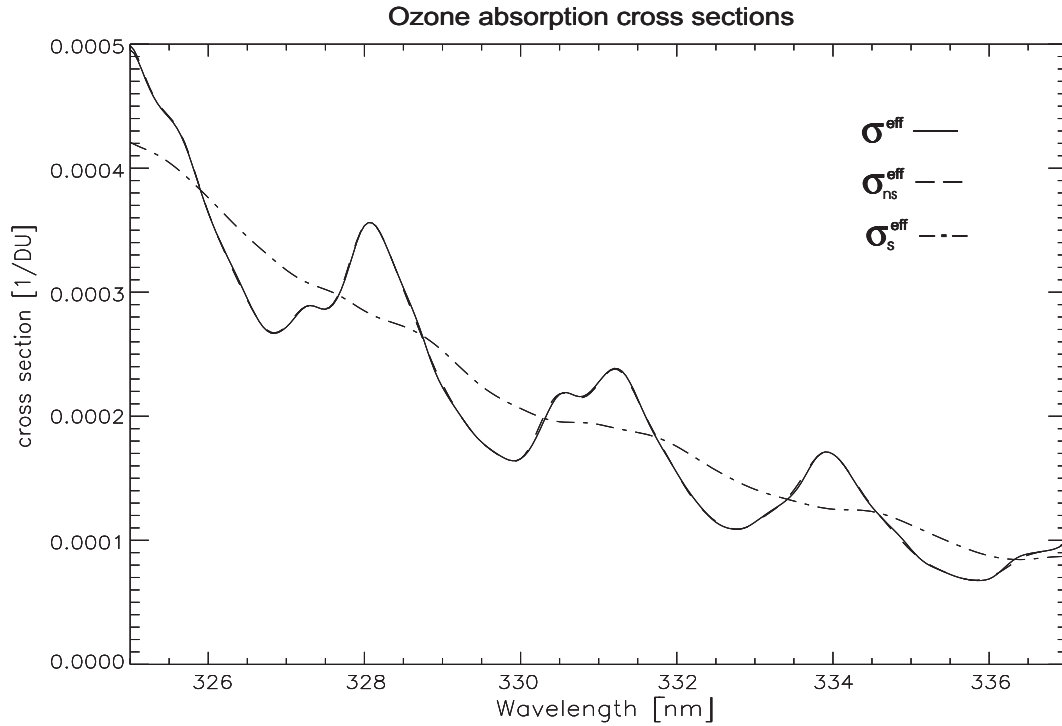


Figure 5.3 Effective ozone cross-sections for elastic scattered light (σ^{eff}) and inelastic scattered light ($\sigma_{\text{ns}}^{\text{eff}}$ and $\sigma_{\text{s}}^{\text{eff}}$), calculated from the Bass and Paur [1985] cross-section data for an absorption temperature of 220 K. The OMI slit function was used (FWHM of 0.45 nm). Note that σ^{eff} and $\sigma_{\text{ns}}^{\text{eff}}$ are almost identical.

the slant column (< 0.5%), retrieved with the GDP and FD algorithms [Van Roozendael et al., 2002b]. However, when the effective spectral resolution of the GOME (ir)radiance spectra is reduced, as is done in the TOGOMI algorithm, the impact on the retrieved slant column becomes more important.

For the inelastic part of the radiance, a similar correction for the effective slit function can be made. Instead of the Ring spectrum defined in Eq. (5.2), an effective Ring spectrum is used:

$$I_{\text{Ring}}^{\text{eff}}(\lambda) = \int_{\lambda_{\text{min}}}^{\lambda_{\text{max}}} S(\lambda, \lambda') \sum_{k=1}^K \frac{\sigma_k(\lambda' - \Delta\lambda_k)}{\sigma_0(\lambda')} F_0(\lambda' - \Delta\lambda_k) d\lambda' \quad (5.7)$$

An effective cross-section for inelastic scattering $\Delta\sigma_{\text{inel}}^{\text{eff}}(\lambda)$ has been derived by De Haan [2003]. In the assumption for weak absorption, Eq (5.4) can be still applied to calculate $\Delta\sigma_{\text{inel}}^{\text{eff}}(\lambda)$ by using an effective not-scrambled cross-section and an effective scrambled cross-section. The effective not-scrambled cross-section is calculated by weighting the ozone cross-section with the effective Ring spectrum:

$$\sigma_{ns}^{eff}(\lambda) = \frac{\int_{\lambda_{min}}^{\lambda_{max}} S(\lambda, \lambda') \sigma(\lambda') \sum_{k=1}^K \sigma_k(\lambda' - \Delta\lambda_k) F_0(\lambda' - \Delta\lambda_k) d\lambda'}{\int_{\lambda_{min}}^{\lambda_{max}} S(\lambda, \lambda') \sum_{k=1}^K \sigma_k(\lambda' - \Delta\lambda_k) F_0(\lambda' - \Delta\lambda_k) d\lambda'} \quad (5.8)$$

The effective scrambled cross-section is calculated by scrambling the ozone cross-sections and weighting with the effective Ring spectrum:

$$\sigma_s^{eff}(\lambda) = \frac{\int_{\lambda_{min}}^{\lambda_{max}} S(\lambda, \lambda') \sum_{k=1}^K \sigma_k(\lambda' - \Delta\lambda_k) \sigma(\lambda' - \Delta\lambda_k) F_0(\lambda' - \Delta\lambda_k) d\lambda'}{\int_{\lambda_{min}}^{\lambda_{max}} S(\lambda, \lambda') \sum_{k=1}^K \sigma_k(\lambda' - \Delta\lambda_k) F_0(\lambda' - \Delta\lambda_k) d\lambda'} \quad (5.9)$$

Thus the new DOAS equation (5.3) can still be applied, using the effective cross-section for elastic scattered light $\sigma^{eff}(\lambda)$, the effective Ring spectrum $I_{Ring}^{eff}(\lambda)$, and the effective cross-section for inelastic scattering $\Delta\sigma_{inel}^{eff}(\lambda)$.

Figure 5.3 shows the effective cross-section for elastic scattered light (Eq. (5.6)), and the effective not-scrambled and scrambled cross-sections (Eq. (5.8) and (5.9)) for the ozone DOAS wavelength 325-337 nm. Figure 5.3 shows that $\sigma^{eff}(\lambda)$ and $\sigma_{ns}^{eff}(\lambda)$ are very similar, but there are small differences due to the slit-function correction. The scrambling by rotational Raman scattering removes a large part of the spectral fine structure of the ozone absorption in this wavelength region, therefore the scrambled cross-section $\sigma_s^{eff}(\lambda)$ shows only weak spectral features. Note that the spectral structures of the ozone cross-sections differ substantially from the Ring spectrum ratio $I_{Ring}(\lambda)/F_0(\lambda)$ shown in Figure 5.2, which is a necessity for a stable DOAS fit.

For each GOME measurement, first the effective cross-section for inelastic scattering $\Delta\sigma_{inel}^{eff}(\lambda)$ is calculated, since $\Delta\sigma_{inel}^{eff}(\lambda)$ depends on the viewing geometry (Eq. (5.4)). Thereafter, the non-linear DOAS Eq. (5.3) is solved for N_s with the Levenberg-Marquardt method.

5.3.4 GOME fit results

As mentioned before, a prerequisite for proper use of the new DOAS Eq. (5.3) is that the elastic and inelastic components of the measured reflectance can be determined separately. That the spectral features of the elastic and inelastic part differ considerably is illustrated in Figure 5.4. In this figure, the reflectance $I^{meas}(\lambda)/F_0^{meas}(\lambda)$, the elastic component of I/F_0 (first term of Eq. (5.3)), and the inelastic component (second term of Eq. (5.3)) are plotted for an arbitrary GOME measurement with a solar zenith angle of 60° . Figure 5.4 shows that the ozone absorption features (see Figure 5.3) are prominent for the elastic scattered part but not for the inelastic part, which is dominated by Ring-spectrum structures. The different spectral

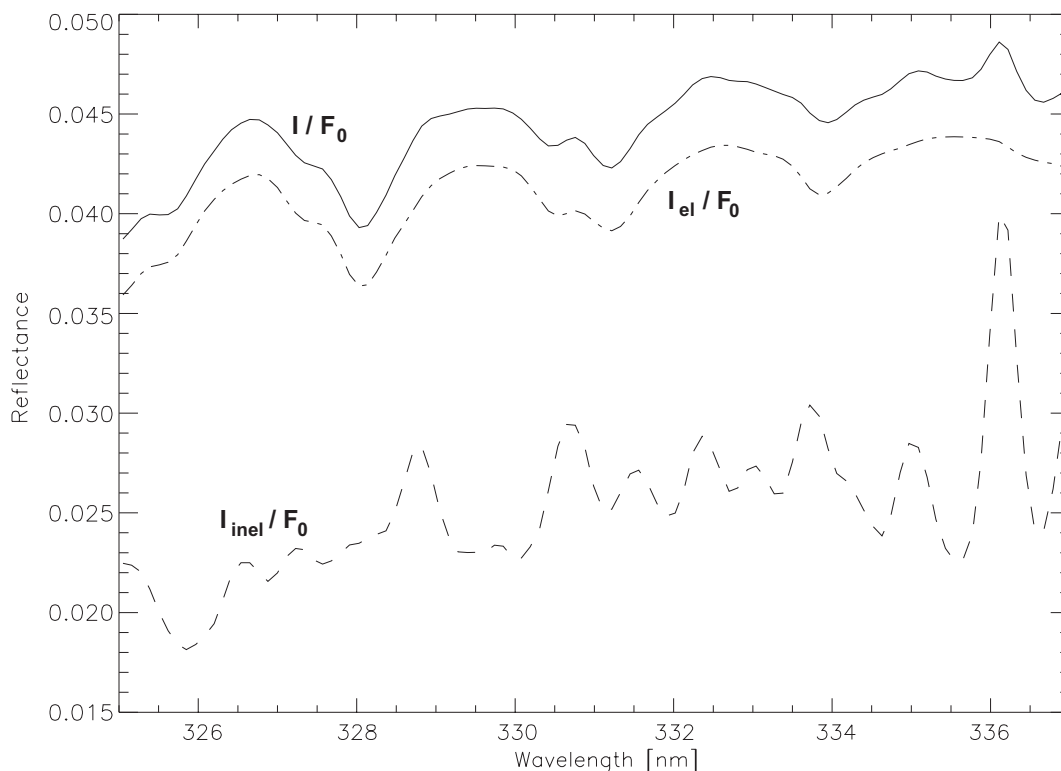


Figure 5.4 Reflectance I/F_0 for a single GOME measurement with a solar zenith angle of 60° (centre pixel). The inelastic and elastic components of I/F_0 are plotted as well (the inelastic component is multiplied by 8 to reveal its spectral features). The OMI slit function was used (FWHM of 0.45 nm). On average, the fraction inelastic scattered light is about 8% for this GOME measurement.

features of the elastic and inelastic part (correlation coefficient < 0.35) make it possible to determine them separately. GOME measurements with other viewing geometries show similar differences between the elastic and inelastic part of I/F_0 , and therefore the improved DOAS Eq. (5.3) can be generally applied.

For the GOME measurement of Figure 5.4, the fraction inelastic scattered light is about 8%, averaged over the wavelength region 325–337 nm. This number is higher than the 4% for a single scattering and is due to multiple scattering. The fraction depends mainly on the wavelength, solar zenith angle and albedo [De Haan, 2003]. Figure 5.5 shows the relative amount of inelastic scattered light for a GOME orbit (#28118) on 5 September 2000. This orbit runs from the Arctic, over Central Europe and Africa, to the Southern Atlantic and Antarctica. Figure 5.5 shows that the relative amount of inelastic scattered light increases from about 6% at low latitude (small solar zenith angles) to 10–13% at high latitudes. The highest values are found over snow/ice in the Antarctic. The relative amount of inelastic scattered light derived from the GOME measurements, and its dependence on albedo and solar zenith angle as shown in Figure 5.5, compare well with the theoretical values calculated by De Haan [2003]. He estimated the relative contribution of inelastic scattered light from theoretical calculations for a solar zenith angle of 45° , and obtained values of 7.5 and 10% for dark ($A_s = 0.05$) and bright ($A_s = 0.8$) surfaces, respectively.

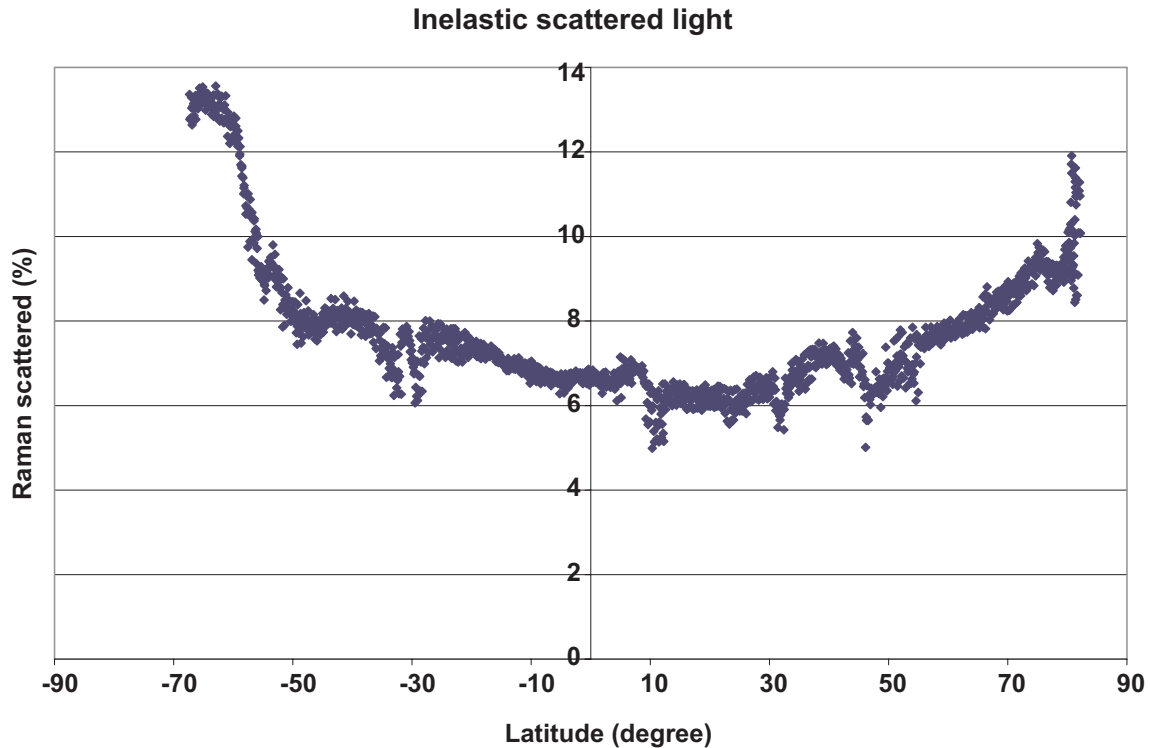


Figure 5.5 Relative amount of inelastic scattered light (in %) for the GOME measurements of orbit #28118 on 5 September 2000, as a function of latitude. The values are averages for the wavelength region 325-335 nm.

The ozone slant columns retrieved with the improved DOAS fit-equation (5.3) have been compared with the slant columns retrieved with the traditional DOAS equation (5.1), using a differential $I_{Ring}(\lambda)/F_0(\lambda)$. Figure 5.6 shows the difference between the ozone slant columns for GOME orbit #28118 on 5 September 2000, using the fit-window 325-335 nm. The improved DOAS equation results in higher slant columns and the difference increases with increasing solar zenith angle. At low latitudes, the improved slant columns are about 3% higher than the slant columns retrieved with the traditional DOAS equation, and the difference increases to 8-10% for high latitudes. For GOME orbits in other months, the slant column differences are comparable, with a similar solar zenith angle dependence. Figure 5.6 also includes slant column differences calculated from synthetic GOME spectra, using the same DOAS equations (5.1) and (5.3) [De Haan, 2003]. These simulated values have been calculated for solar zenith angles of 45°, 60° and 75°, for a surface albedo of 0.05. The measured slant column differences compare very well with the simulated values, as can be seen in Figure 5.6. The DOAS fit also provide an estimate of the precision of the retrieved slant column. With the improved DOAS fit-equation (5.3), a small relative slant column error of 0.3-0.6% is found. Note, however, that this estimated slant column error does not (fully) include the error due to the uncertainty in the ozone cross-section, as described in the next section.

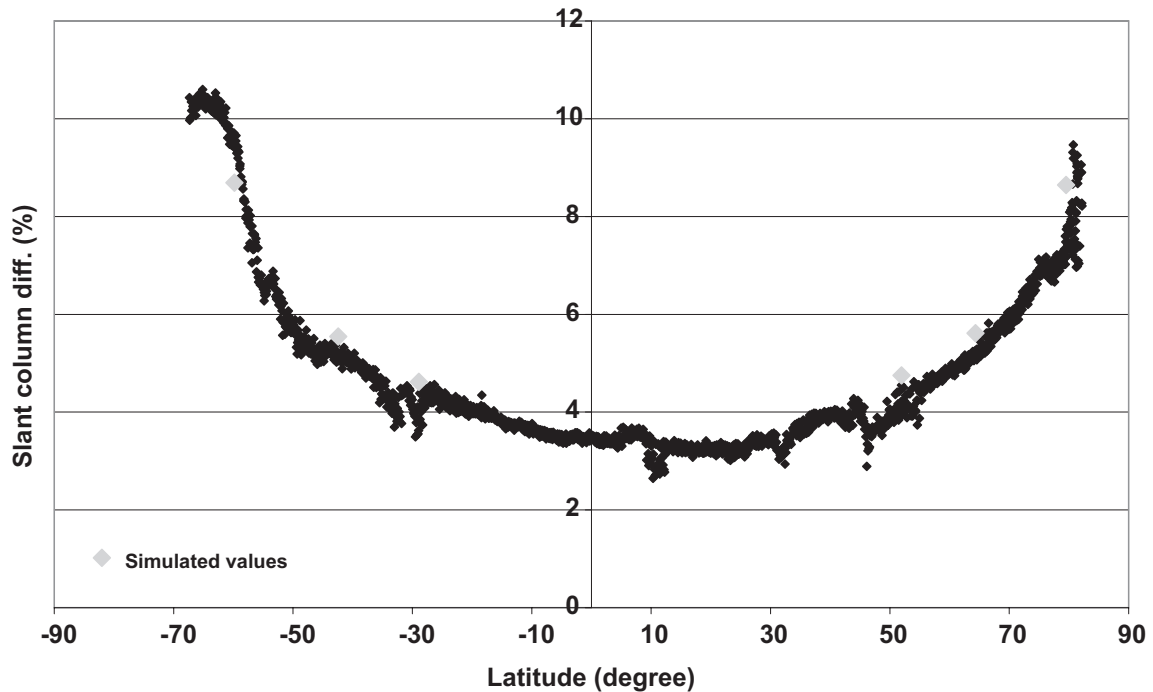


Figure 5.6 Relative difference between the ozone slant columns retrieved with the improved DOAS fit equation (5.3) and the slant columns retrieved with the traditional DOAS equation (5.1), using a differential I_{Ring}/F_0 . The differences for the GOME measurements of orbit #28118 on 5 September 2000 are shown, as a function of latitude. The DOAS fit window was 325-335 nm.

5.4 DOAS fit-window and temperature dependence

5.4.1 Ozone cross-section data sets

The accuracy of the retrieved ozone slant columns depends largely on the accuracy and suitability of the ozone cross-section data sets used in the DOAS fit equation. The ozone absorption cross-section varies with wavelength λ , with temperature T and with total pressure p . In the Huggins band (310-350 nm), the temperature dependence is particularly strong, and this results in increasing differential ozone cross-sections with decreasing temperatures (see Figure 1.4). In order to determine the cross-sections, laboratory measurements have been performed by a several groups. An extensive review of the available laboratory measurements of ozone absorption cross-sections, to be used in retrievals algorithms for satellite instruments like GOME, has been performed by *Orphal* [2002]. In the TOGOMI algorithm, two well-established data sets of temperature dependent ozone cross-sections for GOME retrieval in the Huggins band can be used: the GOME Flight Model (FM98) data [*Burrows et al.*, 1999b] and the *Bass and Paur* [1985] (B&P) data.

The B&P cross-sections have been measured at high spectral resolution (better than 0.025 nm) at 6 different temperatures (203, 218, 228, 243, 273 and 298 K). For the use in the TOGOMI algorithm, the spectral resolution of the B&P cross-sections has been reduced to the OMI resolution (see Section 5.2.2). The FM98 cross-sections have been measured at 5 different temperatures (202, 221, 241, 273 and 293 K) during the pre-flight calibration of

GOME, using the GOME flight model. The spectral resolution of the FM98 cross-sections has also been reduced to the OMI resolution.

Since the DOAS fit is very sensitive to spectral shift errors (see Section 5.2.1), the wavelength calibration of the laboratory cross-section is of particular importance. Both the B&P and the FM98 cross-sections need to be shifted to higher wavelengths in the Huggins band. For the TOGOMI algorithm, the recommendations from *Chance* [Private Comm.] and *Van Roozendael et al.* [2002b] have been followed, i.e. a shift of +0.015 nm for the B&P cross-sections, and +0.017 nm for the FM98 cross-sections.

After the wavelength correction of the B&P and FM98 cross-sections, there remain significant differences between the two cross-sections. For the most important temperatures for GOME-DOAS retrievals, 221 and 243 K, differences of several percent between the two data-sets are found in the Huggins band (e.g. see Figures 7-23 and 7-31 in *Orphal* [2002]). The B&P cross-sections are close to the average value of all available laboratory data at all temperatures, but the B&P cross-sections inhibit the strongest noise [*Orphal*, 2002; *Van Roozendael et al.*, 2002b]. Both the B&P and FM98 cross-sections show only small baseline drifts (wavelength dependent systematic errors) concerning the magnitude of the cross-sections.

The use of B&P or FM98 cross-sections in DOAS Eq. (5.3) results in systematic differences in the retrieved ozone slant columns, due to the differences between the B&P and FM98 cross-sections. The effect on the retrieved ozone slant column depends also on the DOAS fitting window, as discussed in the following sections on the GOME and OMI fit-windows. The use of different cross-section data sets (e.g. B&P and FM98) can also be a source of a bias between the GOME ozone columns and the ozone values retrieved with other instruments. However, to quantify this bias falls beyond the scope of this work. The GOME-DOAS retrieval uses differential cross-sections for 5 to 10 nm wavelength regions between 325 and 337 nm, while other instruments use different retrieval algorithms in different wavelength regions. For example, the Brewer ground-based instrument uses B&P cross-sections at four wavelengths outside the DOAS fitting windows: 310, 313, 316 and 320 nm. This results in a sensitivity for the ozone cross-section temperature, that is very different for the GOME and Brewer retrieval algorithms. As discussed in Chapter 3, the sensitivity of the GOME-DOAS algorithm to the atmospheric temperature is larger, and of opposite sign compared to that of the Brewer instrument.

5.4.2 The 325-335 nm GOME fit-window

In both GDP v2.7 and v3 [*Spurr et al.*, 2002], as well as in the FD algorithm described in Chapter 2, the DOAS fit-window is 325-335 nm. This fit-window choice is based on the TRACEGAS study [*Diebel et al.*, 1995]. The main reasons for choosing this window are the strong spectral features of ozone, and due to the width of 10 nm, it contains three main differential absorption structures (see Figure 5.3). This results in a high signal-to-noise ratio. The very strong Ring structure around 336 nm (see Figure 5.2) falls outside this fit-window, which is an advantage in case the Ring spectrum $I_{Ring}(\lambda)$ is not accurately known.

Furthermore, the absorption by interfering species like NO₂, SO₂, BrO, OClO and HCHO is very small in this fit-window, compared to the ozone absorption.

The main disadvantages of the 325-335 nm fit-window are the strong ozone absorption at the smaller wavelengths, as a result of which the atmosphere can become optically thick, and the large temperature dependence of the ozone absorption cross-sections [e.g. see *Van Roozendaal et al.*, 2002b; *Marquard et al.*, 2000; *Burrows et al.*, 1999a]. The first issue is further discussed in Section 5.5, which deals with the empirical air mass factor calculations; in this section the effect of the temperature dependent ozone cross-sections on the retrieved slant column is analysed.

If the cross-section temperatures used in the DOAS fit deviates from the actual atmospheric temperatures, this results in an error in the retrieved ozone slant column. It can easily be shown that for the 325-335 nm fit-window, a 10 K overestimation of the temperature results in about 3% larger ozone slant columns. A useful method to deal with this temperature dependence is to (pre)calculate an effective absorption temperature:

$$T_{eff} = \frac{\int_0^{\infty} A(z) n(z) T(z) dz}{\int_0^{\infty} A(z) n(z) dz} \quad (5.10)$$

where z is the altitude, $A(z)$ is the GOME sensitivity profile for the fit-window (see the Appendix of Chapter 4), $n(z)$ the ozone number density, and $T(z)$ the atmospheric temperature. For the TOGOMI algorithm, effective temperatures are calculated using daily temperature analyses from the European Centre for Medium-Range Weather Forecasts (ECMWF) model [*Untch and Simmons*, 1998] and the ozone profile climatology from Logan, Labow & McPeters as used in the TOMS v8 total ozone algorithm [see *Bhartia and Wellemeyer*, 2002]. An effective ozone cross-section is calculated using the effective temperature and then applied in the DOAS fit. This method to deal with the ozone temperature dependence is very similar to the one used in the FD algorithm, as described in Section 2.3.2.

Another method is to allow the cross-sections to adjust themselves to the measured ozone absorption features. In this case, the ozone slant column and the effective absorption temperature are simultaneously retrieved by including the derivative of the cross-section with respect to the temperature in the DOAS fit. The fit-equation (5.3) then becomes (assuming weak absorption):

$$\frac{I^{meas}(\lambda)}{F_0^{meas}(\lambda)} = P_{el}(\lambda) \left\{ \exp \left[-N_s \left(\sigma^{eff}(T_0, \lambda) + (T - T_0) \frac{d\sigma^{eff}(T, \lambda)}{dT} \Big|_{T=T_0} \right) \right] + \frac{P_{inel}(\lambda)}{P_{el}(\lambda)} \frac{I_{Ring}^{eff}(\lambda)}{F_0^{meas}(\lambda)} \exp \left[-N_s \left(\Delta\sigma_{inel}^{eff}(T_0, \lambda) + (T - T_0) \frac{d\Delta\sigma_{inel}^{eff}(T, \lambda)}{dT} \Big|_{T=T_0} \right) \right] \right\} \quad (5.11)$$

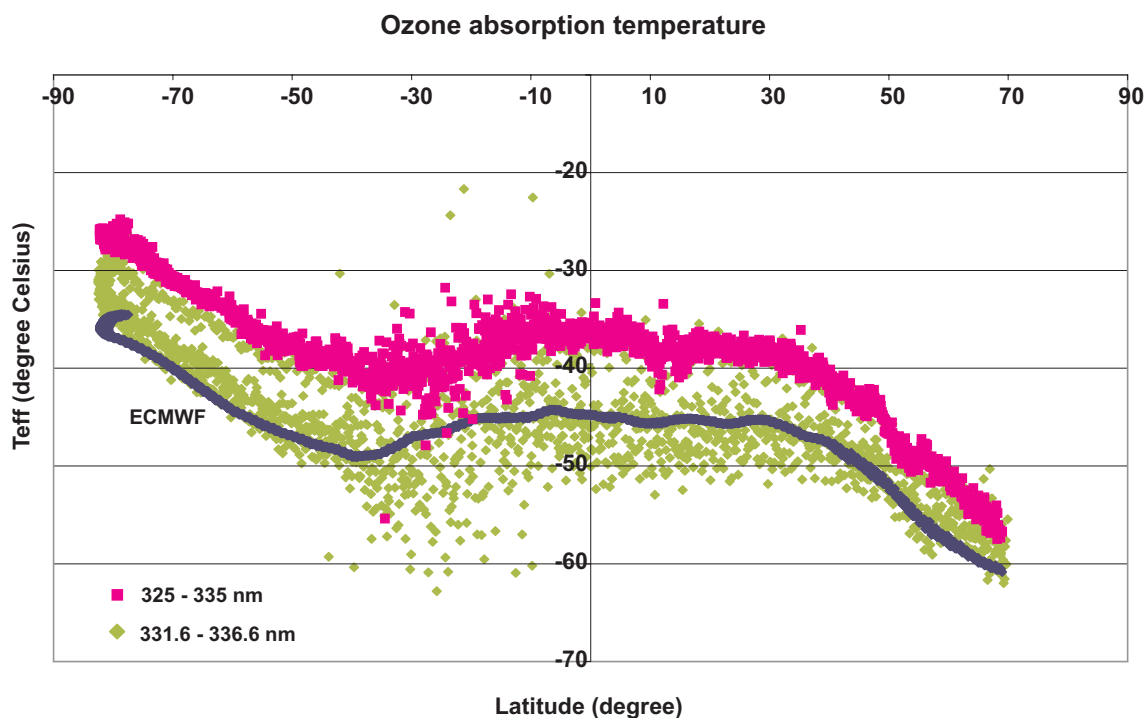


Figure 5.7 Effective absorption temperatures (in °C) fitted with DOAS fit-equation (5.11) and pre-calculated using ECMWF temperature analyses. The temperatures for the GOME measurement of orbit #28992 on 5 November 2000 are shown, as a function of latitude. The temperatures have been retrieved for the GOME and OMI fit-windows, using the FM98 ozone cross-sections.

where T_0 is a fixed (or climatological) reference temperature and T the effective absorption temperature to be fitted. Figure 5.7 shows the fitted absorption temperatures for the GOME measurements of orbit #28992 on 5 November 2000, together with the (pre)calculated ECMWF effective temperatures. The fitted absorption temperature follows the latitudinal structures of the ECMWF temperature well, which demonstrates that the temperature fit method is sensitive to actual variations of the atmospheric temperature. However, the fitted temperatures systematically overestimate the ECMWF temperatures by up to 10 K. Taking into account the sensitivity of the retrieved slant column for the cross-section temperature in the 325-335 nm fit-window (3% / 10 K), the inferred temperature bias directly translate into a 3% systematic overestimation of the slant column, if DOAS fit Eq. (5.11) is used. This systematic overestimation of the fitted temperature in the 325-335 nm fit-window occurs in all months.

The temperature fit method is also used in the GDP v3, using the common DOAS temperature fit method (based on Eq. (5.1), without accounting for Raman scattering [Spurr *et al.*, 2002]). With the common DOAS temperature fit method, a similar systematic overestimation of the fitted temperature is found [Van Roozendaal *et al.* 2002b].

It is likely that the relatively large uncertainty of the ozone cross-section data sets is a main reason for the systematic overestimation of the fitted temperature for the 325-335 nm fit-window. In addition, the partial correlation between the differential structures of $\sigma(\lambda)$ and

$d\sigma(\lambda)/dT$ in the 325-335 nm wavelength region also plays a role [De Haan, 2003; see also next section]. To confirm that the uncertainty in the ozone cross-sections has a large effect on the fitted temperature, DOAS fit Eq. (5.11) has been applied on simulated GOME (ir)radiances calculated with a radiative transfer model (using the method described in Section 5.5.1). In this simulation, the ozone cross-section data set used in the radiative transfer model to calculate the GOME radiances was the same as used in the DOAS fit. Therefore, the uncertainty in the ozone cross-sections had no influence on the retrieved temperature and ozone slant column. This resulted in a good agreement between the fitted absorption temperature and the effective temperature calculated with Eq. (5.10), without a systematic overestimation (not shown). Because of this problem involved with fitted absorption temperatures, the (pre)calculated ECMWF effective temperatures are used in the TOGOMI algorithm, and the DOAS temperature fit Eq. (5.11) is not applied for the 325-335 nm fit-window.

Another important issue mentioned in the previous section is the systematic differences in the retrieved ozone slant columns when the B&P or FM98 cross-sections are used in DOAS Eq. (5.3). For the 325-335 nm fit window, the slant columns retrieved with the B&P cross-sections are about 3% higher than the slant columns retrieved with the FM98 cross-sections. These results are consistent with the analyses of *Van Roozendaal et al.* [2002b].

Finally, it is important to note that the issues related to the ozone cross-sections, as described above, can only be resolved when more accurate cross-sections data sets become available.

5.4.3 The 331.6-336.6 nm OMI fit-window

For the OMI total ozone algorithm, a small 5 nm wide fit-window, centered around 334.1 nm will be used [Veeffkind and de Haan, 2002]. The main reason for this fit-window choice is the very small sensitivity of the retrieved slant column for the cross-section temperature. The correlation between the differential structures of $\sigma(\lambda)$ and $d\sigma(\lambda)/dT$ is minimized for this fit-window, resulting in a temperature sensitivity that is at least five times smaller (0.5% / 10 K) than for the 325-335 nm fit-window. This small sensitivity has the important advantage that a fixed temperature (e.g. 220 K) can be used for the ozone cross-sections, and that it is not necessary to (pre)calculated (ECMWF) effective temperatures. It is also possible to fit an effective temperature using DOAS Eq. (5.11), as is illustrated in Figure 5.7 for the GOME orbit on 5 November 2000. Figure 5.7 shows that the small correlation between $\sigma(\lambda)$ and $d\sigma(\lambda)/dT$ for the OMI fit-window reduces the temperature bias, compared to the bias found for the 325-335 nm fit-window. Note that because of the small temperature sensitivity of the OMI fit-window, differences between the actual absorption temperature and the fitted temperature do not lead to significant errors in the slant column.

An additional advantage of the OMI fit-window is that it is located at longer wavelengths ($\lambda > 330$ nm). The absence of the strong ozone absorption at 325 nm reduces the optical thickness compared to that of the GOME fit window, and thereby reduces the sensitivity of the DOAS algorithm to the ozone profile. This issue is further discussed in Section 5.5 on the air mass factor calculations.

The main disadvantage of the 5 nm wide OMI fit-window is that the spectral features of ozone are smaller, and that it only includes two main differential absorption structures, resulting in a lower signal-to-noise ratio than the 325-335 fit-window. It also contains the very strong Ring structure around 336 nm (see Figure 5.2). The lower signal-to-noise ratio results in larger random errors in the slant columns of 1-2%, compared to the slant columns retrieved with the 325-335 nm fit-window (not shown). This increased random error for the OMI fit-window is also visible in the fitted absorption temperatures (Figure 5.7), and in the vertical ozone columns (Figure 5.10, described in Section 5.7.1).

Just as for the GOME fit-window, the use of B&P or FM98 cross-sections results in systematic differences in the retrieved ozone slant columns. For the OMI fit-window, the slant columns retrieved with the B&P cross-sections are about 4% higher than the slant columns retrieved with the FM98 cross-sections if DOAS Eq. (5.3) is used. Finally, it should be noted that for both the GOME and OMI fit-windows the fitting residuals are smaller when the FM98 cross-sections are used, resulting in an estimated 20-30% smaller slant column error.

5.5 Air Mass Factor calculations

5.5.1 Empirical Air Mass Factor

As explained in the Introduction of this thesis (Section 1.5), the Air Mass Factor (AMF) is used to convert the slant column density into a vertical column density. The air mass factor M resembles the effective atmospheric path length and can be defined as the ratio of the slant column density N_s , and the vertical column density N_v :

$$M = \frac{N_s}{N_v} \quad (5.12)$$

This definition of the air mass factor is based on the traditional DOAS fit-equation (5.1), which only takes into account ozone absorption by elastically scattered light. If one fully accounts for Raman scattering, two air mass factors, M_{el} and M_{inel} , corresponding to atmospheric paths for elastically and inelastically scattered light, need to be considered. A fair approximation for ozone absorption is the assumption that the air mass factor for elastic and inelastic scattering is the same ($M_{inel} = M_{el} = M$). Based on this assumption, DOAS fit Eq. (5.3) and the cross-section for inelastic scattering $\Delta\sigma_{inel}$ (Eq. (5.4)) have been derived, and the single AMF defined in Eq. (5.12) can be used [De Haan, 2003]. The air mass factor depends on the sun-satellite geometry and on the state of the atmosphere, i.e. on the ozone profile, on cloud and aerosol properties, on surface reflectivity properties etc. Because the retrieved slant column N_s depends on the spectral fit-window, there is also a different air mass factor for each fit-window.

For the TOGOMI algorithm, the air mass factors have been calculated using the so-called empirical approach [Marquard *et al.*, 2000; Veefkind and De Haan, 2002]. Using radiative transfer calculations for a model atmosphere and a GOME simulator, synthetic (ir)radiance

spectra are created and a DOAS fit is performed on these synthetic spectra. As the vertical column density N_v is known from the model specification, the air mass factor M can then directly be derived from the fitted slant column density. With this approach, the correct air mass factor is obtained if the atmospheric model used to calculate the synthetic spectrum corresponds to the real atmosphere. The GOME simulator is used to produce synthetic GOME spectra from the reflectivities calculated with a radiative transfer model. In this way, the synthetic spectra resemble best the measured GOME spectra used in DOAS fit Eq (5.3). The advantage of the empirical DOAS method is that the same procedure is used for the measured (ir)radiance spectra and for the synthetic spectra, leading to cancellation of errors. For example, a problem with the 325-335 nm fit window is the strong ozone absorption at the shorter wavelengths. This results in an error in the vertical ozone column at higher solar zenith angles, because the atmosphere becomes optically thick and the DOAS approximation breaks down. With the empirical DOAS method, this error is reduced considerably.

The radiative transfer model used for the simulations of spectra is the Doubling-Adding-KNMI (DAK) model, which solves the radiation transport equation using the full Stokes vector, i.e. accounting for polarization [De Haan *et al.*, 1987; Stammes *et al.*, 1989; Stammes, 2000]. Commonly used scalar models, like DISORT and GOMETRAN [Stammes *et al.*, 1988; Rozanov *et al.*, 1997], compute top-of-atmosphere reflectances that may deviate up to 10% [Mischenko *et al.*, 1994; Lacis *et al.*, 1998]. Single scattering properties of aerosol particles and PSCs are calculated with a Mie scattering code [De Rooij and Van der Stap, 1984] that generates coefficients for the expansion in generalized spherical functions, making efficient calculations for polarized light possible. Only elastic scattering is included in the model, and Cabannes scattering is used instead of Rayleigh scattering for the scattering properties of the molecules [De Haan, 2003]. The DAK version used in this study is based on a plane-parallel atmosphere, therefore only GOME measurements with solar zenith angles $\leq 75^\circ$ are considered here. For the DOAS fit on the synthetic GOME spectra only the first term of Eq (5.3), for elastically scattered light, is used. This results in an air mass factor for elastic scattering, while the air mass factor for inelastic scattering is assumed to be the same, as described above. Besides ozone, absorption by NO_2 , SO_2 , and BrO are accounted for in the radiative transfer calculations. Clouds are represented by Lambertian surfaces situated at the cloud top level with an albedo of 0.8, as recommended by Koелеmeijer and Stammes [1999].

5.5.2 Slant column dependent Air Mass Factor

The dependence of the air mass factor on the ozone profile is of particular importance. The ozone profiles in the atmosphere vary strongly, resulting in changes of several percent in the actual air mass factor. A slant column dependent AMF and an ozone climatology are used to reduce the uncertainty in the air mass factor due to the ozone profile variability. To derive a relation between the slant column density and the air mass factor, a set of ozone profiles is used that cover the natural variability of the ozone profile for a given location and time of year. For each of these profiles, the air mass factor is calculated for a set of sun/satellite geometries and surface properties. This procedure is illustrated in Figure 5.8. The top panel shows a set of ozone profiles that are representative for 55°N for December. These profiles

are taken from the ozone profile climatology from Logan, Labow & McPeters as used in the TOMS V8 total ozone algorithm [see *Bhartia and Wellemeyer, 2002*]. This climatology contains 3 (at low-latitudes) to 10 (at high-latitudes) column classified ozone profiles per 10° latitude band for each month. The bottom panel of Figure 5.8 shows the effective AMF for each of the profiles, plotted as a function of the slant column density. To eliminate most of the geometrical effects, it is convenient to use the effective AMF, defined as M/M_{geo} , with the geometrical AMF M_{geo} given by Eq. (1.4). As can be seen in Figure 5.8, the effective AMF varies almost linearly with the slant column density. This is used in the TOGOMI algorithm, by making the effective AMF a linear function of the slant column density determined in the DOAS fit, as indicated in the bottom panel.

The TOGOMI algorithm uses an AMF look-up-table, avoiding the need for on-line radiative transfer calculations. The look-up-table contains the air mass factor as a function of sun-satellite geometry, surface reflectivity, surface pressure and ozone profile (per latitude, per month).

The empirical air mass factor used in the TOGOMI algorithm has been compared with the air mass factor used in the FD algorithm. Because of the different way the air mass factors are calculated (empirical and slant column dependent AMF vs. single AMF for 325 nm, Cabannes scattering vs. Rayleigh scattering, different ozone climatologies), systematic differences are to be expected. Figure 5.9 shows the difference between the (clear sky) air mass factors for GOME orbit #33930 on 16 October 2001. This orbit runs from the Arctic, over Western Europe and Africa, to the Southern Atlantic and the Antarctic ozone-hole. For low- and mid-latitudes the difference is generally smaller than 2%. The difference increases for large solar zenith angles at high latitudes, where the effect of the ozone absorption on the air mass factor is larger. In the polar regions, the empirical air mass factors are 2-6% smaller than the FD air mass factors. This general pattern as function of solar zenith angle and latitude is also found for GOME orbits in other months. The increased scatter in the Antarctic ozone-hole, south of 60°S , is due to inaccuracies in the air mass factor calculations of the FD-algorithm for high albedos. Another interesting feature visible in Figure 5.9 is the systematic difference between the three ground-pixel types (East, Centre and West). This is caused by an error in the viewing geometry calculations of the FD-algorithm, resulting in small biases in the air mass factors and vertical ozone columns, depending on the ground-pixel type. This problem has been resolved in the TOGOMI algorithm.

5.6 Cloud correction and vertical ozone column

5.6.1 Cloud correction

For a GOME measurements in the presence of clouds, part of the ozone column is covered by the clouds and two air mass factors are needed: one down to the ground surface (M_{clear}), as described in the previous section, and one down to the cloud top (M_{cloudy}). This cloudy air mass factor is determined with the same method as for clear-sky conditions, replacing the surface pressure with the cloud-top pressure and using an albedo of 0.8. In good

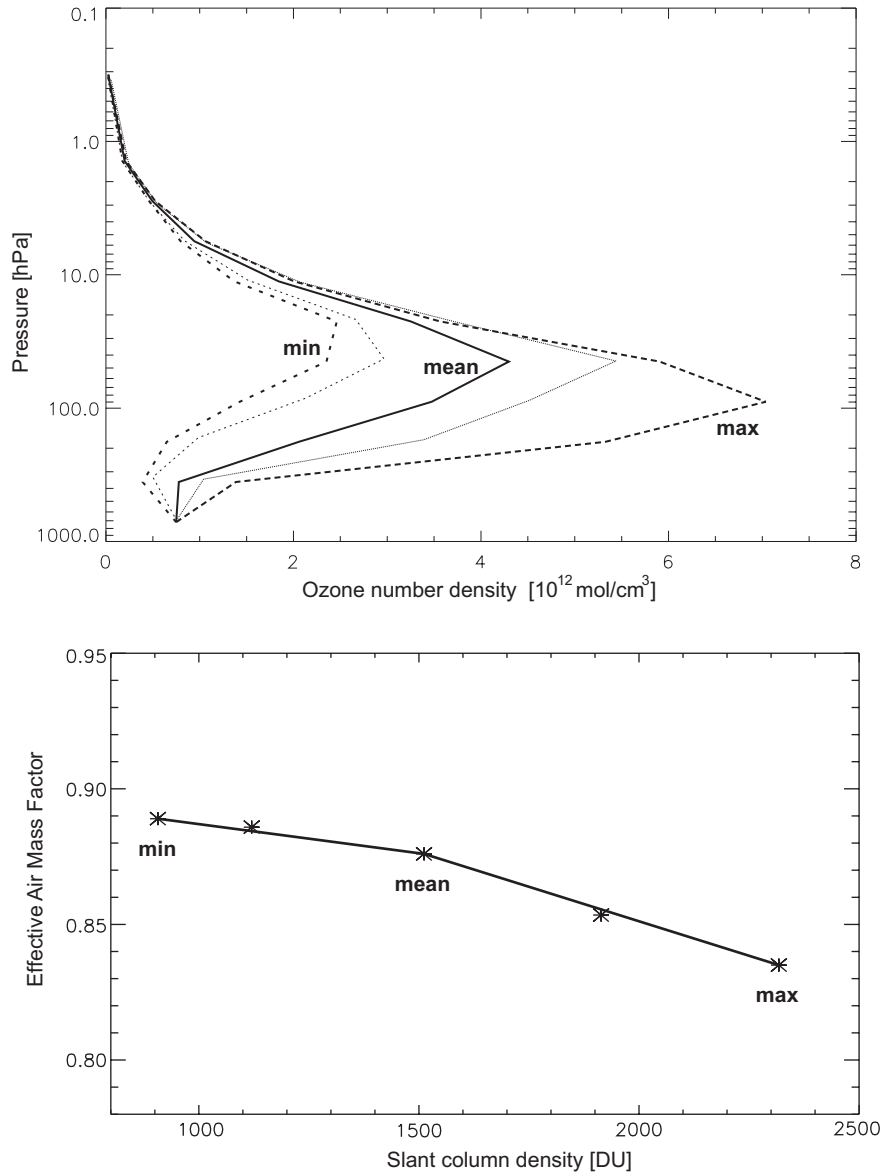


Figure 5.8 Top panel: Five ozone profiles from the Logan, Labow & McPeters climatology [see Bhartia and Wellemeyer, 2002] for 55°N for December. The thick lines denote the ozone profiles with the smallest vertical columns density ($N_v=225$ DU), an average ozone profile ($N_v=375$ DU), and the ozone profile with the largest vertical columns density ($N_v=575$ DU). Two additional ozone profiles with $N_v=275$ DU and $N_v=475$ DU are also plotted. Bottom panel: Effective AMF computed for the five ozone profiles shown in the top panel, plotted as a function of the slant column density. The effective AMFs have been calculated for a solar zenith angle of 75° and a surface albedo of 0.05, using the 325-335 nm DOAS fit-window.

approximation, the air mass factor for a partly cloudy pixel is the area and radiance weighted sum of the air mass factor of a clear and a cloudy pixel [Martin *et al.*, 2002b]:

$$M = w \cdot M_{cloudy} + (1 - w) M_{clear} \quad (5.13)$$

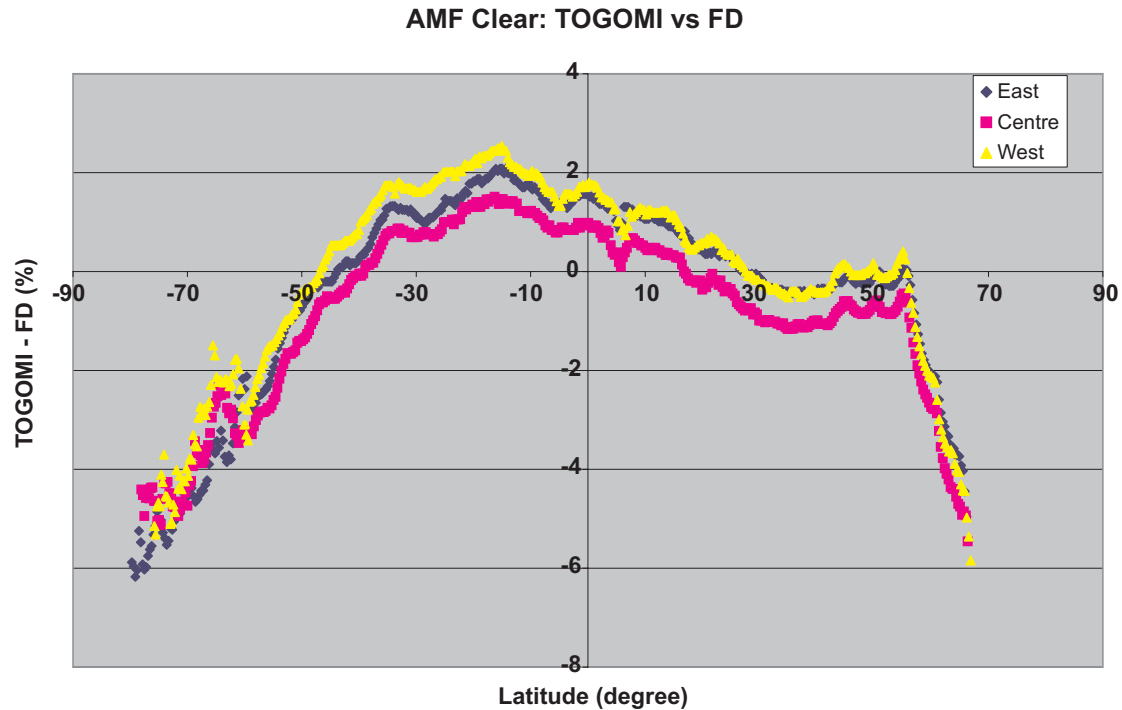


Figure 5.9 Relative difference between the clear-sky AMF calculated with the empirical method of the TOGOMI algorithm and the AMF used in the FD algorithm. The AMF is determined for the 325-335 nm fit window. The differences for the GOME measurements of orbit #33930 on 16 October 2001 are shown, as a function of latitude and ground-pixel type.

The weighting factor w in Eq (5.13) is the fraction of the photons that originates from the cloudy part of the pixel, and can be expressed as:

$$w = \frac{f_c \langle I_{cloudy}(p_c) \rangle}{\langle I \rangle} \quad (5.14)$$

where f_c is the cloud fraction, $\langle I_{cloudy}(p_c) \rangle$ is the average radiance over the fit-window for a ground pixel that is fully covered with a cloud that is located at pressure p_c , and $\langle I \rangle$ is the average measured radiance for the pixel.

The amount of ozone below the cloud-top is called the ghost column N_g , and cannot be measured by GOME. Usually, the ghost column is determined by integrating a climatological ozone profile from the surface to the cloud-top pressure and added to the retrieved vertical column density (see also next section). In the TOGOMI algorithm, the ozone profiles from the Logan, Labow & McPeters climatology are used to calculate the ghost column. With this column-classified climatology, the ghost column can be made a function of the slant column density, latitude and month, just like the air mass factor.

To calculate the ghost column N_g and the cloudy air mass factor M_{cloudy} , the cloud-fraction and cloud-top pressure are needed. These cloud properties are derived with the Fast Retrieval Scheme for Clouds from the Oxygen A-band (FRESCO) method [Koelemeijer *et*

al., 2001, 2002]. The FRESCO algorithm is also used in the FD algorithm and has been described in Section 4.2.1. The retrieval is based on non-linear least squares fitting of the GOME reflectance to a simulated spectrum in the range 758-766 nm, and solving it for cloud-fraction and cloud pressure. The FRESCO cloud model considers all clouds to be thick, single layer clouds (opaque Lambertian surface), with an albedo of 0.8. GOME ground-pixels that are fully covered with thin clouds are represented by partly cloudy pixels with a thick cloud.

5.6.2 Vertical ozone column

For the computation of the vertical ozone column, three cases can be distinguished: cloud-free, cloud covered and partly cloudy GOME measurements. Using the air mass factor definition Eq. (5.12), the vertical column density N_v for a cloud free ground-pixel is simply given by:

$$N_v = \frac{N_s}{M_{clear}} \quad (5.15)$$

where N_s is the fitted slant column density and M_{clear} is the air mass factor for a clear atmosphere. For a cloudy ground-pixel the air mass factor for a cloudy atmosphere M_{cloudy} is used, and the ghost column N_g needs to be added:

$$N_v = \frac{N_s}{M_{cloudy}} + N_g \quad (5.16)$$

For a partly cloudy ground-pixel the vertical column density is given by:

$$N_v = \frac{N_s + w \cdot M_{cloudy} \cdot N_g}{M} \quad (5.17)$$

where the (total) air mass factor M is determined according to Eq. (5.13) and the weighting factor w with Eq. (5.14). The term $w \cdot M_{cloudy} \cdot N_g$ in the numerator of Eq. (5.17) denotes a virtual slant column below the clouds that is not measured by GOME. Note that for a cloud-free scene, Eq. (5.17) reduces to Eq. (5.15), and for fully cloudy ground-pixels it reduces to Eq. (5.16).

5.6.3 Error analysis

An error analysis has been carried out for the TOGOMI ozone columns. Here, the main findings of this error analysis are presented. As shown in Section 5.4, the uncertainty in the ozone absorption cross-sections is an important error source for the DOAS-fit, and contributes

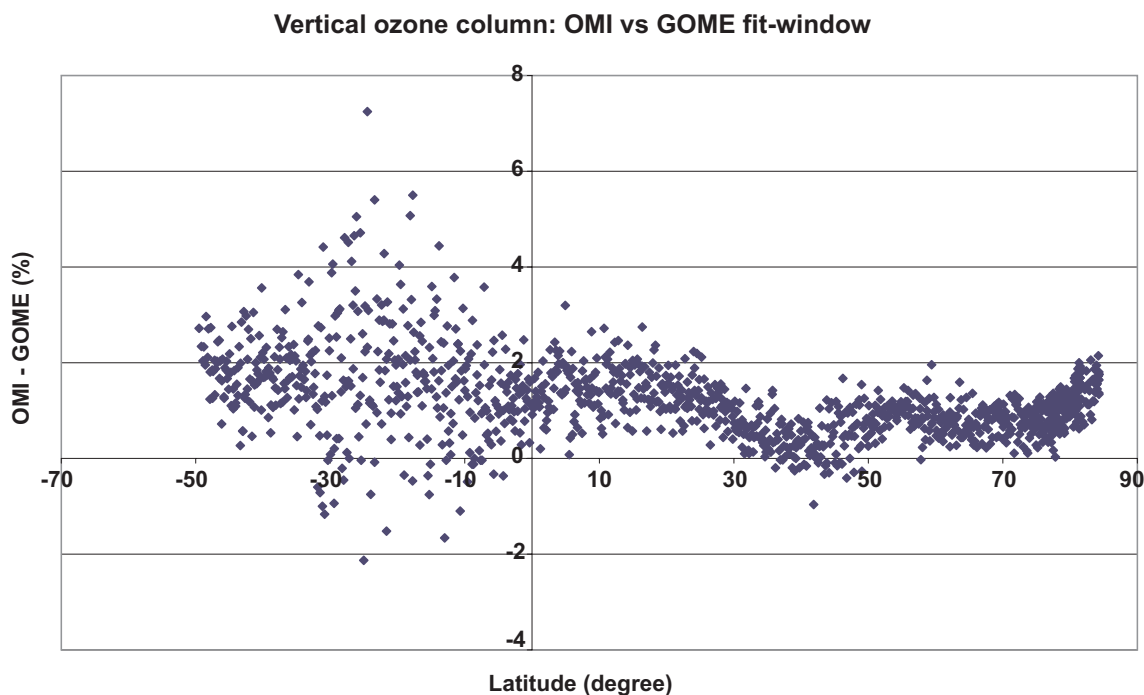


Figure 5.10 *Relative difference between the TOGOMI vertical ozone columns retrieved for the OMI fit-window (331.6-336.6 nm) and the GOME fit window (325-335 nm). The measurements of GOME orbit #32041 on 6 June 2001 are shown, as a function of latitude. The FM98 ozone cross-sections were used for both fit-windows.*

~2% to the error in the slant column. The expected error in the slant column due to the temperature sensitivity of the 325-335 nm fit window is estimated to be less than 0.5%, because of the use of pre-calculated ECMWF effective temperatures. The small temperature sensitivity of 331.6-336.6 nm fit-window further reduces this error to less than 0.3%. The signal-to-noise ration of the GOME instrument in the 325-340 nm range is better than 1000. The expected error in the slant column due to radiometric noise is ~0.5% for the 325-335 nm fit-window, and ~1.5% for the 331.6-336.6 nm fit-window. Finally, the error in the slant column due to the spectral calibration uncertainty (better than 1/100th of a pixel) is estimated to be less than 0.5%.

The error estimates for the air mass factors and the cloud correction are based on the analysis carried out for the OMI total ozone algorithm [Veefkind and De Haan, 2002]. Due to the uncertainty in the cloud fraction and cloud top pressure, the estimated error for the cloudy air mass factor is larger than for the clear-sky air mass factor: ~1.5% and 0.6%, respectively. The most important error source due to the cloud correction is the uncertainty in the ghost column. The average error in the ghost column is estimated to be 40% (about 5-8 DU).

By combining the error estimates of the slant column density, the air mass factor and the ghost column, an estimate of the error in the vertical column density can be made: the estimated total error of the vertical column density is ~2.5% for a cloud free ground-pixel, and increases to ~3.3% for a cloudy ground-pixel. The quality of the TOGOMI ozone columns has also been assessed by comparisons with other satellite and ground-based ozone measurements, as described in the next section.

5.7 Ozone column comparisons

5.7.1 Fit window comparison

Both the GOME fit-window (325-335 nm), as well as the OMI fit-window (331.6-336.6 nm), have been used to calculate vertical ozone columns with the TOGOMI algorithm. Figure 5.10 shows the relative difference between the ozone columns retrieved with the two fit-windows for GOME orbit #32041 on 6 June 2001. Theoretically, there should not be a systematic difference between the two ozone columns. However, Figure 5.10 shows that on average, the ozone columns retrieved with the OMI fit-window are 1-1.5% higher than the ozone columns retrieved with the GOME fit-window. It is very well possible that the relatively large error in the ozone cross-section data sets leads to systematic differences between the ozone columns, since the ozone absorption structures in the two fit-windows differ considerably. In addition, the OMI fit-window contains a strong Ring structure around 336 nm. Therefore, it is likely that inaccuracies in the theoretical Ring spectra (as calculated by *Chance and Spurr* [1997] and *De Haan* [2003]) have a larger effect on the ozone columns retrieved with the OMI fit-window. For GOME orbits in other months similar systematic differences are found, with 1-2% higher ozone columns retrieved with the OMI fit-window.

Figure 5.10 also shows that in the Northern Hemisphere, there is a small scatter of about 1% in the differences, mainly due to the lower signal-to-noise ratio of the (smaller) OMI fit-window, resulting in scatter in the retrieved slant columns, see Section 5.4.3. The large scatter in the Southern Hemisphere is due to the South Atlantic Anomaly (SAA), which strongly reduces the signal-to-noise ratio of the measured GOME reflectance for orbits over the South Atlantic [*REF*]. As expected, the SAA has a larger effect on the ozone columns retrieved with the OMI fit-window than on the ones retrieved with the GOME fit-window.

5.7.2 Comparisons with FD ozone columns

Figure 5.11a shows the vertical ozone columns calculated with the TOGOMI algorithm using the 325-335 nm fit-window, and the ozone columns calculated with the FD algorithm for the same GOME orbit #33930 on 16 October 2001. Figure 5.11b shows the relative difference between the two ozone columns. Because of the larger slant column (see Figure 5.6) and the differences in the air mass factor (Figure 5.9), the TOGOMI ozone columns are higher than the FD ozone columns. The pattern as a function of latitude is similar to that of the slant column, with the largest differences found for large solar zenith angles at high latitudes. An interesting feature clearly visible in Figure 5.11b is the sudden change in the difference around 65°S in the Antarctic ozone hole. These GOME measurements are over a cloud-covered area with cloud top heights of 5-7 km, and therefore a relatively large ghost column is added to the measured ozone column. However, the tropospheric ozone concentrations in the Logan, Labow & McPeters climatology are much smaller at these latitudes than in the *Fortuin and Kelder* [1998] climatology used in the FD algorithm. As a result, a smaller ghost column is added to the measured ozone column in the TOGOMI algorithm ($N_g = \sim 10$ DU) than in the FD algorithm ($N_g = \sim 18$ DU).

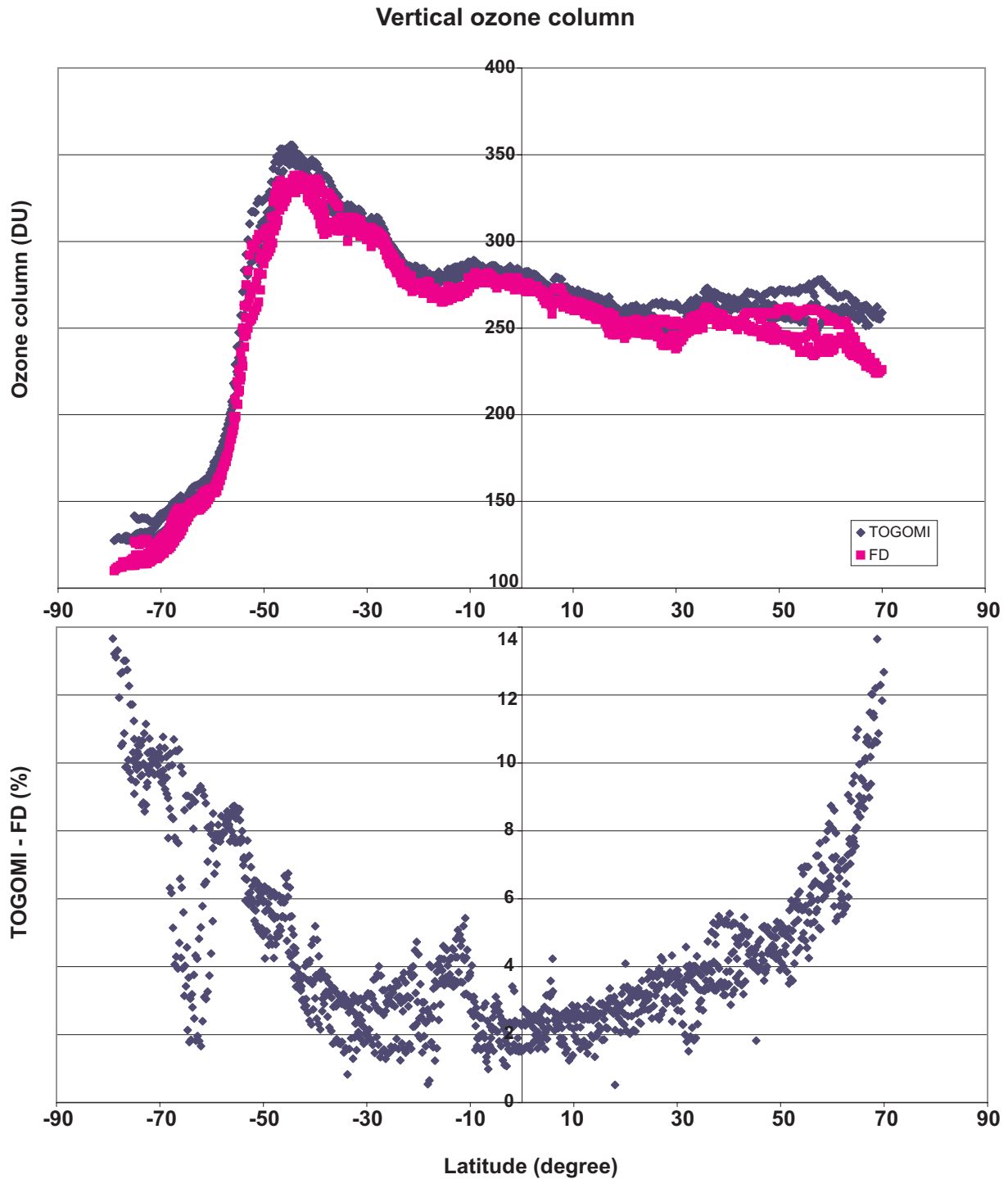


Figure 5.11 Vertical ozone columns retrieved with the TOGOMI and FD algorithms (top) and the relative difference between the ozone columns of the two algorithms (bottom). The measurements of GOME orbit #33930 on 16 October 2001 are shown, as a function of latitude. The 325-335 nm fit window and the FM98 ozone cross-sections were used in both algorithms.

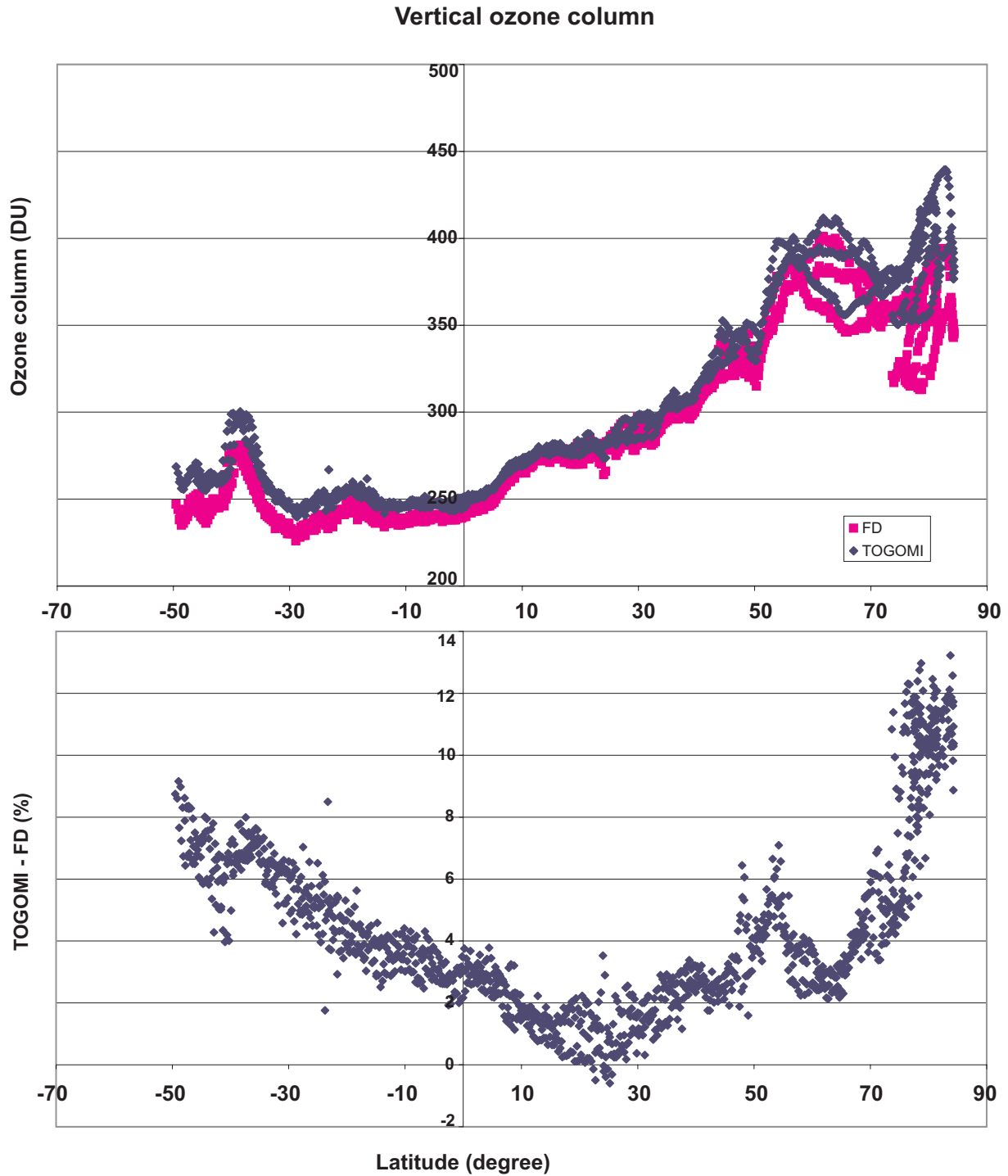


Figure 5.12 Vertical ozone columns retrieved with the TOGOMI and FD algorithms (top) and the relative difference between the ozone columns of the two algorithms (bottom). The measurements of GOME orbit #32041 on 6 June 2001 are shown, as a function of latitude. The 325-335 nm fit window and the FM98 ozone cross-sections were used in both algorithms.

Figure 5.12 shows the vertical ozone columns calculated with the TOGOMI and the FD algorithm, and the relative difference for GOME orbit #32041 on 6 June 2001. The difference plot shows the same pattern as for the October orbit: the TOGOMI ozone columns are higher than the FD ozone columns, with the largest differences found at high latitudes. However, the general pattern of the relative difference has shifted to the north, due to the solar zenith angle dependence. Note also that because of the high total ozone values, the absolute differences at northern high-latitudes are larger than for the October orbit.

5.7.3 Comparisons with GDP ozone columns

The TOGOMI ozone columns have also been compared with the GDP v3 ozone columns. Figure 5.13a shows the relative difference between the slant columns retrieved with the TOGOMI and GDP v3 algorithms. To calculate the slant column, the GDP algorithm uses the temperature fit method, based on the common DOAS fit Eq (5.1), without accounting for Raman scattering (see Section 5.4.2). The use of so-called undersampling cross-sections [Spurr *et al.*, 2002] to deal with the undersampling of GOME instead of reducing the effective spectral resolution, is another difference with the TOGOMI algorithm. Since Raman scattering is not properly accounted for in the GDP, the TOGOMI slant columns are higher than the GDP ozone columns, with the largest differences found for large solar zenith angles at high latitudes (see Figure 5.13a). As explained in Section 5.4.2, the temperature fit method in the GDP results in a ~3% overestimation of the retrieved slant column, which partly compensates the error due the incomplete treatment of Raman scattering. Therefore, the differences for the GDP are smaller than the differences shown in Figure 5.6. The increased scatter on the Southern Hemisphere due to the South Atlantic Anomaly is also clearly visible in Figure 5.13a. The SAA has a larger effect on the GDP v3 ozone columns, because of the sensitivity of the temperature fit method for the SAA, as described by Van Roozendael *et al.* [2002b].

Figure 5.13b shows the relative difference between the vertical ozone columns retrieved with the TOGOMI and GDP v3 algorithm. Although the TOGOMI vertical columns are generally higher than the GDP vertical columns, the comparison differs considerably from that of the slant columns in Figure 5.13a, mainly due to differences in the air mass factors. Because of the different way the air mass factor are calculated in the two algorithms, this is to be expected. The GDP v3 uses an air mass factor for one wavelength (325 nm) based on the TOMS v7 climatology [Spurr *et al.*, 2002], while the TOGOMI algorithm uses an empirical AMF based on the Logan, Labow & McPeters climatology.

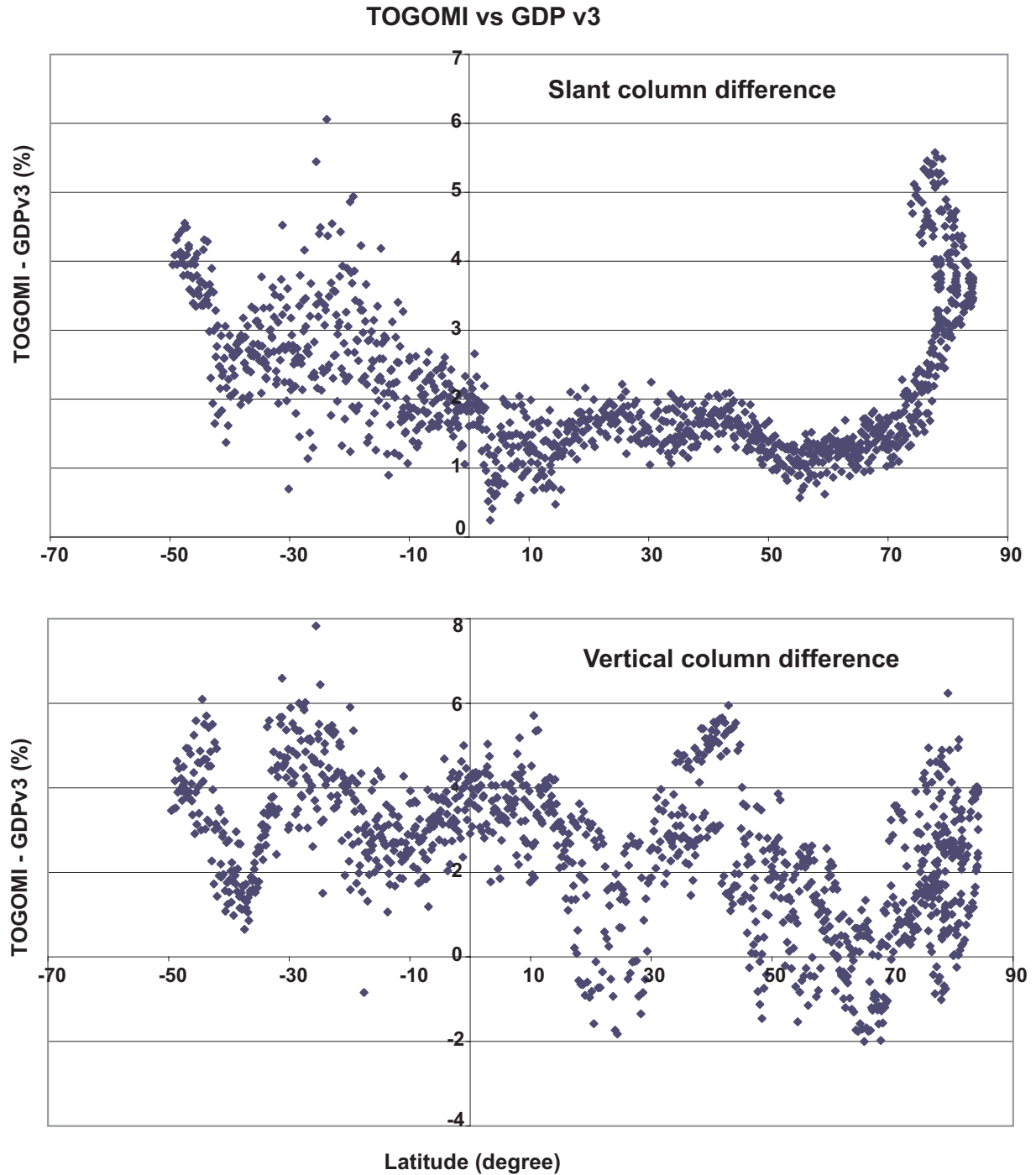


Figure 5.13 Relative difference between the slant columns (top) and vertical ozone columns (bottom) retrieved with the TOGOMI and GDP version 3 algorithms. The measurements of GOME orbit #32041 on 6 June 2001 are shown, as a function of latitude. The 325-335 nm fit window and the FM98 ozone cross-sections were used in both algorithms.

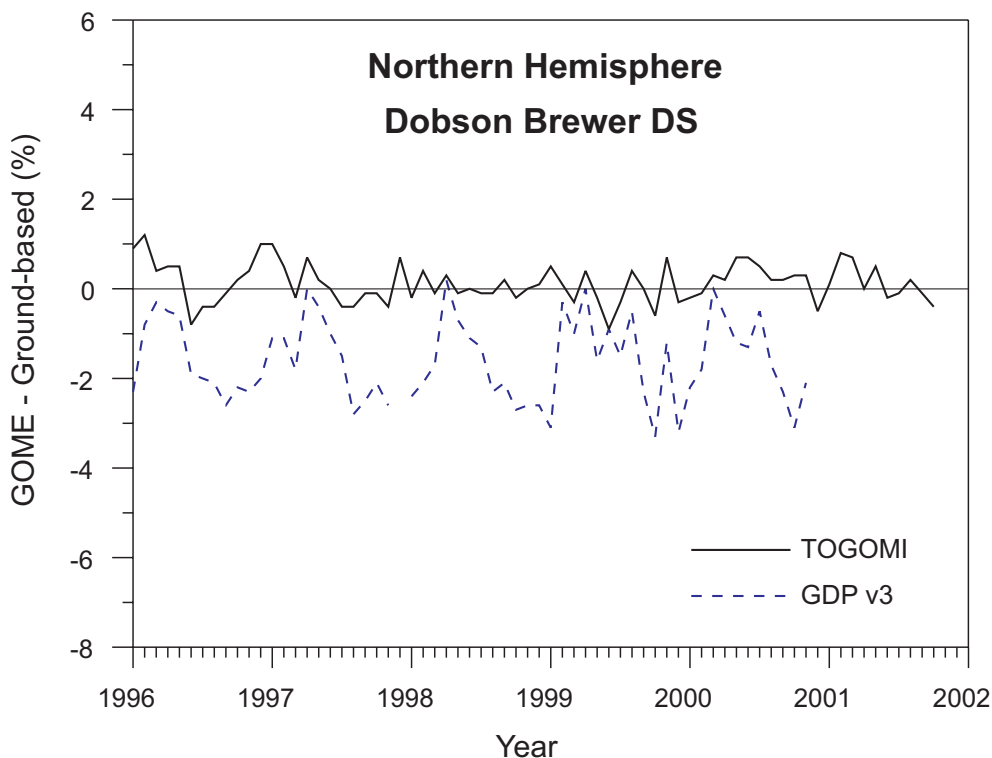


Figure 5.14 Relative difference between the TOGOMI (black line) and GDP v3 (dotted line) ozone columns, and ground-based Dobson and Brewer measurements for the Northern Hemisphere, as a function of time. Adapted from Balis [Private Comm.]

5.7.4 Validation with ground-based measurements

A preliminary global validation of the TOGOMI ozone columns with ground-based ozone measurements has been carried by Balis [Private Comm.]. The results have been compared with the validation results for the GDP and FD ozone columns (see Chapter 2 and Lambert and Zehner [2002]; Kelder *et al.* [2003]). Figure 5.14 shows the comparison of the TOGOMI and GDP v3 ozone columns with ground-based Dobson and Brewer measurements in the Northern Hemisphere for the period 1996-2001. The GDP v3 ozone columns generally underestimate the ground-based measurements, as can be seen in Figure 5.14. However, the underestimation of the GDP v3 is more or less seasonal dependent, with differences between 0 and 3%. The FD (and GDP v2.7) ozone columns exhibit an even stronger seasonal dependence than the GDP v3 ozone columns (not shown): the FD ozone columns show a reasonable agreement during the NH summer, but underestimate the Brewer measurements by 4-5% during the NH winter. Figure 5.14 shows that the improved TOGOMI ozone columns compare very well with the ground-based measurements: the differences are within 1%, and there is no seasonal dependence. This is in agreement with the fact that the TOGOMI ozone columns are generally higher than the FD ozone columns, and that the difference increases with increasing solar zenith angle, as described in the section 5.7.2 (see Figure 5.11 and 5.12).

Figure 5.15 shows the comparison of the TOGOMI, FD and GDP v3 ozone columns with Dobson and Brewer measurements as a function of latitude. It should be noted that for the FD

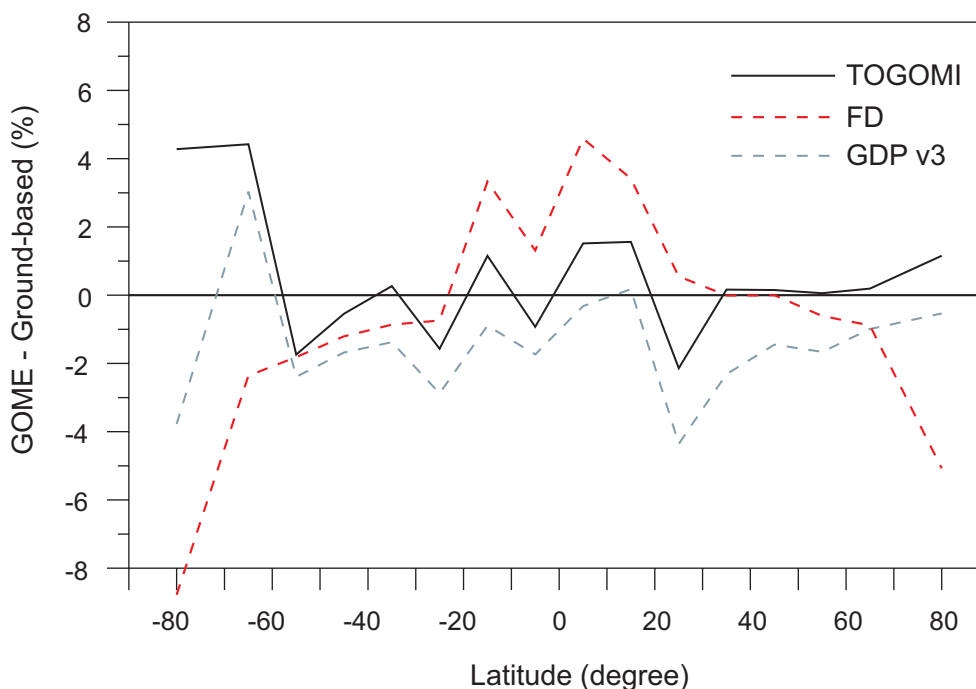


Figure 5.15 Relative difference between the TOGOMI, FD, and GDP v3 ozone columns, and ground-based Dobson and Brewer measurements, as a function of latitude. For the TOGOMI and GDP comparisons, observations for the years 1996-2001 have been used, while for the FD comparisons, observations for 1998-2000 have been used. Adapted from Balis [Private Comm.]

comparison, observations for the years 1998-2000 have been used, while for the TOGOMI and GDP comparisons, observations for 1996-2001 have been used. Figure 5.15 shows that the TOGOMI ozone columns agree very well with the ground-based measurements, with differences smaller than 2%, except for southern high latitudes, where the TOGOMI ozone columns are ~4% larger than the ground-based measurements. The GDP v3 also shows a reasonable good agreement with the ground-based measurements. However, the GDP v3 ozone columns generally underestimate the ground-based measurements by about 2%. Figure 5.15 clearly illustrates the improved accuracy of the TOGOMI algorithm, compared to the FD algorithm. The FD ozone columns overestimate the ground-based measurements by 2-4% at low-latitudes, and underestimate the ground-based measurements by about 5% at high-latitudes.

5.8 Concluding Remarks

An improved total ozone algorithm for the Global Ozone Monitoring Experiment (GOME) instrument has been developed based on the Differential Optical Absorption Spectroscopy (DOAS) method. The new algorithm, called TOGOMI, uses a DOAS fit-equation that properly accounts for inelastic Raman scattering. This results in 3-10% larger ozone slant columns compared to the slant columns retrieved with the common DOAS fit-equation, as

used in the Fast Delivery and GDP algorithms. The largest differences are found for large solar zenith angles at high latitudes, as a result of the increasing relative amount of Raman scattered light due to multiple scattering.

The retrieved ozone slant columns depend on the ozone absorption cross-section data set used in the TOGOMI algorithm: the use of the Bass and Paur cross-sections in the DOAS fit results in 2.5-4% larger slant columns than when the GOME Flight Model (FM98) cross-sections are used. This is a result of the differences between the two cross-section data sets. Since the accuracy of the FM98 and B&P cross-section are comparable, the issue of the best-suited cross-section data set can only be resolved when more accurate cross-sections (better than 2%) become available.

The main advantage of the 325-335 nm spectral fit-window is that it contains three main differential absorption structures, resulting in a high signal-to-noise ratio. However, this fit-window is very sensitive to the temperature dependence of the ozone cross-sections. A simultaneous fit of the ozone slant column and the effective absorption temperature, results in a ~3% overestimation of the slant column. Therefore, a pre-calculated effective temperature is used in the TOGOMI algorithm, based on daily temperature analyses from the ECMWF model and the ozone profile climatology from Logan, Labow & McPeters. The 331.6-336.6 nm fit-window has the important advantage that it is insensitive to the temperature dependence of the ozone cross-sections, and therefore a fixed absorption temperature can be used for the ozone cross-sections in the DOAS-fit. A disadvantage of this 5 nm wide fit-window is that it only contains two main differential absorption structures, resulting in a lower signal-to-noise ratio, and a ~1% larger random error in the ozone column, compared to the ozone column retrieved with the 325-335 nm fit-window.

A fair assumption for ozone absorption is that the air mass factor for elastic and inelastic scattering is the same. Therefore, only elastically scattered light is considered in the air mass factor calculations. The empirical air mass factors approach used in the TOGOMI algorithm, reduces the errors involved in the DOAS method, e.g. when the atmosphere becomes optically thick at high solar zenith angles. The uncertainty in the air mass factor due to the natural ozone profile variability, is reduced by using a slant column dependent air mass factor, based on the ozone profile climatology from Logan, Labow & McPeters.

The improved DOAS fit-equation and empirical air mass factor calculations result in larger vertical ozone columns, compared to the Fast Delivery (FD) ozone columns. The difference depends strongly on the solar zenith angle: at low-latitudes the TOGOMI ozone columns are 0-3% larger than the FD ozone columns, while at high-latitudes the TOGOMI ozone columns are about 10% larger. The difference with the GDP v3 ozone columns is somewhat smaller: between -2 and +6 %. In the GDP v3, the temperature fit method results in a positive bias in the slant column, which partly compensates the error due to the incomplete treatment of inelastic Raman scattering.

The preliminary validation of the TOGOMI ozone columns with ground-based Brewer and Dobson measurements shows a very good agreement. The differences with the ground-based measurements are within 1-2%, and, in contrast to the FD ozone columns, there are no seasonal dependent differences.

As described in the Introduction of this thesis (Section 1.5), satellite ozone measurements are invaluable in detecting long-term trends in ozone. For accurate trend analyses, the satellite instrument should be able to detect a change of 1% in the ozone column over a period of 10

years [WMO, 2003]. This requires a high (relative) accuracy of the ozone columns (i.e. of the order of 2-3%, see *Weatherhead et al.* [1998]). The improved TOGOMI ozone columns will therefore be a valuable addition to existing satellite data sets used in ozone trend studies.

Because the TOGOMI algorithm uses the fast DOAS retrieval method, the ozone columns can also be retrieved in near-real time (i.e. within 3 hours after sensing), just like the FD algorithm. A difficulty with the assimilation of the FD ozone column into the ECMWF model is the negative bias between the satellite ozone values and the modelled ozone fields [*Dethof, 2003*]. The assimilation of the TOGOMI ozone columns in the ECMWF model could reduce this bias considerably.

Chapter 6

Summary and Outlook

6.1 Overview

The retrieval of vertical ozone column densities from Global Ozone Monitoring Experiment (GOME) observations was one of the main topics of this thesis. A Fast Delivery (FD) algorithm has been developed that retrieves GOME ozone columns in near-real time. The FD ozone column data were used to study an ozone mini-hole event over north-western Europe on November 30, and December 1, 1999. Since the validation of the FD ozone columns raised important issues for further improvements, a new algorithm has been developed, based on the total ozone algorithm for the Ozone Monitoring Instrument (OMI).

This thesis also dealt with the variability in tropical tropospheric ozone. GOME ozone columns and GOME cloud measurements were used to determine a monthly-mean tropospheric ozone column for the tropics. The GOME-TTOCs, and the chemistry-transport model TM3, have been used to untangle the intriguing relation of tropical tropospheric ozone to biomass burning emissions, lightning NO_x emissions and large-scale transport. The conclusions from these studies are presented below, formulated as answers to the scientific questions posed in Chapter 1, that guided the investigations in this thesis.

6.2 Summary and Conclusions

6.2.1 Scientific questions

The following questions were addressed in this thesis:

1. *Can ozone columns be retrieved from GOME observations in near real-time, with the required quality for use in Numerical Weather Prediction models?*
2. *How well do the GOME ozone columns agree with ground-based observations, and can the accuracy of the GOME ozone columns be improved further?*

3. *What is the influence of low stratospheric temperature on observations of ozone mini-holes from the ground and from space?*
4. *Can the existing retrieval methods of tropospheric ozone columns in the tropics be improved with GOME observations?*
5. *How to interpret the observed variability of ozone in the tropical troposphere?*

The first two questions relate to the work presented in Chapters 2 and 5, the third question to Chapter 3 and the last two questions to Chapter 4.

6.2.2 Answers to the scientific questions

1. *Can ozone columns be retrieved from GOME observations in near real-time, with the required quality for use in Numerical Weather Prediction models?*

The growing demand for global ozone measurements from satellite instruments motivated the development of the GOME Fast Delivery (FD) algorithm. Applications such as the assimilation of ozone in Numerical Weather Prediction (NWP) models, monitoring the status of the ozone layer and improving surface UV radiation forecasts require that the satellite ozone observations are available within a few hours after sensing, i.e. in near-real time. To meet this demand, the FD algorithm uses only a small part of the raw GOME data, thereby assuring the availability in near-real time. The FD algorithm is based on the algorithm used within the ESA/DLR GOME Data Processor. However, several changes in the algorithms have been made to improve the retrieval of the ozone columns: (1) the use of effective ozone absorption cross-sections based on ECMWF temperature forecast in the ozone slant column fit, (2) the use of the DAK radiative transfer model and the *Fortuin and Kelder* [1998] ozone climatology for the air mass factor calculations and (3) the use of the FRESCO cloud algorithm for the derivation of cloud fraction and cloud-top pressure. A global validation with ground-based measurements showed that the level of quality of the FD ozone columns meets the requirements for near-real time applications (see also Question 2).

The assimilation of satellite ozone observations in NWP models is expected to give a better description of the stratospheric dynamics, the temperatures and the radiation and heating in the model [*Stoffelen and Eskes*, 1999; *Struthers et al.*, 2002]. At the European Centre for Medium-Range Weather Forecasts (ECMWF), experiments with the assimilation of the GOME-FD ozone columns (together with SBUV ozone profiles) started in August 2001. An important issue regarding the assimilation of the FD ozone columns in the ECMWF model is the bias between the FD ozone columns and the modelled ozone fields, especially for high latitudes. North of 40°N and south of 50°S, the FD values are lower than the model values, with differences of more than 10% at high latitudes. As inferred from a validation with ground-based measurements, the difference is partly due to a negative bias in the FD ozone columns at high latitudes in winter (i.e. for large solar zenith angles). It should be noted that the ECMWF model also has a bias: the modelled ozone values are too low in the tropics and too high at high latitudes [*Dethof*, 2003].

2. *How well do the GOME ozone columns agree with ground-based observations, and can the accuracy of the GOME ozone columns be improved further?*

The accuracy of the FD ozone columns has been determined by a global validation study involving ground-based total ozone observations from about 15 sites, associated with the international Network for the Detection of Stratospheric Change. The near-real time ozone columns are in reasonable agreement with the ground-based measurements (within 5% for low- and mid-latitudes, within -10 to +5% for high latitudes). An important issue is that the FD algorithm underestimates the winter ozone values at higher latitudes. This solar zenith angle / latitudinal dependence of the FD ozone columns was also found by a validation with ground-based Brewer and Dobson measurements [Balis and Zerefos, 2001].

To resolve the inaccuracies of the FD algorithm, an improved GOME total ozone algorithm was developed. The new algorithm, named TOGOMI, is based on the total ozone algorithm for the OMI instrument, to be launched on EOS-Aura in 2004 [Veefkind and De Haan, 2002]. The main improvements of this algorithm are: (1) a new DOAS fit-equation that properly accounts for inelastic Raman scattering, (2) the use of an empirical DOAS method to account for the wavelength dependence of the air mass factor, and (3) the use of a slant column dependent air mass factor to account for atmospheric variability. In addition, the new algorithm offers the possibility to use a smaller (5 nm) spectral fit window at longer wavelengths, which reduces the sensitivity to the ozone profile and atmospheric temperature. The improved DOAS fit-equation and empirical air mass factor calculations result in larger ozone column values, compared to the ozone columns retrieved with the FD algorithm. The difference depends on the solar zenith angle: at low-latitudes the TOGOMI ozone columns are 0-3% larger than the FD ozone columns, while at high-latitudes the TOGOMI ozone columns are about 10% larger. A preliminary validation of the improved ozone columns with ground-based Brewer and Dobson measurements showed a very good agreement. The differences with the ground-based measurements are within 1-2%, and, in contrast to the FD ozone columns, there are no seasonal dependent differences.

For ozone trend studies, the satellite instrument should be able to detect a change of 1% in the ozone column over a period of 10 years [WMO, 2003]. This requires a high (relative) accuracy of the ozone column (i.e. of the order of 2-3%, see Weatherhead *et al.* [1998]). The favourable (preliminary) validation results indicate that the improved TOGOMI ozone columns will be a valuable addition to existing satellite data sets used in ozone trend studies.

Since the TOGOMI algorithm is fast enough to allow ozone column processing in near-real time, the improved ozone columns can also be used for assimilation in the ECMWF model. With the TOGOMI algorithm, the bias between the GOME ozone columns and the ECMWF model can largely be resolved (see Question 1).

3. *What is the influence of low stratospheric temperature on observations of ozone mini-holes from the ground and from space?*

A region of extreme low ozone column densities passed over North-western Europe during November 30, and December 1, 1999. This ozone mini-hole was mainly caused by poleward transport of subtropical air with small ozone mixing ratios into the North Atlantic storm track region [Van Velthoven, Private Comm.]. Total ozone values well below 200 DU were measured from the ground, with a Brewer Spectrophotometer at De Bilt (52°N, 5°E), and from space with the GOME and TOMS satellite instruments. An ozonesonde measurement and a retrieved GOME ozone profile at De Bilt showed that the main reduction in the ozone concentration occurred between the tropopause (210 hPa) and the ozone maximum (31 hPa).

Sonde measurements and ECMWF temperature analyses showed that the low ozone values over Europe coincided with very low temperatures in the stratosphere. The adiabatic cooling associated with the large scale uplifting of air in the lowermost stratosphere created favourable conditions for formation of Polar Stratospheric Clouds (PSCs). Although this has the potential for ozone destruction by heterogeneous chemistry, it does not seem to have affected the ozone column densities in the ozone mini-hole itself.

Because of the temperature dependence of the ozone cross-sections, the low stratospheric temperature has significant consequences for both the Brewer and GOME total ozone retrieval algorithms. The effective ozone temperature in the ozone mini-hole was -62°C , as derived from sonde measurements. The use of a fixed ozone temperature (-46.3°C) in the standard ozone retrieval software for the Brewer spectrophotometer resulted in total ozone values which are $\sim 2\%$ too low. In the Fast Delivery algorithm, used to retrieve the GOME total ozone values in the ozone mini-hole, the error in the effective ozone temperature is minimised by using ECMWF temperature profiles. The GOME algorithm has the opposite sensitivity to the atmospheric temperature: if climatological temperature profiles are used to calculate the ozone temperature, the GOME total ozone values are $\sim 4\%$ too high. From this analysis, one can conclude that it is essential to take the stratospheric temperature sensitivity of both the GOME and Brewer instruments into account, especially when comparing coincident Brewer and GOME ozone measurements.

4. *Can the existing retrieval methods of tropospheric ozone columns in the tropics be improved with GOME observations?*

Tropical tropospheric ozone columns (TTOCs) have been determined with an improved convective-cloud-differential (CCD) method, using GOME ozone column and cloud measurements. A limitation of the existing TOMS-CCD method is that cloud height information is not measured by TOMS, and the assumption is made that tropical high-reflectivity clouds often have cloud tops at the tropopause (~ 100 hPa) [Ziemke *et al.*, 1998]. However, the cloud fractions and cloud top pressures derived with the GOME-FRESCO algorithm, indicate that most tropical convective cloud tops are between 300 and 500 hPa, and do not extend up to the tropopause. The GOME-CCD method takes this tropical transition layer below the tropopause into account, and uses above-cloud and clear-sky ozone columns

to derive a monthly-mean TTOC below 200 hPa. The comparisons with ozonesonde measurements from the Southern Hemisphere ADditional OZonesondes (SHADOZ) network showed that the assumption of the GOME-CCD method of a zonally invariant ozone column above 200 hPa, including both ozone in the stratosphere and the transition layer, has good validity in the tropics.

The monthly-averaged TTOCs have been calculated for the period July 1995-December 2001 on a 2.5° latitude by 5° degree longitude grid. The validation of the GOME-TTOCs for the southern tropics with seven ozonesonde sites showed a good agreement, with an RMS difference of about 5 DU. In the northern tropics, comparisons have been made with ozonesonde measurements at Paramaribo ($6^\circ\text{N}, 55^\circ\text{W}$) and with MOZAIC aircraft observations at Abidjan ($5^\circ\text{N}, 4^\circ\text{W}$). At these sites, the GOME-TTOCs also compare favourably with in-situ measurements. The seasonal variation at the northern tropical site Paramaribo is captured reasonably well.

The GOME-TTOCs do not show the occasionally strong deviations from ozonesonde and aircraft measurements as seen in the TOMS-TTOCs. However, for both the GOME and TOMS instruments, the low sensitivity for ozone changes in the lower most troposphere forms a fundamental limitation in detecting lower tropospheric ozone from space. This is especially of importance for the northern tropics, where the increases in ozone concentrations during the biomass burning season occur mainly in the lower troposphere.

5. *How to interpret the observed variability of ozone in the tropical troposphere?*

The presence of a seasonal maximum in tropical tropospheric ozone over the southern tropical Atlantic and a persistent minimum over the tropical Pacific has been the focus of many past and present studies. This zonal wave-one pattern in tropospheric ozone has been measured from the ground (e.g. by ozonesondes) and with satellites, using the tropospheric ozone residual technique from *Fishman et al.*, [1990], the TOMS-MR method [*Hudson and Thompson*, 1998], and the CCD method described in this thesis. The wave-one pattern and the variability in the TTOC can be attributed to a complex interaction of several processes, including biomass burning, lightning, and large-scale transport. For example, analysis of the GOME-TTOCs, with the aid of the TM3 model, showed that the pronounced difference between the seasonal South Atlantic maximum in 2000 and 2001 can be explained by the difference in transport between the two years.

The highest TTOC during the northern biomass burning season (December-February) are usually observed over the South Atlantic, even though burning in the Southern Hemisphere is then at its seasonal minimum; this is the so-called “tropical Atlantic paradox” [*Thompson et al.*, 2000]. The upper tropospheric ozone production from lightning NO_x emissions, and the persistent subsidence over the southern tropical Atlantic contribute to the tropical Atlantic paradox and the persistent wave-1 pattern in the TTOC. However, the tropical Atlantic paradox can also be partly explained by the low sensitivity of the GOME and TOMS instruments for ozone changes in the lower troposphere (see also Question 4). In the northern tropics, the increases in ozone during the biomass burning season occur mainly in the lower troposphere, while the largest increases over the southern Atlantic occur in the middle troposphere. Due to the efficiency correction for the reduced sensitivity of GOME for ozone

in the lower troposphere in the GOME retrieval algorithm, the GOME-TTOC captures the seasonal variation in the northern tropics better than the TOMS-TTOC, which reduces the magnitude of the observed tropical Atlantic paradox.

6.3 Outlook and future work

6.3.1 Total ozone columns

Satellite instruments offer the possibility to measure the distribution of atmospheric constituents on a global scale and on a long-term basis. The launch of the GOME instrument on the ERS-2 satellite in April 1995 provided new possibilities to determine the global atmospheric abundance of ozone and other trace gases, such as nitrogen dioxide (NO₂), formaldehyde (HCHO), sulfur dioxide (SO₂), bromine oxide (BrO), and the chlorine specie OClO. Since 1997, the Fast Delivery system at KNMI produces total ozone columns from GOME observations in near-real time, and makes them available on the Internet. The FD ozone columns are assimilated in the TM3 chemical transport model to calculate a global ozone field and a 5-day ozone forecast [Eskes *et al.*, 2002, 2003]. The FD ozone columns and the assimilated ozone fields and forecast are distributed to numerous end-users for various applications. For example, the WMO uses the GOME ozone columns for monitoring the status of the ozone layer, and several meteorological organisations use the GOME ozone columns for improving their surface UV radiation forecasts. With the implementation of the new TOGOMI retrieval algorithm and the adaptation of this algorithm to the SCIAMACHY instrument, the Fast Delivery service can be continued over the coming years, and the quality of the near-real time ozone columns and assimilated ozone fields can be improved further.

An extensive global validation of the TOGOMI ozone columns with ground-based Brewer and Dobson instruments is ongoing. An analysis of the quality of the total ozone columns will be made for a range of observing conditions and atmospheric circumstances, e.g. solar zenith angle, surface albedo, seasonal variations and the Antarctic ozone hole. Further developments for the TOGOMI algorithm include the use of a new version of the DAK radiative transfer model, based on a spherical atmosphere. This is especially of importance for the calculation of the air mass factor for solar zenith angles $> 75^\circ$. To improve the accuracy of the ozone columns for higher latitudes, daily snow and sea-ice maps from the ECMWF model will be used. The presence of snow or ice has a large effect on the surface albedo and thus on the air mass factor. Another issue is the relative large uncertainty in the ozone absorption cross-sections, as described in Chapter 5. The availability of more accurate cross-sections data-sets becomes increasingly important for future improvements of the TOGOMI algorithm and of ozone retrieval algorithms in general.

As noted above, the assimilation of satellite ozone data in the ECMWF model started in 2001, using FD-GOME ozone columns and SBUV ozone profiles. Since April 2002, the FD ozone columns are assimilated in the operational ECMWF model. For the operational assimilation, the bias between the FD ozone columns and the modelled ozone fields for higher latitudes is an important issue. It is expected that the bias between the GOME ozone columns and the modelled ozone fields can largely be resolved with the improved TOGOMI algorithm,

and GOME ozone columns for higher latitudes can be included in the ECMWF assimilation system.

Another development is the adaptation of the TOGOMI algorithm to the SCIAMACHY instrument. SCIAMACHY is an extended version of GOME and was launched on ENVISAT in 2002. The most important improvement for the ozone columns is the higher spatial resolution of SCIAMACHY compared to GOME: the ground-pixel size of SCIAMACHY is $30 \times 60 \text{ km}^2$ for latitudes between 50°S and 50°N , and about $30 \times 240 \text{ km}^2$ for higher latitudes. The spectral measurements of SCIAMACHY in the DOAS fitting region for ozone are very similar to those of the GOME instrument, making the implementation of the TOGOMI algorithm relatively straightforward.

The OMI instrument, to be launched in 2004 on EOS-AURA, will have an even smaller ground-pixel ($13 \times 24 \text{ km}^2$), with global coverage in one day. Since the TOGOMI algorithm is based on the total ozone algorithm developed for the OMI instrument, the two algorithms are very similar. This has the important advantage that the experience gained with the GOME observations and the TOGOMI algorithm can be used for further improvements of the OMI algorithm. The results of the global validation of the TOGOMI ozone columns with ground-based measurements will also be beneficial for the improvement of both algorithms.

6.3.2 Tropical tropospheric ozone

The variability of ozone in the tropical troposphere and the interplay of biomass burning, lightning, and large-scale transport are the subject of ongoing research, in which satellite and ground-based measurements are used in conjunction with chemical transport models. The satellite analyses described in Chapter 4 demonstrate the strength of the cloud-differential method to determine the tropical tropospheric ozone column (TTOC). The cloud-differential method can be extended to a cloud slicing method, in which ozone column measurements are used above clouds with different cloud-top pressures. With the cloud slicing method, it is possible to retrieve ozone information for different tropospheric layers, as has been demonstrated by Ziemke *et al.* [2001], using TOMS total ozone measurements and THIR cloud top pressure data for the period 1979-1984. Because of the large ground pixel of GOME, the number of cloudy and clear sky measurements is generally too small to apply such a cloud slicing method. However, the upcoming satellite instruments will greatly enhance the possibilities to retrieve information about the tropospheric ozone profile, as explained below.

The SCIAMACHY instrument provides collocated ozone and cloud data with a ground-pixel of $30 \times 60 \text{ km}^2$ for the (sub)tropics and mid-latitudes. With SCIAMACHY, it is possible to continue and improve the present TTOC time series from the GOME and TOMS instruments. Furthermore, the small pixel size in the (sub)tropics allows the retrieval of tropospheric profile information with the cloud slicing method. The even smaller ground-pixel of OMI and the three GOME-2 instruments, the first one to be launched on the METOP-1 satellite in 2005, will allow more frequent observations between clouds, thus giving better penetration into the troposphere. This makes it possible to extend the cloud slicing method to the sub-tropics and mid-latitudes. The combination of TTOC measurements with ozone

profile measurements, and the combination with chemistry transport models through data-assimilation techniques, will further improve the measurement of the global tropospheric ozone distribution.

Measurements of ozone precursors, such as CO and NO₂, are invaluable for understanding the processes affecting the tropical tropospheric ozone distribution. For example, recent studies show how MOPITT-CO retrievals allow investigation of convection of biomass burning plumes at the ITCZ and inter-hemispheric transport, while GOME-NO₂ measurements enable identification of two important tropical sources of this ozone precursor, biomass burning and lightning [e.g. *Edwards et al.*, 2003]. With the upcoming satellite instruments, such as SCIAMACHY, the possibilities to measure ozone precursors in the troposphere are extended considerably. Furthermore, the continuation of satellite measurements until 2020 with OMI and the three GOME-2 instruments will make it possible to monitor trends in (sub)tropical tropospheric ozone and its precursors over a long period. This is of great importance, since large ozone trends are expected in view of the rapid development of several (sub)tropical countries [*Prather et al.*, 2001].

Bibliography

- Aberle, B., W. Balzer, A. von Bargaen, E. Hegels, D. Loyola and R. Spurr, GOME Level 0 to 1 Algorithms Description, Tech. Note ER-TN-DLR-GO-0022 (Issue 5/B), Deutsches Zentrum für Luft und Raumfahrt, Oberpfaffenhofen, Germany, 2002.
- Aliwell, S.R., M. Van Roozendaal, P.V. Johnston, A. Richter, T. Wagner, B. Arlander, J.P. Burrows, D.J. Fish, R.L. Jones, J.-C. Lambert, I. Pundt, K. K. Tornkvist, Analysis for BrO in zenith-sky spectra : An intercomparison exercise for analysis improvement, *J. Geophys. Res.*, 107, No. D23, 10.1029/2001JD000329, 2002.
- Allaart, M., P. Valks, R. van der A, A. Piters, H. Kelder and P. van Velthoven, Ozone mini-hole observed over Europe, influence of low stratospheric temperature on observations, *Geophys. Res. Lett.*, 27, 4089-4092, 2000.
- Arino, O., M. Simon, I. Piccolini, J.M. Rosaz, The ERS-2 ATSR-2 World Fire Atlas and the ERS-2 ATSR-2 World Burnt Surface Atlas projects, paper presented at *8th ISPRS conference on Physical Measurement and Signatures in Remote Sensing*, Int. Soc. for Photogramm. and Remote Sensing., Aussois, France, 8-12 January, 2001.
- Balis, D.S. and C.S. Zerefos, Extensive validation of the total-ozone fields for the period 1995-2000, based on ground based total ozone measurements, paper presented at GOA Project Meeting, 5 Oct., 2001, Thessaloniki, Greece, 2001.
- Bass, A.M., and R.J. Paur, The Ultraviolet Cross-Sections of Ozone, I, The Measurements, in: *Atmospheric Ozone*, edited by C. S. Zerefos and A. Ghazi, pp. 606-610, D. Reidel, Norwell, Mass., 1985.
- Berk, A., L. S. Bernstein, and D. C. Robertson, MODTRAN: A moderate resolution model for LOWTRAN-7, *GL-TR-89-0122*, Geophysics Laboratory, Hanscom AFB, MA 01732, 1989.
- Bhartia, P.K. and C.W. Wellemeyer, OMI Algorithm Theoretical Basis Document, Barthia, P.K (ed), Volume II - Chapter 2, TOMS-V8 Total O3 Algorithm, *ATBD-OMI-02*, Version 2.0, Augustus 2002.
- Bovensmann, H., J.P. Burrows, M. Buchwitz, J. Frerick, S. Noël and V.V. Rozanov, SCIAMCHY: Mission Objectives and Measurements Modes, *J. Atmos. Sciences*, 56, no. 2, 127-150, 1999.
- Brasseur, G.P., R.A. Cox, D. Hauglustaine, I.S.A. Isaksen, J. Lelieveld, D.H. Lister, R. Sausen, U. Schumann, A. Wahner, and P. Wiesen, European scientific assessment of the atmospheric effects of aircraft emissions, *Atmos. Environ.*, 32, 2329-2418, 1998.
- Brewer, A.W., Evidence for a world circulation provided by the measurements of helium and water vapor distribution in the stratosphere, *Q. J. R. Meteorol. Soc.*, 75, 351-363, 1949.

- Brewer, A.W., A replacement for the Dobson spectrophotometer, *Pure Appl. Geophys.* 106, 919-927, 1973.
- Burrows, J.P., M. Weber, M. Buchwitz, V. Rozanov, A. Ladstätter-Weissenmayer, A. Richter, R. Debeek, R. Hoogen, K. Bramstedt, K.-U. Eichmann, M. Eisinger, D. Perner, The Global Ozone Monitoring Experiment (GOME): Mission concept and first results, *J. Atmos. Sciences*, 56, no. 2, 151-175, 1999a.
- Burrows, J.P., A. Richter, A. Dehn, B. Deters, S. Himmelmann, S. Voigt, J. Orphal, Atmospheric remote-sensing reference data from GOME - 2. Temperature-dependent absorption cross-sections of O₃ in the 231-794 nm range. *J. Quant. Spectrosc. Radiat. Transfer*, 61, 509-517, 1999b.
- Burrows, J.P., M. Weber, R. de Beek, V. Rozanov, A. Richter, *Gome-2 Error Assessment, Final Report*, Kerridge, B. (ed.), Chapter 17, Reduction in Spectral Resolution & Column Retrieval, EUMETSAT EUM/CO/01/901/DK, January 2003.
- Caspar, C. and K. Chance, GOME wavelength calibration using solar and atmospheric spectra. *Proceedings of the 3rd ERS symposium*, Florence, 17-21 March, 1997, pp. 609, ESA SP-414, ESA/ESTEC, Noordwijk, The Netherlands, 1997.
- Chance, K.V. and R.J.D. Spurr, Ring effect studies: Rayleigh scattering, including molecular parameters for rotational Raman scattering, and the Fraunhofer spectrum, *Applied Optics*, 36, 5224-5230, 1997.
- Chance, K. V., J. P. Burrows, D. Perner, and W. Schneider, Satellite measurements of atmospheric ozone profiles, including tropospheric ozone, from ultraviolet/visible measurements in the nadir geometry: a potential method to retrieve tropospheric ozone, *J. Quant. Spectrosc. Radiat. Transfer*, 57, 467-476, 1997.
- Chapman, A theory of upper-atmospheric ozone, *Memoirs Roy. Meteorol. Soc.*, III, 103, 1930.
- Chatfield, R.B., J.A. Vastano, L. Li, G.W. Sachse and V.S. Connors, The great African plume from biomass burning: Generalization from a three-dimensional study of TRACE A carbon monoxide, *J. Geophys. Res.*, 103, 28,059-28,077, 1998.
- Crutzen, P.J., The influence of nitrogen oxides on the atmospheric ozone content, *Q. J. R. Meteorol. Soc.*, 96, 320-325, 1970.
- Crutzen, P.J. and M.O. Andreae, Biomass burning in the tropics – Impact on atmospheric chemistry and biogeochemical cycles, *Science*, 250, 1669-1678, 1990.
- De Haan, J.F., P.B. Bosma, and J.W. Hovenier, The adding method for multiple scattering calculations of polarized light, *Astron. Astrophys. Vol 183*, 371-391, 1987
- De Haan, J.F., Accounting for Raman Scattering in DOAS, *SN-OMIE-KNMI-409*, KNMI, De Bilt, 2003.
- De Maziere, M., O. Hennen, M. Van Roozendaal, P. Demoulin, H. De Backer, Daily ozone vertical profile model built on geophysical grounds, for column retrieval from atmospheric high-resolution infrared spectra, *J. Geophys. Res.*, 104, 23,855-23,869, 1999.
- Dentener, F., M. van Weele, M. Krol, S. Houweling and P. van Velthoven, Trends and inter-annual variability of methane emissions derived from 1979-1993 global CTM simulations, *Atmos. Chem. Phys.*, 3, 73-88, 2003.
- De Rooij, W.A., van der Stap, C.C.A.H., Expansion of Mie Scattering Matrices in Generalized Spherical Functions, *Astron. & Astrophys, Vol 131*, 237-248, 1984

- Dethof, A., Assimilation of ozone data in the ECMWF model, paper presented at *TEMIS User Workshop*, ESA-ESRIN, Frascati, Italy, 15-16 May, 2003.
- Diebel, D., J. Burrows, R. de Beek, B. Kerridge, L. Marquard, K. Muirhead, R. Munro and U. Platt, Detailed Analysis of the Retrieval Algorithms Selected for the Level 1-2 Processing of GOME Data, *Final Report*, ESA 10728/94/NL/CN, Noordwijk, The Netherlands, October 1995.
- Dirksen, R. and M. Dobber, Analysis of PFM TV slit function measurements, *RP-OMIE-KNMI-342*, KNMI, De Bilt, 2002.
- Dobson, G.M.B., Observations of the amount of ozone in the Earth's atmosphere and its relation to other geophysical conditions, *Proc. Roy. Soc. London, Sec. A 129*, 411, 1930.
- Dobson, G.M.B., Origin and distribution of the polyatomic molecules in the atmosphere, *Proc. R. Soc. London, Ser. A*, 236, 187-193, 1956.
- Dobson, G.M.B., Forty years' research on atmospheric ozone at Oxford: A history, *Appl. Optics* 7, 405, 1968.
- Edwards, D.P., J.-F. Lamarque, J.-L. Attié, L.K. Emmons, A. Richter, J.-P. Cammas, J.C. Gille, G.L. Francis, M.N. Deeter, J. Warner, D.C. Ziskin, L.V. Lyjak, J.R. Drummond and J.P. Burrows, Tropospheric ozone over the Atlantic: A satellite perspective, *J. Geophys. Res.*, 108(D8), 4237, doi: 10.1029/2002JD002927, 2003.
- Eisinger, M. and J.P. Burrows, Tropospheric sulfur dioxide observed by the ERS-2 GOME Instrument, *Geophys. Res. Lett.*, 25, 4177-4180, 1998.
- ESA, GOME Users Manual, *ESA SP-1182*, ESA/ESTEC, Noordwijk, The Netherlands, 1995.
- Eskes, H., P. Van Velthoven, G. El Serafy, and H. Kelder, GOME ozone data assimilation and the ozone mini-hole of 30 november 1999. *Proceedings of the ERS-ENVISAT symposium*, 16-20 October 2000, Gothenburg, Sweden, CD-ROM: ESA SP-461, ESA/ESTEC, Noordwijk, The Netherlands, 2001.
- Eskes, H.J., P.F.J. van Velthoven and H.M. Kelder, Global ozone forecasting based on ERS-2 GOME observations, *Atmos. Chem. Phys.*, 2, 271-278, 2002.
- Eskes, H.J., P.F.J. van Velthoven, P.J.M. Valks, and H. M. Kelder, Assimilation of GOME total ozone satellite observations in a three-dimensional tracer transport model, *Quart. J. Roy. Meteor. Soc.*, 129, 1663, 2003.
- Farman, J.C., B.G. Gardiner and J.D. Shanklin, Large losses of total ozone in Antarctica reveal seasonal ClO_x/NO_x interaction, *Nature*, 315, 207-210, 1985.
- Fiedler, M. H. Frank, T. Gomer, M. Hausmann, K. Pfeilsticker, and U. Platt, The 'Minihole' event on Feb. 6, 1990, Influence of Mie-scattering on the evaluation of spectroscopic measurements, *Geophys. Res. Lett.*, 20, 10, 959-962, 1993.
- Fishman, J., C.E. Watson, J.C. Larsen, and J.A. Logan, Distribution of tropospheric ozone determined from satellite data, *J. Geophys. Res.*, 95, 3599-3617, 1990.
- Fishman, J., V.G. Brackett, E.V. Browell, and W.B. Grant, Tropospheric ozone derived from TOMS/SBUV measurements during TRACE-A, *J. Geophys. Res.*, 101, 24,069-24,082, 1996.
- Fishman, J., and A.E. Balok, Calculation of daily tropospheric ozone residuals using TOMS and empirically improved SBUV measurements: Application to an ozone pollution episode over the eastern United States, *J. Geophys. Res.*, 104, 30,319-30,340, 1999.

- Folkins, I., M. Loewenstein, J. Podolske, S. Oltmans, and M. Proffitt, A barrier to vertical mixing at 14 km in the tropics: Evidence from ozonesondes and aircraft measurements, *J. Geophys. Res.*, *104*, 22,095-22,101, 1999.
- Fortuin, J.P.F., and H.M. Kelder, Ozone climatology based on ozone sonde and satellite measurements, *J. Geophys. Res.*, *103*, 31,709-31,734, 1998.
- Fortuin, J.P.F., H.M. Kelder, M. Sigmond, R. Oemraw, and C.R. Becker, Inertial instability flow in the troposphere over Suriname during the South American Monsoon, *Geophys. Res. Lett.*, *30*, 1482, doi: 10.1029/2002GL016754, 2003.
- Garcia, O., Atlas of highly reflective clouds for the global tropics: 1971-1983. *U.S. Dept. of Commerce, NOAA, Environmental Research Lab., Boulder, Co.*, 365 pp., 1985.
- Grainger, J.F., and J. Ring, Anomalous Fraunhofer line profiles, *Nature*, *193*, 762, 1962.
- Guenter, A., et al., A global model of natural volatile organic compound emissions, *J. Geophys. Res.*, *100*, 8873-8892, 1995.
- Hansen, J.E., M. Sato, and R. Ruedy, Radiative forcing and climate response, *J. Geophys. Res.*, *102*, 6831-6864, 1997.
- Hansen, G., A. Dahlback, F. Tønnessen, and T. Svenøe, Validation of GOME total ozone by means of the Norwegian ozone monitoring network. *Ann. Geophysicae*, *17*, 430-436. 1999.
- Hao, W.M., M.H. Liu and P.J. Crutzen, Estimates of annual and regional releases of CO₂ and other trace gases to the atmosphere from fires in the tropics, based on the FAO statistics for the period 1975-180. In: *Fire in the Tropical Biota: Ecosystem Processes and Global Challenges, Ecol. Studies 84* (ed. J.G. Goldammer), pp. 440-462. Springer-Verlag, New York, 1990.
- Hao, W.M., and M.H. Liu, Spatial and temporal distribution of tropical biomass burning, *Global Biogeochem. Cycles*, *8*, 495-503, 1994.
- Herman, J.R., and E.A. Celarier, Earth surface reflectivity climatology at 340-380 nm from TOMS data, *J. Geophys. Res.*, *102*, 28,003-28,011, 1997.
- Highwood, E.J., and B.J. Hoskins, The tropical tropopause, *Q. J. R. Meteorol. Soc.*, *124*, 1579-1604, 1998.
- Hoogen, R., V. V. Rozanov, and J. P. Burrows, Ozone profiles from GOME satellite data: Algorithm description and first validation, *J. Geophys. Res.*, *104*, no. D7, 8263-8280, 1999.
- Houweling, S., F. Dentener, and J. Lelieveld, The impact of non-methane hydrocarbon compounds on tropospheric photochemistry, *J. Geophys. Res.*, *103*, 10673-10696, 1998.
- Hudson, R.D., J.H. Kim and A.M. Thompson, On the derivation of tropospheric column ozone from radiances measured by the total ozone mapping spectrometer, *J. Geophys. Res.*, *100*, 11,137-11,145, 1995.
- Hudson, R.D., and A. M. Thompson, Tropical tropospheric ozone (TTO) from TOMS by a modified-residual method, *J. Geophys. Res.*, *103*, 22,129-22,145, 1998.
- Huntrieser, H., H. Schlager, C. Feigl and H. Höller, Transport and production of NO_x in electrified thunderstorms: survey of previous studies and new observations at midlatitudes, *J. Geophys. Res.*, *103*, 28247-28264, 1998.
- Intergovernmental Panel on Climate Change (IPCC), *Aviation and the global atmosphere*, edited by J. E. Penner et al., Cambridge University Press, New York, 1999.

- Intergovernmental Panel on Climate Change (IPCC), *Climate Change 2001: Contribution of Working group I to the Third assessment report*, edited by J.T. Houghton et al., 881 pp., Cambridge University Press, New York, 2001.
- Jacob, D.J., B.G. Heikes, S.-M. Fan, J.A. Logan, D.L. Mauzerall, J.D. Bradshaw, H.B. Singh, G.L. Gregory, R.W. Talbot, D.R. Blake, and G.W. Sachse, Origin of ozone and NO_x in the tropical troposphere: A photochemical analysis of aircraft observations over the South Atlantic basin, *J. of Geophys. Res.*, *101*, 24,235-24,250, 1996.
- James, P. M., A climatology of ozone mini-holes over the Northern hemisphere, *Int. J. of Climatol.*, *18*, 1287-1303, 1998.
- Jeuken, A.B.M., H.J. Eskes, P.F.J. Van Velthoven, H.M. Kelder, and E.V. Hólm, Assimilation of total ozone satellite measurements in a three-dimensional tracer transport model. *J. of Geophys. Res.*, *104*, 5551-5563, 1999.
- Kelder, H.M., H.J. Eskes, F. Boersma, I. Isaksen, M. Gauss, C.S. Zerefos, D. Balis, U. Platt, M. Wenig, T. Wagner, G.H. Hansen, O.F. Vik, and C. Zehner, GOA: GOME Assimilated and Validated Ozone and NO₂ Fields for Scientific Users and for Model Validation, *Final Report*, EU project EVK2-CT-2000-00062, April, 2003.
- Kim, J.H., R.D. Hudson and A.M. Thompson, A new method of deriving time-averaged tropospheric column ozone over the tropics using total ozone mapping spectrometer (TOMS) radiances: Intercomparison and analysis using TRACE A data, *J. of Geophys. Res.*, *101*, 24,317-24,330, 1996.
- Klenk, K.F., P.K. Bhartia, A.J. Fleig, V.G. Kaveeshwar, R.D. McPeters, and P.M. Smith, Total ozone determination from the backscattered ultraviolet (BUV) experiment, *J. Appl. Meteorol.*, *21*, 1672-1684, 1982.
- Koelemeijer, R.B.A., and P. Stammes, Effects of clouds on ozone column retrieval from GOME UV measurements, *J. Geophys. Res.*, *104*, NO. D7, 8,281- 8,294, 1999.
- Koelemeijer, R.B.A., P. Stammes, J. W. Hovenier, and J. F. de Haan, A fast method for retrieval of cloud parameters using oxygen A-and measurements from the Global Ozone Monitoring Experiment, *J. of Geophys. Res.*, *106*, 3475-3490, 2001.
- Koelemeijer, R.B.A., P. Stammes, J. W. Hovenier, and J. F. de Haan, Global distributions of effective cloud fraction and cloud top pressure derived from oxygen A band spectra measured by the Global Ozone Monitoring Experiment: comparison to ISCCP data, *J. Geophys. Res.*, *107*(D12), 4151, doi: 10.1029/2001JD000840, 2002.
- Koelemeijer, R.B.A., J.F. de Haan and P. Stammes, A database of spectral surface reflectivity in the range 335-772 nm derived from 5.5 years of GOME observations, *J. Geophys. Res.*, *108*(D2), 4070, doi: 10.1029/2002JD002429, 2003.
- Komhyr, W.D., Nonreactive gas sampling pump, *Rev. Sci. Instrum.*, *38*, 981-983, 1967.
- Krishnamurti, T.N., H. Fuelberg, M.C. Sinha, D. Oosterhof, E.L. Bensman, and V.B. Kumar, The meteorological environment of the tropospheric ozone maximum over the Tropical South Atlantic Ocean, *J. Geophys. Res.*, *98*, 10,621-10,641, 1993.
- Krishnamurti, T.N., M.C. Sinha, M. Kanamitsu, D. Oosterhof, H. Fuelberg, R. Chatfield, D.J. Jacob, and J. Logan, Passive tracer transport relevant to the TRACE A experiment, *J. Geophys. Res.*, *101*, 23,889-23,907, 1996.
- Krol, M., and M. van Weele, Implications of variation of photodissociation rates for global atmospheric chemistry, *Atmos. Env.*, *31*, 1257-1273, 1997.

- Krueger, A.J., B. Guenther, A.J. Fleig, D.F. Heath, E. Hilsenrath, R.D. McPeters, and C. Prabhakara, Satellite ozone measurements, *Phil. Trans. R. Soc. Lond.*, A296, 191-204, 1980.
- Lacis, A.A., D.J. Wuebbles, and J.A.A. Logan, Radiative forcing of climate by changes in the vertical distributions of ozone, *J. Geophys. Res.*, 95, 9971-9981, 1990.
- Lacis, A.A., J. Chowdhary, M.I. Mischenko, and B. Cairns, Modelling errors in diffuse-sky radiation: Vector vs. scalar treatment, *Geophys. Res. Lett.*, 25, 135-138, 1998.
- Lambert, J.-C., M. Van Roozendaal, M. De Mazière, P.C. Simon, J.-P. Pommereau, F. Goutail, A. Sarkissian, and J.F. Gleason, Investigation of Pole-to-Pole Performances of Spaceborne Atmospheric Chemistry Sensors with the NDSC. *J. Atmos. Sciences*, 56, 176-193, 1999.
- Lambert, J.-C., M. Van Roozendaal, P.C. Simon, et al., Combined characterisation of GOME and TOMS total ozone measurements from space using ground-based observations from the NDSC. *Adv. Space Res.*, 26, 1931-1940, 2000.
- Lambert, J.-C. and C. Zehner, ERS-2 GOME GDP 3.0 Implementation and Delta Validation, *Validation Report for GOME Level-1-to-2 Data Processor Upgrade to Version 3.0*, ERSE-DTEX-EOAD-TN-02-0006, ESA-ESRIN, Frascati, Italy, 2002.
- Landgraf, I., and P.J. Crutzen, An efficient method for online calculations of photolysis and heating rates, *J. Atmos. Sci.*, 55, 863-878, 1998.
- Lauscher, F., Ozonbeobachtungen in Wien von 1853 bis 1981. Zusammenhänge zwischen Ozon und Wetterlagen. *Arbeiten a.d. Zentralanstalt f. Met. U. Geodynamik*, Heft 60, Wien, 1984.
- Lelieveld, J., and F. Dentener, What controls Tropospheric Ozone?, *J. Geophys. Res.*, 105, 3531– 3551, 2000.
- Leue, C., T. Wagner, M. Wenig, U. Platt and B. Jähne, Determination of the tropospheric NO_x source strength from GOME data, paper presented at *ESAMS Conference*, Eur. Space Agency, Netherlands, Jan. 18-22, 1999.
- Marengo, A., V. Thouret, P. Nedelec, H. Smit, M. Helten, D. Kley, F. Karcher, P. Simon, K. Law, J. Pyle, G. Poschmann, R. Vonwrede, C. Hume, and T. Cook, Measurement of ozone and water vapor by Airbus in-service aircraft: The MOZAIC airborne program, An overview, *J. Geophys. Res.*, 103, 25631-25642, 1998.
- Marland, G., T.A. Boden, and R.J. Andres, CO₂ emissions trends: A compendium of data on global change, *Tech. Rep.*, Carbon Dioxide Analysis Center, Oak Ridge National Laboratory, Oak Ridge, Tenn USA, 2000.
- Marquard, L.C., T. Wagner, and U. Platt, Improved air mass factor concepts for scattered radiation differential optical absorption spectroscopy of atmospheric species. *J. Geophys. Res.*, 105, 1315-1327, 2000.
- Martin, R.V., D.J. Jacob, J.A. Logan, I. Bey, R.M. Yantosca, A.C. Staudt, Q. Li, A.M. Fiore, B.N. Duncan, H. Liu, P. Ginoux, V. Thouret, Interpretation of TOMS observations of tropical tropospheric ozone with a global Model and in-situ observations, *J. Geophys. Res.*, 107(D18), 4351, doi: 10.1029 / 2001JD001480, 2002a.
- Martin, R.V., K. Chance, D.J. Jacob, T.P. Kurosu, R.J.D. Spurr, E. Bucsela, J.F. Gleason, P.I. Palmer, I. Bey, A.M. Fiore, Q. Li, R.M. Yantosca, and R.B.A. Koелеmeijer, An improved retrieval of tropospheric nitrogen dioxide from GOME, *J. Geophys. Res.*, 107(D20), 4437, doi: 10.1029/2001JD001027, 2002b.

- McDermid, I.S., S.M. Godin, and T.D. Walsh, Lidar measurements of stratospheric ozone and intercomparisons and validation, *Appl. Opt.*, 29, 4914-4923, 1990.
- McKenna, D. S., R. L. Jones, J. Austin, E. V. Browell, M. P. McCormick, A. J. Krueger, and A. F. Tuck, Diagnostic studies of the Antarctic vortex during the 1987 Airborne Antarctic Ozone Experiment: ozone miniholes, *J. Geophys. Res.*, 94(D9), 11641-11668, 1989.
- McKinlay, A.F., and B.L. Diffey, A reference action spectrum for ultraviolet induced erythema in human skin, *CIE J.*, 6, 17-22, 1987.
- McPeters, R.D., P.K. Bhartia, A.J. Krueger, J.R. Herman, C.G. Wellemeyer, C.J. Seftor, G. Jaross, O. Torres, L. Moy, G. Labow, W. Byerly, S.L. Taylor, T. Swissler, and R.P. Cebula, Earth Probe Total Ozone Mapping Spectrometer (TOMS) Data Products User's Guide. *NASA Technical Publication 1998-206895*, NASA Goddard Space Flight Center, Greenbelt, Maryland 20771., 1998.
- Meijer, E., P. van Velthoven, D. Brunner, H. Huntrieser and H. Kelder, Improvement and evaluation for the parameterisation of nitrogen oxide production by lightning, *Phys. Chem. of the Earth*, 26, 577-583, 2001.
- Miller, A.J., A review of satellite observations of atmospheric ozone, *Planet. Space Sci.*, 37, 1539-1554, 1989.
- Mischenko, M.I., A.A. Lacis, and L.D. Travis, Errors induced by the neglect of polarization in radiance calculations for rayleigh-scattering atmospheres, *J. Quant. Spectrosc. Radiat. Transfer*, 51, 491-510, 1994.
- Molina, M.J., and F.S. Rowland, Stratospheric sink for chlorofluoromethanes: chlorine atom catalyzed destruction of ozone, *Nature*, 249, 810-812, 1974.
- Müller, R., P.J. Crutzen, J.-U. Grooß, C. Brühl, J.M. Russel, H. Gernandt, D.S. McKenna, and A.F. Tuck, Severe chemical ozone loss in the Arctic during the winter of 1995-96, *Nature*, 389, 709-712, 1997.
- Munro, R., R. Siddans, W. J. Reburn, and B. J. Kerridge, Direct measurement of tropospheric ozone distributions from space, *Nature*, 392, 1998.
- Newman, P.A., L.R. Lait, and M.R. Schoeberl, The morphology and meteorology of Southern-Hemisphere spring total ozone mini-holes, *Geophys. Res. Lett.*, 15, 923-926, 1988.
- Newman, P.A., J.F. Gleason, R.D. McPeters, and R.S. Stolarski, Anomalously low ozone over the Arctic, *Geophys. Res. Lett.*, 24, 2689-2692, 1997.
- Newman, P. A., et al., An overview of the SOLVE/THESEO 2000 campaign, *J. Geophys. Res.*, 107(D20), 8259, doi:10.1029/2001JD001303, 2002.
- Noxon, J.F., Nitrogen dioxide in the stratosphere and troposphere measured by ground-based absorption spectroscopy, *Science*, 189, 547-549, 1975.
- Olivier, J.G.J., et al., Description of EDGAR Version 2.0: A set of global emission inventories of greenhouse gases and ozone-depleting substances for all anthropogenic and most natural sources on a per country basis and on 1°x1° grid, *RIVM report nr. 771060 002*, Bilthoven, The Netherlands, 1996.
- Orphal, J., A critical review of the absorption cross-sections of O₃ and NO₂ in the 240-790 nm region, *ESA Technical Note MO-TN-ESA-GO-0302*, 2002.
- Parrish, A., B.J. Connor, J.J. Tsou, I.S. McDermid, and W.P. Chu, Ground-based microwave monitoring of stratospheric ozone, *J. Geophys. Res.*, 97, 2541-2546, 1992.

- Peters, W., M. Krol, F. Dentener, A. M. Thompson and J. Lelieveld, Chemistry-transport modeling of the satellite observed distribution of tropical tropospheric ozone, *Atmos. Chem. Phys.* 2, 103-120, 2002a.
- Peters, W., J.P.F. Fortuin, H. Kelder, C.R. Becker, P.J. Crutzen, A.M. Thompson and J. Lelieveld, Tropospheric ozone over a tropical Atlantic station in the northern hemisphere: Paramaribo, Surinam (6N, 55W), *Tellus B*, in press, 2002b.
- Pickering, K.E., A.M. Thompson, Y. Wang, W.-K. Toa, D.P. McNamara, V.W.J.H. Kirchoff, B.G. Heikes, G.W. Sachse, J.D. Bradshaw, G.L. Gregory, and D.R. Blake, Convective transport of biomass burning emissions over Brazil during Trace A, *J. Geophys. Res.*, 101, 23,993-24,012, 1996.
- Piters, A.J.M., R.J. Van Der A, J.H.G.M. Van Geffen, R.F. Van Oss, and P.J.M. Valks, Retrieving spectral reflectivities from Extracted GOME Instrument header data. *Proceedings of the ERS-ENVISAT symposium*, 16-20 October 2000, Gothenburg, Sweden, CD-ROM: ESA SP-461, ESA/ESTEC, Noordwijk, The Netherlands, 2001.
- Platt, U., D. Perner and Pätz, Simultaneous measurement of atmospheric CH₂O, O₃, and NO₂ by differential optical absorption, *J. Geophys. Res.*, 84, 6329-6335, 1979.
- Platt, U., Differential optical absorption spectroscopy (DOAS), Air Monitoring by Spectroscopic Techniques, M. Siegrist, Ed., *Chemical Analysis Series*, 127, 1994.
- Prather, M., et al., Atmospheric chemistry and greenhouse gases, in *Climate Change 2001, The scientific basis: Contribution of working group I to the Third assessment report of the Intergovernmental Panel on Climate*, edited by J. T. Houghton, et al., Chapter 4, pp. 239-287, Cambridge University Press, Cambridge, United Kingdom and New York, NY, US., 2001.
- Price, C., J. Penner and M. Prather, NO_x from lightning 1. Global distribution based on lightning physics, *J. Geophys. Res.*, 102, 5929-5941, 1997.
- Reid, S. J., A. F. Tuck and G. Kildaris, On the changing abundance of ozone minima at Northern midlatitudes, *J. Geophys. Res.*, 105(D10), 12169-12180, 2000.
- Rex, M. et al., Prolonged stratospheric ozone loss in the 1995-96 Arctic winter, *Nature*, 389, 835-838, 1997.
- Richter, A., F. Wittrock, M. Eisinger and J.P. Burrows, GOME observation of tropospheric BrO in northern hemispheric spring and summer 1997, *Geophys. Res. Lett.*, 25, 2683-2686, 1998.
- Richter, A. and J. P. Burrows, Tropospheric NO₂ from GOME measurements, *Adv. Space Res.* 29, 1673-1683, 2002.
- Rodgers, C. D., Characterization and error analysis of profiles retrieved from remote sounding measurements, *J. Geophys. Res.*, 95(D5), April, 1990.
- Rossow, W. B., A. W. Walker, and L. C. Garder, Comparison of ISCCP and other cloud amounts, *J. Clim.*, 6, 2394-2418, 1993.
- Rossow, W. B., and R. A. Schiffer, Advances in understanding clouds from ISCCP, *Bull. Am. Meteor. Soc.*, 80, 2261-2287, 1999.
- Rozanov, V., D. Diebel, R. Spurr and J. Burrows, GOMETRAN: A radiative transfer model for the satellite project GOME – the plane parallel version, *J. Geophys. Res.*, 102, 16,683-16,695, 1997.
- Schutgens, N. and P. Stammes, Parameterisation of Earth's polarisation spectrum in the ultraviolet, *J. Quant. Spectrosc. Radiat. Transfer*, 75, 239-255, 2002.

- Siegert, F., G. Ruecker, A. Hinrichs et al., Increased damage from fires in logged forests during droughts caused by El Nino, *Nature*, 414, 437-440, 2001.
- Sigmond M., P.C. Siegmund, H. Kelder, and E. Manzini, A simulation of the separate climate effects of middle atmospheric and tropospheric CO₂ doubling, *J. Climate*, in press, 2003.
- Spurr, R., Improved Climatologies and New Air Mass Factor Look-up Tables for O₃ and NO₂ Column Retrievals from GOME and SCIAMACHY Backscatter Measurements. *Proceedings of the ESAMS '99 Symposium*, 18-22 January, ESA-WPP-161, ESA-ESTEC, Noordwijk, The Netherlands, 1999.
- Spurr, R., W. Thomas and D. Loyola, GOME Level 1 to 2 Algorithms Description, Tech. Note ER-TN-DLR-GO-0025 (Issue 3/A), Deutsches Zentrum für Luft und Raumfahrt, Oberpfaffenhofen, Germany, 2002.
- Stammes, P., J.F. de Haan, and J.W. Hovenier, The polarized internal radiation field of a planetary atmosphere, *Astron. Astrophys.*, 225, 239-259, 1989.
- Stammes, P., Spectral radiance modelling in the UV-Visible range, in *IRS2000: Current Problems in Atmospheric Radiation*, edited by W.L. Smith and Y.M. Timofeyev, pp. 385-388, A. Deepak Publishing, Hampton (VA), 2000.
- Stammes, K., S.-C. Tsay, W. Wiscombe, and K. Jayaweera, Numerically stable algorithm for discrete ordinate method radiative transfer in multiple scattering and emitting layered media, *Applied Optics*, 27, 2502-2509, 1988.
- Stoffelen, A. and H. Eskes, Final Report of the SODA (Satellite Ozone Data Assimilation) project, KNMI, De Bilt, The Netherlands, 1999.
- Stolarski, R.S., P. Bloomfield, R.D. McPeters, and J.R. Herman, Total Ozone trends deduced from Nimbus 7 TOMS data, *Geophys. Res. Letters*, 18, 1015-1018, 1991.
- Struthers, H., R. Brugge, W.A. Lahoz, and A. O'Neill, Assimilation of ozone profiles and total ozone column measurements into a global general circulation model, *J. Geophys. Res.*, 107, 2002.
- Thompson, A.M., K.E. Pickering, D.P. Menamara, M.R. Schoeberl, R.D. Hudson, J.H. Kim, E.V. Browell, V.W.J.H. Kirchoff, and D. Nganga, Where did tropospheric ozone over southern Africa and the tropical Atlantic come from in October 1992? – Insight from TOMS, GTE, TRACE A, and SAFARI 1992, *J. Geophys. Res.*, 101, 24,251-24,278, 1996.
- Thompson, A. M., and R. D. Hudson, Tropical tropospheric ozone (TTO) maps from Nimbus 7 and Earth Probe TOMS by the modified-residual method: Evaluation with sondes, ENSO signals, and trends from Atlantic regional time series, *J. Geophys. Res.*, 104, 26,961-26,975, 1999.
- Thompson, A. M., B.G. Doddridge J.C. Witte, R.D. Hudson, W.T. Luke, J.E. Johnson, B.J. Johnson, S.J. Oltmans, and R. Weller, A tropical Atlantic paradox: Shipboard and satellite views of a tropospheric ozone maximum and wave-one in January-February 1999, *Geophys. Res. Lett.*, 27, 3317-3320, 2000.
- Thompson, A.M., J.C. Witte, R.D. Hudson, H. Guo, J.R. Herman, and M. Fujiwara, Tropical tropospheric ozone and biomass burning, *Science*, 291, 2128-2132, 2001.

- Thompson, A. M., J. C. Witte, R. D. McPeters, S. J. Oltmans, F. J. Schmidlin, J. A. Logan, M. Fujiwara, V. W. J. H. Kirchhoff, F. Posny, G. J. R. Coetzee, B. Hoegger, S. Kawakami, T. Ogawa, B. J. Johnson, H. Vömel and G. Labow, Southern Hemisphere Additional Ozonesondes (SHADOZ) 1998-2000 tropical ozone climatology: 1. Comparison with Total Ozone Mapping Spectrometer (TOMS) and ground-based measurements, *J. Geophys. Res.*, *108* (D2), 8238, doi:10.1029/2001JD000967, 2003a.
- Thompson, A. M., J. C. Witte, S. J. Oltmans, F. J. Schmidlin, J. A. Logan, G. J. R. Coetzee, B. Hoegger, V. W. J. H. Kirchhoff, T. Ogawa, S. Kawakami, F. Posny, J. P. F. Fortuin, H. M. Kelder and M. Fujiwara, Southern Hemisphere Additional Ozonesondes (SHADOZ) 1998-2000 tropical ozone climatology: 2. Tropospheric variability and the zonal wave-one, *J. Geophys. Res.*, *108* (D2), 8241, doi:10.1029/2002JD002241, 2003b.
- Uchino, O., R.D. Bojkov, D.S. Balis, K. Akagi, M. Hayashi, and R. Kajiwara, Essential characteristics of the Antarctic ozone decline: Update to 1988, *Geophys. Res. Lett.*, *26*, 1377-1380, 1999.
- Untch, A., and A. Simmons, Increased stratospheric resolution in the ECMWF forecasting system, *ECMWF Newsletter*, *82*, 2-8, 1998.
- Valks, P.J.M., and G.J.M. Velders, The present-day and future impact of NO_x emissions from subsonic aircraft on the atmosphere in relation to the impact of NO_x surface sources, *Ann. Geophysicae*, *17*, 1064-1079, 1999.
- Valks, P.J.M., A.J.M. Piters, J.C. Lambert, C. Zehner and H. Kelder, A Fast Delivery System for the retrieval of near-real time ozone columns from GOME data, *Int. J. Remote Sensing*, *24*, 423-436, 2003a.
- Valks, P. J. M., R. B. A. Koelemeijer, M. van Weele, P. van Velthoven, J. P. F. Fortuin, and H. Kelder, Variability in tropical tropospheric ozone: Analysis with Global Ozone Monitoring Experiment observations and a global model, *J. Geophys. Res.*, *108*(D11), 4328, doi: 10.1029 /2002JD002894, 2003b.
- Van Aardenne, J.A., F.J. Dentener, C.G.M. Klein Goldewijk, J. Lelieveld and J.G.J. Olivier, A high resolution data set of historical anthropogenic trace gas emissions for the period 1890-1990, *Global. Biogeochem. Cycles*, *15*, 909– 928, 2001.
- Van der A, R.J., R.F. van Oss, A.J.M. Piters, J.P.F. Fortuin, Y.J. Meijer and H.M. Kelder, Ozone profile retrieval from recalibrated Global Ozone Monitoring Experiment data, *J. Geophys. Res.*, *107*(D15), 4239, doi: 10.1029/2001JD000696, 2002.
- Van der Werf, G.R., J.T. Randerson, G.J. Collatz and L. Giglio, Carbon emissions from fires in tropical and subtropical ecosystems, *Global Change Biology*, *9*, 547-562, 2003.
- Van Geffen, J.H.G.M., Documentation of the software package GomeCal (version 1.0), *Technical report, KNMI*, De Bilt, The Netherlands, in press, 2002.
- Van Geffen, J.H.G.M., and R.F. van Oss, Wavelength calibration of spectra measured by GOME using a high-resolution reference spectrum, *Appl. Opt.*, *42*, 2739-2753, 2003.
- Van Roozendaal, M., P. Peeters, H. K. Roscoe, H. de Backer, A. E. Jones, L. Bartlett, G. Vaughan, F. Goutail, J.-P. Pommereau, E. Kyro, C. Wahlstrom, G. Braathen, P. C. Simon, Validation of ground-based visible measurements of total ozone by comparison with Dobson and Brewer spectrophotometers. *J. Atm. Chem.*, *29*, 55-83, 1998.
- Van Roozendaal, M., et al., Intercomparison of BrO measurements from ERS-2 GOME, ground-based and balloon platforms, *Adv. Space Res.*, *29*, 1661-1666, 2002a.

- Van Roozendael, V. Soebijanta, C. Fayt, and J.-C. Lambert, Investigation of DOAS issues affecting the accuracy of the GDP Version 3.0 total ozone product; In: ERS-2 GOME GDP 3.0 Implementation and Delta Validation, *Validation Report for GOME Level-1-to-2 Data Processor Upgrade to Version 3.0*, Lambert, J.-C. and C. Zehner (ed), Chapter 6, ERSE-DTEX-EOAD-TN-02-0006, ESA-ESRIN, Frascati, Italy, 2002b.
- Van Velthoven, P.F.J. and H. Kelder, Estimates of stratosphere-troposphere exchange: Sensitivity to model formulation and horizontal resolution, *J. Geophys. Res.*, *101*, 1429-1434, 1996.
- Vaughan, G., and C. Timmis, Transport of near-tropopause air into the lower midlatitude stratosphere. *Q. J. R. Meteorol. Soc.* *124*, 1559-1578, 1998.
- Veefkind, J.P. and J.F. De Haan, OMI Algorithm Theoretical Basis Document, Barthia, P.K (ed), Volume II - Chapter 3, DOAS Total Ozone Algorithm, *ATBD-OMI-02*, Version 2.0, Augustus 2002.
- Velders, G. J. M., C. Granier, R. W. Portmann, K. Pfeilsticker, M. Wenig, T. Wagner, U. Platt, A. Richter, and J. P. Burrows, Global tropospheric NO₂ column distributions: Comparing three-dimensional model calculations with GOME measurements, *J. Geophys. Res.*, *106*, 12,643-12,660, 2001.
- Wagner, T. and U. Platt, Satellite mapping of enhanced BrO concentrations in the troposphere, *Nature*, *395*, 486-490, 1998.
- Waliser, D.E., and C. Gautier, A Satellite-derived Climatology of the ITCZ, *J. Clim.*, *6*, 2162-2174, 1993.
- Wauben, W. M. F, and F. Kuik, Sensitivity study of the Brewer direct sun ozone retrieval algorithm using numerical simulations, in *Proc. XVIII Quadr. Ozone Symp., Aquila, 1996*, edited by R. D. Bojkov and G. Visconti, 85-88, 1998.
- Weatherhead, E.C., G.C. Reinsel, G.C. Tiao, X. Meng, D. Choi, W. Cheang, T. Keller, J. DeLuisi, D.J. Wuebbles, J.B. Kerr, A.J. Miller, S.J. Oltmans, and J.E. Frederick, Factors affecting the detection of trends: Statistical considerations and applications to environmental data, *J. Geophys. Res.*, *103*, 17149-17161, 1998.
- Weber, M., K.-U. Eichmann, F. Wittrock, K. Bramstedt, L. Hild, A. Richter, J.P. Burrows, and R. Müller, The cold Arctic winter 1995/96 as observed by GOME and HALOE: Tropospheric wave activity and chemical ozone loss, *Quart. J. Roy. Meteorol. Soc.*, *128*, 1293-1319, 2002.
- Wellemeyer, C.G., S.L. Taylor, C.J. Seftor, R.D. McPeters, and P.K. Barthia, A correction for total ozone mapping spectrometer profile shape errors at high latitude, *J. Geophys. Res.*, *102*, 9029-9038. 1997.
- World Meteorological Organization (WMO), Report of the WMO-NOAA Expert Meeting on GAW Data Acquisition and Archiving (Asheville, NC, USA, 4-8 November 1995), World Meteorological Organization Global Atmosphere Watch, *Environmental Pollution Monitoring and Research Programme Report Series*, No. 110, 61 pp, 1995.
- World Meteorological Organization (WMO), *Scientific Assessment of Ozone Depletion: 2002*, WMO Global Ozone Research and Monitoring Project – Report No. 47, 498 pp., Geneva, 2003.
- Yienger, J.J. and Levy, H., Global inventory of soil-biogenic NO_x emissions, *J. Geophys. Res.*, *100*, 11,447-11,464, 1995.

- Young, A.T., Revised depolarization corrections for atmospheric extinction, *Appl. Opt.*, *19*, 3427-3428, 1980.
- Ziemke, J. R., S. Chandra, and P. K. Bhartia, Two new methods for deriving tropospheric column ozone from TOMS measurements: The assimilated UARS MLS/HALOE and convective-cloud differential techniques, *J. Geophys. Res.*, *103*, 22,115-22,127, 1998.
- Ziemke, J. R. and S. Chandra, Seasonal and interannual variabilities in tropical tropospheric ozone, *J. Geophys. Res.*, *104*, 21,425-21,442, 1999.
- Ziemke, J.R., S. Chandra, J. Herman, and C. Varotsos, Erythemally weighted UV trends over northern latitudes derived from Nimbus 7 TOMS measurements. *J. Geophys. Res.*, *105*, pp 7373-7382, 2000.
- Ziemke, J. R., S. Chandra, and P. K. Bhartia, Cloud slicing: A new technique to derive upper tropospheric ozone from satellite measurements, *J. Geophys. Res.*, *106*, 9853-9867, 2001.

Abbreviations and Acronyms

The following is a list of acronyms and abbreviations used in this thesis.

| | |
|---------|---|
| AMF | Air Mass Factor |
| ATBD | Algorithm Theoretical Basis Document |
| ATSR | Along-Trace Scanning Radiometer |
| AVHRR | Advanced Very High Resolution Radiometer |
| B&P | Bass and Paur |
| CCD | Convective Cloud Differential |
| CTM | Chemical Transport Model |
| DAK | Doubling Adding KNMI |
| DISORT | Discrete Ordinate Radiative Transfer |
| DOAS | Differential Optical Absorption Spectroscopy |
| DLR | Deutsches Zentrum für Luft- und Raumfahrt |
| DU | Dobson Unit |
| ECC | Electrochemical Concentration Cell |
| ECMWF | European Centre for Medium-range Weather Forecast |
| EDGAR | Emission Database for Global Atmospheric Research |
| EGOC | Extracted GOME Calibration data |
| EGOI | Extracted GOME Instrument Header |
| ENSO | El Nino-Southern Oscillation |
| ENVISAT | Environmental Satellite |
| EOS | Earth Observation System |
| EP | Earth Probe |
| ERS | European Remote Sensing Satellite |
| ESA | European Space Agency |
| FD | Fast Delivery |
| FM | Flight Model |
| FRESCO | Fast Retrieval Scheme for Cloud Observables |
| FWHM | Full Width Half Maximum |
| GCM | Global Circulation Model |
| GDP | GOME Data Processor |
| GEOS | Goddard Earth Observing System |
| GOME | Global Ozone Monitoring Instrument |
| HALOE | Halogen Occultation Experiment |
| HRC | High Reflectivity Cloud |

| | |
|-----------|--|
| IPCC | Intergovernmental Panel on Climate Change |
| ISCCP | International Satellite Cloud Climatology Project |
| ITCZ | Inter Tropical Convergence Zone |
| KNMI | Koninklijk Nederlands Meteorologisch Instituut |
| LIDAR | Light Detection and Ranging |
| LUT | Look Up Table |
| MLS | Microwave Limb Sounder |
| MOPITT | Measurement of pollution in the troposphere |
| MOZAIC | Measurements of Ozone and Water Vapor by Airbus In-Service Aircraft |
| MR | Modified Residual |
| NDSC | Network for the Detection of Stratospheric Change |
| NH | Northern Hemisphere |
| NIR | Near Infrared |
| NMHC | Non-Methane Hydrocarbons |
| NRT | Near Real Time |
| NWP | Numerical Weather Prediction |
| OMI | Ozone Monitoring Instrument |
| PAF | Processing and Archiving Facility |
| PSC | Polar Stratospheric Cloud |
| RMS | Root Mean Square |
| RTM | Radiative Transfer Model |
| SAA | South Atlantic Anomaly |
| SAGE | Stratospheric Aerosol and Gas Experiment |
| SBUV | Solar Backscatter Ultra-Violet |
| SCIAMACHY | Scanning Imaging Absorption spectrometer for Atmospheric Cartography |
| SH | Southern Hemisphere |
| SHADOZ | Southern Hemisphere Additional Ozone Sounding |
| SOLVE | SAGE III Ozone Loss and Validation Experiment |
| SZA | Solar Zenith Angle |
| THESEO | Third European Stratospheric Experiment on Ozone |
| THIR | Temperature-Humidity and Infrared Radiometer |
| TM | Tracer Model |
| TOGOMI | Total Ozone algorithm for Gome using the OMI algorithm |
| TOMS | Total Ozone Mapping Spectrometer |
| TOR | Tropospheric Ozone Residual |
| TOVS | Tiros Operational Vertical Sounder |
| TRACEGAS | Trace Constituents Extraction from Global Atmospheric Sounding |
| TTOC | Tropical Tropospheric Ozone Column |
| UARS | Upper Atmosphere Research Satellite |
| UV | Ultra Violet |
| VIS | Visible |
| WMO | World Meteorological Organisation |
| WOUDC | World Ozone and UV Radiation Data Centre |

Nawoord

Toen ik eind 1997 bij het KNMI solliciteerde waren er twee onderwerpen waar ik aan zou kunnen gaan werken, de zogenaamde 'ozonwinden' of het bepalen van ozonhoeveelheden uit ruwe satellietdata. Omdat ik niet zoveel affiniteit had met ruwe satellietdata, had ik mijn voorkeur uitgesproken voor de 'ozonwinden'. Echter, nadat ik mijn onderzoek bij het RIVM naar de effecten van vliegverkeer op de samenstelling van de atmosfeer had afgerond en bij het KNMI begon, kon ik toch aan de slag met het 'retrieven' van ozonkolommen uit ruwe GOME satellietdata. Toen bleek ook het werken met ruwe satellietdata heel leuk. Niet alleen het wetenschappelijk onderzoek, maar ook de meer technische zaken, zoals het snel beschikbaar maken van de ozongegevens voor de buitenwereld, heb ik met veel plezier gedaan. Dat de ozonlaag en het ozongat boven de Zuidpool zulke tastbare onderwerpen zijn die veel mensen aanspreken, was zeker een belangrijke stimulans.

Toen ik over de snelle retrieval van GOME ozonkolommen een artikel kon schrijven was dat eigenlijk het begin van mijn promotieonderzoek. In de jaren die volgden heb ik interessante uitstapjes kunnen maken naar mini-ozongaten en de tropische troposfeer. Ook de dertig buitenlandse reizen die ik heb gemaakt om mijn werk te presenteren en om samen te werken met de vele internationale collega's waren heel leerzaam. Het was niet alleen interessant onderzoek, ik vond ook de werkomgeving bij de afdeling Atmosferische Samenstelling van het KNMI zeer stimulerend. Met plezier kijk ik daarom terug op deze leuke tijd bij het KNMI.

Dit proefschrift had niet tot stand kunnen komen zonder de hulp en bijdragen van vele anderen. Ik wil dan ook graag een aantal mensen hier in het bijzonder noemen. In de eerste plaats wil ik mijn promotor Hennie Kelder en co-promotor Roeland van Oss bedanken. Hennie en Roeland, bedankt voor de mogelijkheid en grote vrijheid die jullie me gegeven hebben om dit onderzoek te doen en voor het vertrouwen dat jullie in mij hadden. Eveneens wil ik Ulrich Platt (mijn tweede promotor), Peter Bultjes en Frans Sluijter bedanken voor hun getoonde interesse en de nuttige commentaren.

Uiteraard wil ik het GOFAP/TEMIS team, Ankie Piters, Ronald van der A, Jos van Geffen en Henk Eskes, bedanken. Met jullie heb ik vele jaren vrijwel dagelijks samengewerkt en jullie bijdrage aan het tot stand komen van dit proefschrift is dan ook zeer groot. Ik ben Robert Koelemeijer, Michiel van Weele, Peter van Velthoven veel dank verschuldigd voor hun bijdragen aan het tropische gedeelte van dit proefschrift. Verder zouden zonder het werk en de hulp van Johan de Haan en Pepijn Veeffkind de GOME ozonkolommen van het KNMI niet zo'n hoge kwaliteit bereikt hebben als nu het geval is en zou het proefschrift niet zo'n

mooi slot hebben gehad. Voorts wil ik Marc Allaart bedanken voor de belangrijke mini-ozongat bijdrage aan dit proefschrift en voor alles wat met de 'Brewer' te maken heeft.

I would like to thank Jean-Cristopher Lambert and Dimitris Balis for their important 'ground-based' contribution. Your quality stamps are crucial for a satellite ozone product. Many thanks also to Claus Zehner from the European Space Agency. This work would not have been possible without the technical and financial support from ESA. The cooperation with you and with other colleagues from ESA, like the people from the 'ATSR World Fire Atlas' group, was excellent. Furthermore, I need to thank many other colleagues within the GOME and SCIAMACHY community for the helpful discussions on the many different aspects of satellite measurements.

Natuurlijk wil ik mijn aardige en behulpzame collega's van de groep Atmosferische Samenstelling bedanken. Sinds mijn start bij het KNMI is de groep groter geworden, maar de uitstekende sfeer is gebleven. Een aantal AS'ers wil ik graag met name noemen: Michael, Renske, Ernst, Jeroen, Hans, Paul, Mijke, Jojanneke, Gé, Dirk, Folkert, bedankt voor jullie hulp en de gezellige sfeer.

Tot slot wil ik graag mijn ouders bedanken voor hun steun en vertrouwen.

Curriculum Vitae

Pieter Valks is op 7 september 1969 geboren in Velsen. In 1987 behaalde hij zijn VWO diploma aan het Mendelcollege in Haarlem. In datzelfde jaar begon hij aan de studie Technische Natuurkunde aan de TU Delft. Zijn interesse ging uit naar de meer tastbare fysica. Daarom heeft hij de laatste twee jaar van zijn studie doorgebracht bij de vakgroep Akoestiek en Seismiek en studeerde hij af op geluidoverdracht in de atmosfeer. Voor zijn vervangende dienstplicht kwam hij terecht bij TNO Milieuwetenschappen, waar hij met satellietmetingen van troposferisch ozon en met atmosferische modellen ging werken. Het atmosferisch onderzoek sprak hem aan en hij bleef dan ook nog anderhalf jaar bij TNO werken. Hierna heeft hij ruim een jaar gewerkt bij het RIVM aan de effecten van vliegverkeer op de samenstelling van de atmosfeer, waarna hij in 1998 de overstap maakte naar het KNMI. Daar kon hij zich weer bezig houden met satellietmetingen van ozon en ontstond het idee om hiervan een promotieonderzoek te maken. Hij heeft vervolgens een aantal jaren met veel plezier aan dit onderwerp gewerkt, met dit proefschrift als resultaat.

Stellingen behorend bij het proefschrift:

"Retrieval of total and tropospheric ozone from observations by the Global Ozone Monitoring Experiment"

Pieter Valks, 18 december 2003

1. Bij de bepaling van de troposferische ozonkolom in de tropen met de "Convective Cloud Differential" methode, dient rekening gehouden te worden met het feit dat de meeste convectieve wolken niet hoger reiken dan de tropische overgangslaag, verscheidene kilometers onder de tropopause. (hoofdstuk 4)
2. De tropische "ozonparadox" (het opvallende verschil tussen de locaties van het troposferisch ozonmaximum en de biomassa-verbrandingen in de periode december-februari) kan gedeeltelijk worden verklaard door de lage gevoeligheid van satellietinstrumenten, zoals GOME en TOMS, voor ozonveranderingen in de lage troposfeer. (hoofdstuk 6)
3. De verwachte sterke toename van de emissies van ozonprecursors, zoals NO_x en CO, in de (sub)tropen vormt een ernstige bedreiging voor de mondiale luchtkwaliteit in de tweede helft van deze eeuw. (Prather et al., Geophys. Res. Lett., 2003)
4. De ozonkolomdichtheid van de atmosfeer kan alleen nauwkeurig worden bepaald uit GOME radiantiemetingen met de DOAS methode, als rekening wordt gehouden met inelastische (Raman) verstrooiing. (hoofdstuk 5)
5. De onnauwkeurigheid in de absorptiedoorsneden van ozon is een belangrijke oorzaak voor de verschillen tussen ozonkolomdichtheden gemeten vanaf de grond en vanuit de ruimte. (hoofdstuk 2 en 5)
6. De berichten in de media in het najaar van 2002 over het herstel van de ozonlaag, naar aanleiding van de kleine omvang van het Zuidpool-ozongat in dat jaar, waren nogal voorbarig gezien de bijzondere meteorologische condities boven de Zuidpool in die tijd.
7. De bijdrage aan het broeikaseffect van natuurlijke ondergrondse kolenbranden is groter dan de bijdrage van het verkeer in de Verenigde Staten.
8. Het op kunstzinnige wijze weergeven van satellietmetingen van ozon in beeld en geluid draagt bij tot een betere houding van mensen tegenover de kwetsbare aardse biosfeer. (Stéphan Barron, kunstenaar)
9. Als we een wetenschappelijke monocultuur in het leven roepen, waarbij iedereen bezig is met dezelfde paar vragen (vragen die door politici, zakenlieden en technocraten belangrijk worden gevonden), zal het resultaat helemaal geen wetenschap zijn. (Len Fisher)
10. De opmars van de digitale fotografie heeft als gevolg dat foto's uit de donkere kamer steeds vaker als ambachtelijk en artistiek worden ervaren.
11. Het is mede aan een Amsterdamse drukker ten tijde van de Gouden Eeuw te danken, dat Johann Sebastian Bach zich heeft kunnen ontwikkelen tot de componist die hij geworden is.